

**The effect of block molecular weight distribution on  
morphologies of polystyrene-*block*-poly(acrylic acid)  
aggregates in solution**

by

**Owen L. Terreau**

A thesis submitted to the Faculty of Graduate Studies and research in partial fulfillment of  
the requirements for the degree of

**Doctor of Philosophy**

Department of Chemistry  
McGill University  
Montreal, Quebec  
Canada  
H3A 2K6

© Owen L. Terreau, 2004

June 2004



Library and  
Archives Canada

Bibliothèque et  
Archives Canada

Published Heritage  
Branch

Direction du  
Patrimoine de l'édition

395 Wellington Street  
Ottawa ON K1A 0N4  
Canada

395, rue Wellington  
Ottawa ON K1A 0N4  
Canada

*Your file    Votre référence*

*ISBN: 0-494-06344-0*

*Our file    Notre référence*

*ISBN: 0-494-06344-0*

#### NOTICE:

The author has granted a non-exclusive license allowing Library and Archives Canada to reproduce, publish, archive, preserve, conserve, communicate to the public by telecommunication or on the Internet, loan, distribute and sell theses worldwide, for commercial or non-commercial purposes, in microform, paper, electronic and/or any other formats.

The author retains copyright ownership and moral rights in this thesis. Neither the thesis nor substantial extracts from it may be printed or otherwise reproduced without the author's permission.

#### AVIS:

L'auteur a accordé une licence non exclusive permettant à la Bibliothèque et Archives Canada de reproduire, publier, archiver, sauvegarder, conserver, transmettre au public par télécommunication ou par l'Internet, prêter, distribuer et vendre des thèses partout dans le monde, à des fins commerciales ou autres, sur support microforme, papier, électronique et/ou autres formats.

L'auteur conserve la propriété du droit d'auteur et des droits moraux qui protègent cette thèse. Ni la thèse ni des extraits substantiels de celle-ci ne doivent être imprimés ou autrement reproduits sans son autorisation.

---

In compliance with the Canadian Privacy Act some supporting forms may have been removed from this thesis.

Conformément à la loi canadienne sur la protection de la vie privée, quelques formulaires secondaires ont été enlevés de cette thèse.

While these forms may be included in the document page count, their removal does not represent any loss of content from the thesis.

Bien que ces formulaires aient inclus dans la pagination, il n'y aura aucun contenu manquant.

  
**Canada**

---

## ABSTRACT

---

The effect of the molecular weight distribution of both the soluble and the insoluble blocks on the solution self-assembly of the amphiphilic block copolymer polystyrene-*block*-poly(acrylic acid) was studied. Copolymers of a variety of block lengths but with narrow molecular weight distributions were synthesized by sequential anionic synthesis. Mixing two or more copolymers of differing block length (while the second block length was identical) artificially increased the polydispersity index (PDI) of one block. Self-assembly was induced by adding water slowly to a copolymer solution until a desired solvent composition was attained. The resulting aggregates were compared using transmission electron microscopy and dynamic light scattering.

The first experiments, presented in chapter 2, studied the effect of the corona (PAA) polydispersity on the size of vesicular aggregates. For a constant solvent composition and copolymer concentration, the size of the vesicles was generally found to decrease with increasing PAA polydispersity. In chapter 3, a partial phase diagram of morphology as a function of water content and PAA polydispersity is presented. The phase boundaries between spheres and rods, and rods and vesicles were found to shift to lower water contents with increased PAA polydispersity.

While chapters 2 and 3 show that the PAA polydispersity affects both the morphology and the size of vesicles, chapter 4 presents work that indicates that the shape of the PAA molecular weight distribution plays an important part in determining the degree to which the PAA polydispersity affects the morphology. A subsequent study also

shows that the molecular weight distribution effect only occurs when the relative PAA/PS block length ratio is low.

The polystyrene molecular weight distribution studies, presented in chapter 5, show that the opposite effect to that of the PAA molecular weight distribution occurs with an increase in the PS PDI. The morphological boundary from spheres to rods was found to move to higher water contents with an increase in PS PDI. Even at very high water contents, where vesicles are usually found for low molecular weight distribution samples, only spherical micelles were found for the samples with increased PS PDI.



---

## RÉSUMÉ

---

L'influence de la distribution des masses moléculaires des blocs solubles et insolubles sur l'auto-assemblage d'un copolymère amphiphile de polystyrène-*bloc*-poly(acide acrylique) (PS-*b*-PAA) a été étudié. Des copolymères comportant des longueurs de bloc variées, mais avec une distribution de masses moléculaires étroite, ont été produits par synthèse anionique séquentielle. Pour accroître la polydispersité d'un des deux blocs, au moins deux copolymères avec des longueurs différentes du bloc en question ont été mélangés (le deuxième bloc ayant une longueur constante). L'auto-assemblage a été provoqué par l'addition lente d'eau à une solution de copolymère jusqu'à l'obtention de la composition désirée de solvant. Les agrégats obtenus ont été comparés par microscopie électronique à transmission et par diffusion dynamique de la lumière.

La première série d'expériences, présentée au chapitre 2, a porté sur l'étude de l'influence de la polydispersité de la couronne (PAA) sur la taille des agrégats vésiculaires. Pour une composition constante du solvant et une concentration unique de copolymère, la taille des vésicules diminue avec une augmentation de la polydispersité du PAA. Le troisième chapitre présente un diagramme de phases partiel, montrant les morphologies en fonction de la teneur en eau et de la polydispersité du PAA. Les frontières entre sphères/cylindres et cylindres/vésicules sont déplacées vers des teneurs en eau inférieures avec une polydispersité accrue du PAA.

Tandis que les chapitres 2 et 3 montrent que la polydispersité du PAA influence la morphologie et la taille des vésicules, le chapitre 4 indique que la forme de la distribution des masses moléculaires du PAA joue un rôle important. Par ailleurs, une étude subséquente démontre que l'effet de la distribution des masses moléculaires entre seulement en jeu lorsque le quotient des longueurs de blocs PAA/PS est bas.

Les études des distributions de masses moléculaires du polystyrène, chapitre 5, montrent qu'un effet opposé à celui obtenu avec le PAA se produit avec une élévation de l'index de polydispersité (IPD) du PS. La frontière entre les morphologies de sphère et de tige s'est déplacée vers des teneurs en eau plus élevées avec une augmentation de l'IPD du PS. Même avec des teneurs en eau élevées, où des vésicules sont habituellement observées pour des échantillons ayant une distribution de masse moléculaire étroite, seules des micelles sphériques ont été trouvées avec un IPD élevé de PS.

---

## PREFACE

---

In accordance with the Thesis Specifications of the “Guidelines for Thesis Preparation” (Faculty of Graduate Studies and Research, McGill University), the following text is cited:

“As an alternative to the traditional thesis format, the dissertation can consist of a collection of papers of which the student is an author or co-author. These papers must have a cohesive, unitary character making them a report of a single program of research. The structure for the manuscript-based thesis must conform to the following:

Candidates have the option of including, as part of the thesis, the text of one or more papers submitted, or to be submitted, for publication, or the clearly-duplicated text (not the reprints) of one or more published papers. These texts must conform to the "Guidelines for Thesis Preparation" with respect to font size, line spacing and margin sizes and must be bound together as an integral part of the thesis. (Reprints of published papers can be included in the appendices at the end of the thesis.)

The thesis must be more than a collection of manuscripts. All components must be integrated into a cohesive unit with a logical progression from one chapter to the next. In order to ensure that the thesis has continuity, connecting texts that provide logical bridges preceeding (*sic*) and following each manuscript are mandatory.

As manuscripts for publication are frequently very concise documents, where appropriate, additional material must be provided (e.g., in appendices) in sufficient detail to allow a clear and precise judgement (*sic*) to be made of the importance and originality of the research reported in the thesis.

In general, when co-authored papers are included in a thesis the candidate must have made a substantial contribution to all papers included in the thesis. In addition, the candidate is required to make an explicit statement in the thesis as to who contributed to such work and to what extent. This statement should appear in a single section entitled "Contributions of Authors" as a preface to the thesis. The supervisor must attest to the accuracy of this statement at the doctoral oral defence. Since the task of the examiners is made more difficult in these cases, it is in the candidate's interest to clearly specify the responsibilities of all the authors of the co-authored papers.

When previously published copyright material is presented in a thesis, the candidate must include signed waivers from the publishers and submit these to the Graduate and Postdoctoral Studies Office with the final deposition, if not submitted previously. The candidate must also include signed waivers from any co-authors of unpublished manuscripts."

This thesis is written in the alternative format. The duplicated text of two published manuscripts (published in *Langmuir*) constitute chapters 2 and 3. Chapters 4 and 5 have

been written as chapters but shortened versions will be submitted for publication in scientific journals.

Chapter 2: Terreau, O.; Luo, L.; Eisenberg, A. *Langmuir* **2003**, *19*, 5601-5607

Chapter 3: Terreau, O.; Bartels, C.; Eisenberg, A. *Langmuir* **2004**, *20*, 637-645

Chapter 4: Terreau, O.; Eisenberg, A. *to be submitted*

Chapter 5: Terreau, O.; Eisenberg, A. *to be submitted*

### **Contributions of Authors**

In all of the studies, the author performed the experiments, analyzed the data, provided preliminary theories as explanations of the data, wrote the original drafts of the papers, and helped with the editing of papers. Professor Adi Eisenberg was included as a coauthor since he was the research supervisor. Through discussion with professor Eisenberg, the explanations were refined, and the papers were edited. Dr. Laibin Luo was included as a coauthor on chapter 2 because he synthesized the polymers that were used for the studies presented in chapter 2. The author made polymers that were used in the studies presented in chapters 3 and 4, while the polymers that were used for the experiments presented in chapter 5 were left over from previous members of the Eisenberg group. Dr. Carl Bartels helped in the complex analysis of the dynamic light scattering data presented in chapter 3, and is thus included as a coauthor for chapter 3.

---

## ACKNOWLEDGEMENTS

---

My time as a graduate student has been a great experience, especially because of the people who have helped during this time.

- Professor Adi Eisenberg for his supervision and guidance in the research presented in this thesis, his encouragement in the lab, his help in the preparation of manuscripts (and my writing skills), and for allowing me to travel to conferences to present our research.
- Dr. Carl Bartels for his help with the editing of this thesis, training on the DLS, helpful suggestions with polymer synthesis, an introduction to Linux and for being a great friend.
- Members of the Eisenberg group: Past (Neil, Carl, Muriel, Michael, Sachiko, Kui, Hongwei, Laibin, Yisong, Futian, Christine, Susan, Luc) and present (Patrick, Amira, Qingwua, Renata, Nicolas, Tony, Enya), My thanks especially to Neil Cameron, Carl Bartels and Patrick Lim Soo for passing on their knowledge of polymer chemistry to me in the earlier stages of this degree.
- Ms. Jeannie Mui, Dr. S. Kelly Sears, and Dr. Hojatollah Vali for training on the TEM.
- Claudia Gributs for the translation of numerous abstracts into French.
- Alfred Kluck for all of his help with any machine that breaks down. Fred can fix anything, and no, I am not playing hockey today!
- Rick Rossi for his help with electronics in the laboratory and George Kopp for his well made glassware, essential for anionic polymerizations.

- The administrative staff: Renée Charron, Chantal Marotte, Fay Nurse, Paulette Henault, Carol Brown and Sandra Aerssen for their assistance and making day to day operations within the Otto Maass building run smoothly.
- Rhodia US, and the National Science and Engineering Research Council of Canada for funding of this research
- My friends within the department for allowing me to be active in many social scenes. The chemistry graduate student society (especially ex-president Stephanie Warner, for getting me involved) and volunteers for running and funding social activities. Members of such esteemed intramural teams as; the Maassholes (softball), Studly Hungwell (ball hockey), the Ex-Men (hockey), and the Otto Massochists (broomball). Many thanks to those who captained such teams; Shane Pawsey, Claudia Gributs, Francois Ravenelle, Petr Furasik, and Mike McCalduf.
- Those who found time to go relax, and relieve some stress by hitting a little white ball around a field; Lee Fader, Brain Seivewright, Andrew Oliver, Mike Rybak and the rest of the weekend golfers from the department.
- My family: Mom, Dad and Sheila, thanks for always being there to support me, for being there during the sad times and celebrating during the good times. Not only throughout my graduate school career but also through my entire life. I couldn't have had a better family.
- To my love, Diane. Thank you for your support, motivation and always giving me a reason to smile.

---

## TABLE OF CONTENTS

---

Abstract.....	ii
Résumé.....	iv
Preface.....	vi
Acknowledgements.....	xii
Table of Contents.....	xiv
Table of Figures.....	xviii

### Chapter 1: Introduction 1

---

1.0 Introduction.....	1
1.1 Polymers.....	2
1.2 Polymer Synthesis and Characterization.....	3
1.2.1 Molecular Weight and Molecular Weight Distribution.....	4
1.2.2 Ionic Synthesis.....	8
1.2.3 Controlled Free Radical Synthesis.....	13
1.2.4 Polymer Characterization.....	16
1.2.4.1 Spectroscopic techniques.....	16
1.2.4.2 Molecular Weight Measurements.....	17
1.2.4.3 Size Exclusion Chromatography.....	18
1.2.4.4 MALDI TOF.....	21
1.3 Self Assembly.....	22
1.3.1 Block Copolymers in the Bulk.....	22
1.3.2 Micellization of Block Copolymers in Solution.....	25
1.3.2.1 Critical Micelle Concentration.....	28
1.3.2.2 Thermodynamic Considerations.....	28
1.3.2.3 Factors Affecting Morphologies.....	33
1.3.2.4 Kinetics of Morphological Transitions.....	38
1.3.2.5 Aggregate Characterization.....	40
1.4 Summary of Purpose and Scope.....	44
1.5 References.....	46

### Chapter 2: Effect of Poly(Acrylic Acid) Block Length Distribution on Polystyrene-*b*-Poly(Acrylic Acid) Aggregates in Solution. 1. Vesicles. 54

---

Abstract.....	54
2.1 Introduction.....	55
2.2 Experimental.....	58
2.2.1 Anionic Synthesis.....	58
2.2.2 Molecular Weight Distributions.....	59



2.2.3 Preparation of Vesicles.....	61
2.2.4 Transmission Electron Microscopy.....	61
2.2.5 Dynamic Light Scattering.....	62
2.3 Results and Discussion.....	62
2.3.1 Molecular Weight Distributions of Blends.....	62
2.3.2 THF / DMF System.....	65
2.3.3 Dioxane System.....	74
2.3.4 Is There Segregation into Different Aggregates? .....	76
2.4 Conclusions.....	78
2.5 Linking Text.....	79
2.6 Acknowledgements.....	79
2.7 References.....	79

**Chapter 3: Effect of Poly(Acrylic Acid) Block Length Distribution on Polystyrene-*b*-Poly(Acrylic Acid) Aggregates in Solution. 2. A Partial Phase Diagram.** 83

Abstract.....	83
3.1 Introduction.....	84
3.2 Experimental.....	88
3.2.1 Anionic Synthesis.....	88
3.2.2 Fractionation.....	89
3.2.3 Molecular Weight Distributions.....	90
3.2.4 Preparation of Aggregates.....	91
3.2.5 Transmission Electron Microscopy.....	92
3.2.6 Dynamic Light Scattering.....	93
3.3 Results and Discussion.....	93
3.3.1 Effect of Corona Polydispersity on Spheres .....	97
3.3.2 Effect of corona polydispersity on rods.....	104
3.4 Conclusions.....	109
3.5 Linking Text.....	110
3.6 Acknowledgements.....	110
3.7 References.....	111

**Chapter 4: Effect of Poly(Acrylic Acid) Block Length Distribution on Polystyrene-*b*-Poly(Acrylic Acid) Aggregates in Solution. 3. The Shape of the Molecular Weight Distribution Curve.** 114

Abstract.....	114
4.1 Introduction.....	115
4.2 Experimental.....	119
4.2.1 Anionic Synthesis.....	119
4.2.2 Fractionation.....	120
4.2.3 Molecular Weight Distributions.....	120

4.2.4 Preparation of Aggregates.....	121
4.2.5 Transmission Electron Microscopy.....	122
4.3 Results and Discussion.....	123
4.3.1 Molecular Weight Distribution Effects.....	123
4.3.2 Phase Diagrams for Mixtures of Two Copolymers.....	130
4.4 Conclusions.....	133
4.5 Linking Text.....	134
4.6 Acknowledgements.....	134
4.7 References.....	134

## **Chapter 5: Effect of Polystyrene Block Length Distribution on Polystyrene-*b*-Poly(Acrylic Acid) Aggregates in Solution. 137**

Abstract.....	137
5.1 Introduction.....	138
5.2 Experimental.....	141
5.2.1 Anionic Synthesis.....	141
5.2.2 Fractionation.....	142
5.2.3 Molecular Weight Distributions.....	143
5.2.4 Preparation of Aggregates.....	146
5.2.5 Transmission Electron Microscopy.....	146
5.3 Results and Discussion.....	146
5.3.1 Are These Equilibrium Morphologies?.....	154
5.4 Conclusions.....	155
5.5 Acknowledgements.....	156
5.6 References.....	156

## **Chapter 6: Conclusions, Contributions to Original Knowledge 159**

6.1 Effects of Poly(Acrylic Acid) Polydispersity.....	159
6.1.1 Vesicles.....	159
6.1.2 Spheres and Rods.....	160
6.1.3 The Shape of the Molecular Weight Distribution.....	161
6.2 Effects of Polystyrene Polydispersity.....	162
6.3 Future Work.....	162
6.4 Contributions to Original Knowledge.....	163
6.5 References.....	164

<b>Appendices</b>	<b>166</b>
<hr/>	
<b>Appendix A: Polymer Synthesis .....</b>	<b>166</b>
<b>Appendix B: Measurement of <math>M_N</math> and <math>M_W</math>.....</b>	<b>170</b>
<b>Appendix C: Polymer Characterization.....</b>	<b>178</b>
<b>Appendix D: Molecular Weight Distributions.....</b>	<b>185</b>
<b>Appendix E: Calculations.....</b>	<b>190</b>




---

## TABLE OF FIGURES

---

<b>Figure 1-1:</b> Possible arrangements of two monomers in a copolymer. The filled circles represent one type of repeat unit while the empty circles represent a second type of repeat unit.....	3
<b>Figure 1-2:</b> Hypothetical Gaussian molecular weight distribution, the different molecular weight averages are indicated.....	6
<b>Figure 1-3:</b> Molecular weight distributions for two samples with different number $M_n$ . The peaks are superimposed to show the width of the distribution more clearly.....	7
<b>Figure 1-4:</b> Molecular weight distributions of a sample with $M_n = 20$ repeat units...	12
<b>Figure 1-5:</b> Theoretical phase diagram.....	23
<b>Figure 1-6:</b> Morphologies of crew-cut aggregates of amphiphilic diblock copolymers in solution. (HHH: Hexagonally packed hollow hoops).....	27
<b>Figure 1-7:</b> Schematic of 2-stage transmission electron microscope.....	41
<b>Figure 2-1:</b> Molecular weight distributions of PAA blocks of the individual copolymers assuming that the polydispersity of the block is the same as that of a homopolystyrene of similar length prepared under identical conditions.....	64
<b>Figure 2-2:</b> Molecular weight distributions of the PAA blocks in the mixtures.....	64
<b>Figure 2-3:</b> Comparison TEM photos of vesicles made from different mixtures of copolymers in the THF/DMF system. The number at the top left corner refers to the polydispersity index of the PAA block.....	66
<b>Figure 2-4:</b> Size as a function of polydispersity of vesicles in the THF/DMF system. TEM data, ♦ DLS data.....	67

- Figure 2-5:** Vesicle sizes as measured by DLS and TEM..... 68
- Figure 2-6:** Schematic illustration of why an increase in polydispersity of the PAA block results in smaller vesicles. A) A vesicle made with a narrow molecular weight distribution of  $\text{PS}_{310}\text{-}b\text{-PAA}_{28}$  lengths. B) A vesicle made from a mixture of two different blocks with different PAA chain lengths. The smaller  $\text{PS}_{310}\text{-}b\text{-PAA}_{11}$  chains segregate preferentially to the inside surface of the vesicle and therefore the hollow core of the vesicle can become smaller. The dotted lines are meant as guides for the eye to indicate the vesicle size..... 70
- Figure 2-7:** Spheres made from mixtures of  $\text{PS}_{300}\text{-}b\text{-PAA}_{74}$  and  $\text{PS}_{300}\text{-}b\text{-PAA}_{11}$ . The longer PAA chains are kept away from each other by regions containing only the short PAA chains, thereby reducing the repulsions among corona chains..... 73
- Figure 2-8:** Size as a function of polydispersity for vesicles in the dioxane system. The first point is courtesy of Choucair et al.<sup>38</sup>..... 76
- Figure 2-9:** Partial phase diagram of individual copolymers. - ● Large compound micelles; • - Spheres; ○ - Spheres and rods; + - Rods; ⊕ - Rods and vesicles; O - Vesicles. The arrows indicate the conditions at which the mixtures were made.....78
- Figure 3-1:** Molecular weight distributions of PAA block of individual copolymers assuming that the polydispersity of the block is the same as that of a homopolystyrene of similar length prepared under identical conditions..... 91
- Figure 3-2:** Partial phase diagram of PAA PDI and water content for mixtures with a number-average composition of  $\text{PS}_{325}\text{-}b\text{-PAA}_{48}$  at a constant concentration. •spheres,

 rods and spheres, 
  rods and vesicles, 
 O vesicles, 
  spheres and LCMs. The dotted lines are meant as guides for the trend in the morphological boundaries.....94

**Figure 3-3:** Comparison micrographs of spherical aggregates made from mixtures of block copolymers, with an artificially broadened PAA block polydispersity, at 8% water (w/w). The polydispersity of the PAA block increases from 1.25 (a) to 1.58 (b) to 1.89 (c) to 2.17 (d) to 2.46 (e) to 3.28 (f). In all cases, spherical aggregates were observed ..... 100

**Figure 3-4:** Average aggregate diameter (and population standard deviation) as a function of PAA polydispersity, as measured by TEM ( $\blacklozenge$ ) and DLS ( $\bullet$ ). The TEM measurements are an average of 250-300 particles. The DLS measurements are the result of the Contin program (number average) at a detection angle of 90°..... 101

**Figure 3-5:** Spherical micelle with a polydisperse corona. The longer chains will stretch further away from the core and prevent secondary aggregation or LCM formation.... 101

**Figure 3-6:** Effect of PAA PDI on rods. At 14% water (w/w), at a low PAA PDI of 1.25 rods are observed, and as the polydispersity of the PAA block is increased to 1.58 a mixture of rods and vesicles is observed. A further increase to a PAA PDI of 1.89 shows rods and spheres, while increasing the PAA PDI further to 2.17, 2.46, or 3.28 results in the formation of vesicles..... 105

**Figure 3-7:** Effect of the PAA PDI at 12% water (w/w). The complete range of morphologies from spheres to rods to vesicles is observable. At a low PAA PDI of 1.25, spheres are seen. Increasing the PAA PDI to 1.58, 1.89, and 2.17 shows spheres that are elongated along one axis (i.e., starting to form rods). Vesicles are observed in a mixture

of rods and spheres at a PAA PDI of 2.46, while only vesicles are observed at a PAA PDI of 3.28..... 106

**Figure 3-8:** Aggregate made of the same number of chains with (A) a monodisperse corona and (B) a polydisperse corona. The dotted lines are guides to the radius of the corona. Chain repulsion in the corona causes curvature in part A. In part B the long chains cause an increase in the corona volume. Since the number of corona units is the same in parts A and B, because  $M_n$  of the corona block is the same, the repulsions per unit volume are smaller in part B; this allows more aggregation of chains. As more chains aggregate, the size of the micelle increases; this also increases stretching of the core chains, which is not geotropically favored. Eventually, the micelle will elongate to reduce the stretching of the core chains resulting in an elongated sphere (C)..... 108

**Figure 4-1:** Molecular weight distributions of PAA block in mixtures..... 122

**Figure 4-2:** Schematic of aggregates made from copolymers with A) a monodisperse corona PDI, B) a polydisperse, bimodal corona PDI, and C) a polydisperse, monomodal PDI. In B the corona volume is larger than either A or C..... 130

**Figure 4-3:** A two-polymer phase diagram for mixtures of  $PS_{325}-b-PAA_{10}$  and  $PS_{325}-b-PAA_{210}$ ..... 132

**Figure 4-4:** Two-polymer phase diagrams of the: A)  $PS_{325}-b-PAA_{10}$  /  $PS_{325}-b-PAA_{124}$  system, and B)  $PS_{325}-b-PAA_{124}$  /  $PS_{325}-b-PAA_{210}$  system..... 133

**Figure 5-1:** Molecular Weight Distributions of PS Block of Individual Copolymers .. 144

**Figure 5-2:** Molecular Weight Distributions of PS block in Mixtures..... 145

**Figure 5-3:** TEM micrographs of the PS PDI samples at 50 % water. A change in morphology from vesicles to spheres is observed with an increase in the PS PDI..... 149

**Figure 5-4:** Schematic of aggregates formed from a diblock with a narrow distribution (low PS PDI), and a polydisperse (high PS PDI) distribution of the size of the core block. In both cases the single chains are dissolved in a good solvent. As water is added the chains start to aggregate. At low water contents spherical micelles are formed for both cases; however, the degree of stretching of the chains, which span from the surface to the middle of the micelle core, is higher for the sample made of copolymers with a narrow core block length distribution. A further increase in water content results in a change in morphology for the narrow molecular weight distribution sample in order to relax the high degree of stretching of the core chains. The degree of stretching on the polydisperse sample is not very high; therefore, at high water concentrations, large spherical micelles are obtained..... 150

**Figure C-1:** GPC chromatogram of polystyrene precursor..... 178

**Figure C-2:** GPC chromatogram of diblock copolymer..... 179

**Figure C-3:** NMR spectrum of PS-*b*-Pt-BuA block copolymer..... 180

**Figure C-4:** FTIR spectrum of PS-*b*-Pt-BuA..... 181

**Figure C-5:** FTIR spectrum of PS-*b*-PAA..... 182

**Figure C-6:** GPC chromatogram of inverse micelles. The extra peak is due to homopolymer..... 183

**Figure C-7:** GPC chromatogram of inverse micelles after removal of homopolystyrene. .... 184



<b>Figure D-1:</b> The measured polydispersity of homopolystyrene of degree of polymerization $X_n$ . The solid line is the theoretical limit (Poisson distribution). The dotted line is the experimental fit. <sup>1</sup> .....	<b>185</b>
Molecular weight distributions from Chapter 2.....	<b>186</b>
Molecular weight distributions from Chapter 3.....	<b>187</b>
Molecular weight distributions from Chapter 4.....	<b>188</b>
Molecular weight distributions from Chapter 5.....	<b>189</b>

## CHAPTER 1

---

# INTRODUCTION

---

### 1.0 Introduction

The goal of the research presented in this thesis was to investigate the effect of the block molecular weight distribution on the sizes and morphologies of diblock copolymers in solution. Nanoscience has emerged as a huge field, especially as technology is constantly improving. Computers are becoming faster and, at the same time, microprocessors are being incorporated into more devices. The general trend is to make such devices smaller, and thus, more compact. For example, people with diabetes can measure the levels of glucose in their body using a device that is the size of a credit card. As the devices become smaller, the parts within them must also become smaller. The field of nanotechnology has emerged as a solution to this problem. By scaling down macroscopic materials to the nano level, smaller devices are possible. Once materials are of the atomic size, their macroscopic properties may change. The properties of nanoscale materials have potential for use in many applications<sup>1-8</sup>; however, they must first be understood.

The self-assembly of diblock copolymers is an interesting area of nanotechnology. The physical process of the self-assembly is, in itself, a complex process with many aspects still not understood. More and more potential applications of block copolymers, in areas such as drug delivery<sup>2-4</sup>, separations<sup>5-6</sup>, electronics<sup>7</sup> and catalysis<sup>8</sup> are becoming possible; therefore, a more detailed understanding of how to control the self-assembly process is needed in order to optimize the resulting materials and conditions in which they

are used. While it is clear to those in the field that block copolymers, like other polymers, have a distribution of molecular weights, the effect that the molecular weight distribution of the copolymer has on solution self-assembly has not been extensively studied. Since block copolymers are showing potential for use in specific applications, much effort has been put into developing polymerization methods that allow for their low cost production. Some success has been made in the development of such low cost synthetic methods<sup>9-11</sup>; however, the resulting products usually have broader molecular weight distributions than those prepared by anionic polymerization, a relatively expensive method. Therefore, the effect that the molecular weight distribution has on the self-assembly properties needs to be investigated.

## **1.1 Polymers**

To start a discussion on block copolymer self-assembly, a brief introduction to the field of polymer chemistry is needed. A polymer, or macromolecule, is a molecule that is made of many similar units (called monomers before polymerization or repeat units when they are part of a chain) that are all connected together in a repeating fashion during the polymerization.<sup>12</sup> The simplest example of a polymer is a linear homopolymer, a large molecule consisting of only one kind of repeating unit (polystyrene, for example, contains many styrene units covalently bound together). The introduction of a second monomer can result in many different polymer compositions and architectures. For instance, two types of repeating units can be placed in a statistical fashion (a statistical copolymer) or in alternating, gradient (or tapered), graft, or block fashions as shown in figure 1-1.<sup>13</sup>

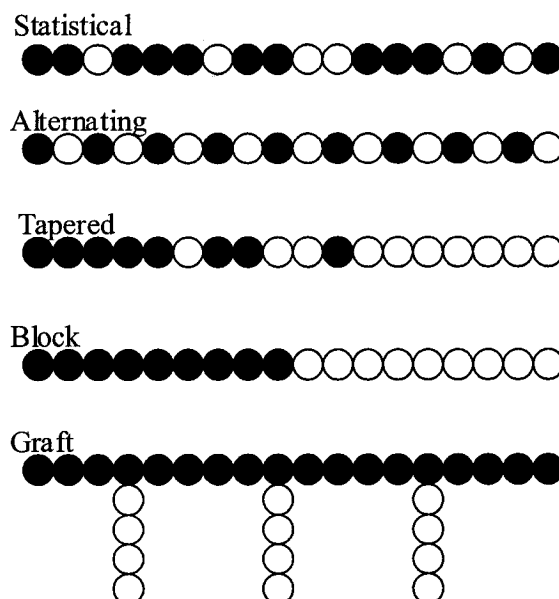


Figure 1-1: Possible arrangements of two monomers in a copolymer. The filled circles represent one type of repeat unit while the empty circles represent a second type of repeat unit.<sup>13</sup>

## 1.2 Polymer Syntheses and Characterization

The architecture of the polymer can be controlled by the synthetic method of preparation. Synthetic polymers can be produced by many different techniques, some give more control of the resulting polymer architecture than others, and still others allow for the low cost production of polymers of simple architectures. Simple organic chemistry can be used between molecules with two reactive end groups in step growth polymerizations, usually condensation reactions. An example is the reaction of the alcohol group in ethylene glycol and the acid functionality in terephthalic acid, which results in the ester linkage in the production of the polyester poly(ethylene terephthalate), sold under the trade name Dacron, among others.<sup>13</sup> Esters, amides, and urethanes are common linkages formed from step growth polymerizations.<sup>13</sup> Vinylic monomers

(monomers containing a carbon-carbon double bond) are polymerized by one of many other techniques such as free radical or ionic polymerizations. Due to their relative ease and low cost, free radical polymerizations are very commonly used in industry to produce a variety of plastics and elastomers.

In nature, biopolymers (i.e. biomaterials such as DNA and proteins) are synthesized by complex processes, utilizing many species including things such as enzymes and ribosomes.<sup>14</sup> These systems work to control the addition of each monomer unit by a series of complex steps that control the molecular weight, molecular weight distribution and stereochemistry of the natural polymer. Synthetic techniques in the laboratory are not as controlled. Some techniques will allow for control of some properties of the resulting polymers. For example, co-ordination compounds, such as Ziegler-Natta catalysts, can be used as catalysts to control the tacticity of synthetic polymers.<sup>15</sup> They do so by controlling the orientation of the monomer with respect to the growing polymer chain.

The most common polymerizations used in industry, other than the Ziegler-Natta catalyzed processes, are the free radical procedures, which give very little control of the molecular weight distribution or the architecture of the resulting polymers. The use of ionic initiators to polymerize monomers with vinylic moieties gives an increase in the control of the resulting polymer properties such as molecular weight or polydispersity.

### **1.2.1 Molecular Weight and Molecular Weight Distributions of Polymers**

Polymers are long chains that are created by the addition of monomer to a growing chain; therefore, due to the frequently random nature of such processes as initiation, propagation, and termination, all of the chains in a given polymer reaction will

not have the same number of repeat units. Rather, there will be a distribution of sizes. The molecular weight is an average quantity. Many different averages can be defined for a polymer sample. The simplest average is the number average molecular weight,  $M_n$ , defined as<sup>13</sup>

$$M_n = \frac{\sum n_i M_i}{\sum n_i} \quad (1-1)$$

where  $n_i$  is the number of chains of molecular weight  $M_i$ . Methods of detection that are dependent on the colligative properties of a polymer are used to determine  $M_n$  (see section 1.2.4 below). Another average is determined by the mass of material of each molecular weight in the sample, the weight average molecular weight,  $M_w$ , is determined.  $M_w$  is defined as<sup>13</sup>

$$M_w = \frac{\sum n_i M_i^2}{\sum n_i M_i} \quad (1-2)$$

Due to the fact that the molecular weight of each chain in the distribution is squared in the calculation of the weight average molecular weight,  $M_w$  is always larger than the number average molecular weight. To get an idea of the heterogeneity of the polymer sample, the heterogeneity index or polydispersity index, PDI, is calculated as the weight average molecular weight divided by the number average molecular weight.<sup>13</sup>

$$\text{PDI} = M_w / M_n \quad (1-3)$$

It can be seen that for a hypothetical sample where all of the chains are the same length  $M$ ,  $M_n = M_w = M$  and the  $\text{PDI} = M/M = 1$ .

It should be pointed out that  $M_n$  is the first moment of the distribution and  $M_w$  is the ratio of the second moment to the first moment of the distribution. Higher order

molecular weights are possible. The ratio of the third moment to the second moment of the distribution is the z-average molecular weight and is defined as<sup>13</sup>

$$M_z = \frac{\sum n_i M_i^3}{\sum n_i M_i^2}; \quad (1-4)$$

however, the number and weight average molecular weights are the two most common average molecular weights associated with polymer samples. Figure 1-2 shows the relationship of the different molecular weights for a sample with a hypothetical Gaussian distribution of chains.

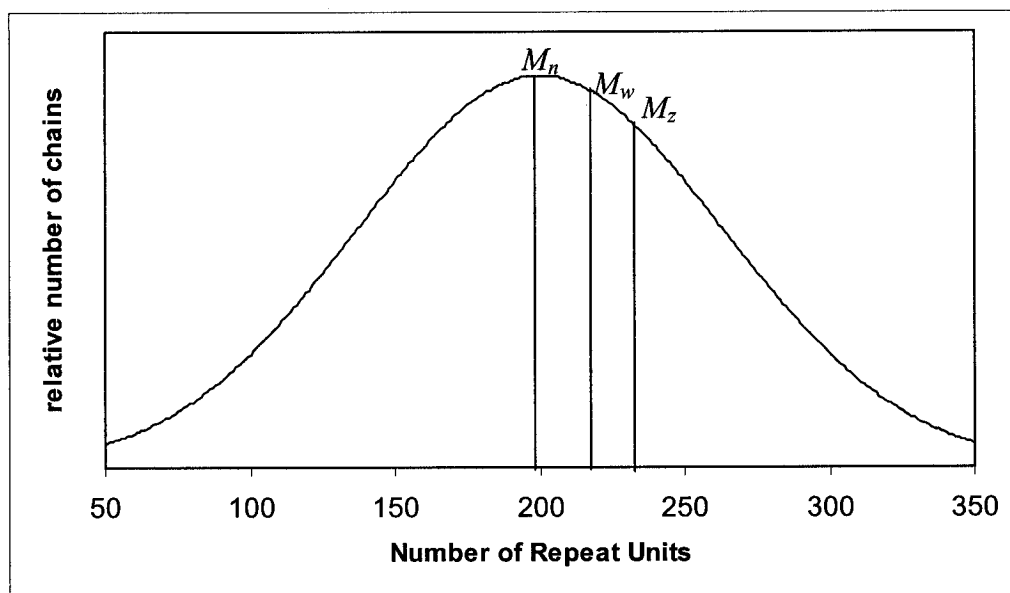


Figure 1-2: Hypothetical Gaussian Molecular Weight Distribution, the different molecular weight averages are indicated.

Two samples that have the same PDI but different  $M_n$  will have different distributions. The sample with a smaller  $M_n$  will have a distribution that is not as broad, as shown in figure 1-3. The x-axis in figure 1-3 has been changed from the normal number of repeat units to  $x - x_n$ , where  $x$  is the number of repeat units and  $x_n$  is the average

degree of polymerization. For a given PDI of 1.1, the width of the  $x_n = 20$  curve is much more narrower than that of the  $x_n = 200$  curve.

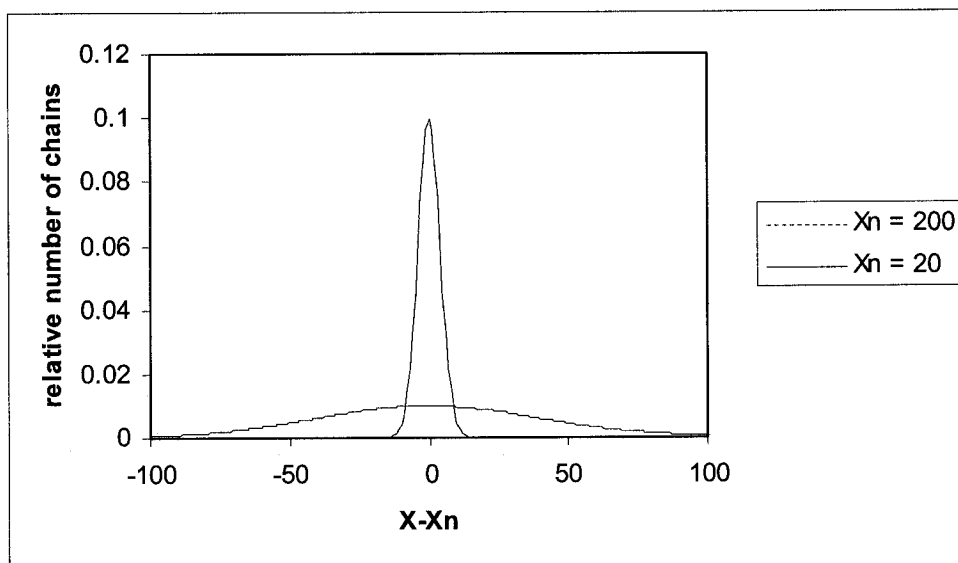


Figure 1-3: Molecular Weight Distributions for two samples with different number  $M_n$ . The peaks are superimposed to show the difference in the widths of the distributions more clearly.

Depending on the polymerization technique, PDIs can vary from 1.01 to over 10.<sup>16</sup> Most free radical polymerizations give PDIs close to 2. For more control of the average molecular weight and for narrower distributions of the molecular weight more sophisticated polymerization techniques, such as ionic<sup>16</sup>, controlled free radical<sup>9-11</sup>, ring opening metathesis (ROMP)<sup>17</sup>, and reversible addition-fragmentation chain transfer (RAFT)<sup>18</sup> can be employed. ROMP and RAFT were not used in the research presented within this thesis, and, therefore, are not discussed.



### 1.2.2 Ionic Synthesis

While ionic polymerizations can be used to form polymers with a higher control of their molecular weight, the range of monomers that can be polymerized is not as broad as that in free radical polymerizations. Ionic initiators can be either cationic or anionic. In either case, a counter-ion (also referred to as the gegen-ion) is present. The type of gegen-ion and the interactions of the ions with the solvent will affect the ionic polymerization. Polar solvents that are highly solvating may result in unwanted side reactions with the initiator. Solvents that promote greater proximity of the gegen-ion to the propagating chain allow more control of the polymerization, but generally reduce the kinetics of the chain growth. In general solvents with relatively low dielectric constants, such as tetrahydrofuran (THF), methylene chloride, etc... are favoured.<sup>16</sup>

Cationic initiators are generally strong Lewis acids; they can be split into three main categories: classical protonic acids, Lewis acids / Friedel-Crafts catalysts, and carbenium ion salts. They will initiate the polymerization of vinylic monomers containing electron-donating groups. The initiator also requires a co-catalyst to generate the carbocation that will attack the vinylic bond in the monomer. The polymerization can be terminated by unimolecular rearrangement of the ion pair or by bimolecular transfer with the monomer.<sup>19</sup>

Anionic initiators can be used to polymerize monomers with strong electronegative groups (i.e. acrylonitrile, styrene, methyl methacrylate). Some typical anionic initiators include *sec*-butyl lithium, diphenyl-methyl potassium, and in some cases Grignard reagents (alkyl magnesium bromides). The anionic polymerizations are rapid at low temperatures, and their rates depend on the solvent, the resonance stability of the carbocation, the electronegativity of the initiator and the degree of solvation of the ion

pair. Due to the nature of the carbanion used in anionic polymerization, trace impurities such as water, alcohol, carbon dioxide and oxygen will inhibit polymerization. Rigorous experimental procedures are needed in order to remove these impurities.<sup>20</sup>

As an example of an anionic polymerization, let us consider a monomer M polymerized by  $N_0$  number of initiators, BuLi. The initiation occurs in two steps:



The second reaction is the rate-determining step and, therefore, the rate of initiation,  $v_i$ , is

$$v_i = k_i c [\text{M}] \quad (1-7)$$

where  $c$  is the concentration of  $\text{Bu}^-$  and  $[\text{M}]$  is the concentration of monomer. The propagation can be written as follows



And the rate of propagation,  $v_p$ , is

$$v_p = k_p [\text{M}] [\text{M}^-] \quad (1-9)$$

where,  $[\text{M}^-]$  is the concentration of the living polymer chain. The advantage of anionic polymerization is that there is no formal termination step.<sup>20</sup> Thus, addition of more monomer will result in a longer polymer chain. Another advantage is that the addition of an aliquot of a second monomer, after the batch of the first monomer has completely reacted will result in a second block, and the formation of diblock copolymers. The lack of a formal termination step also allows for a “living” polymerization.<sup>21</sup> As long as  $v_i$  is greater than  $v_p$  all of the chains will start growing at the same time. The fact that the chains all start growing at the same time allows for the control of the molecular weight.<sup>21</sup>

Chain growth will start at  $N_0$  centers. The number of chains with  $n$  added monomers at a given time,  $N_n(t)$ , can be determined by:

$$\frac{dN_n}{dt} = \lambda[M](N_{n-1} - N_n), \quad (1-10)$$

where  $N_{n-1}$  is the number of chains of length  $n-1$  units,  $N_n$  is the number of chains of length  $n$  units and  $\lambda$  is a constant.

The rate of consumption of monomer can be determined by:

$$\frac{d[M]}{dt} = -\lambda[M]N_0. \quad (1-11)$$

This can be solved:

$$[M](t) = [M]_0 \exp(-\lambda N_0 t). \quad (1-12)$$

Hence,

$$\frac{dN_n}{dt} = \lambda[M]_0 (N_{n-1}(t) - N_n(t) \exp[-\lambda N_0 t]) \quad (1-13)$$

which, can be solved by letting

$$G_z(t) \cong \sum_{n=0}^{\infty} z^n N_n(t) \quad (1-14)$$

giving

$$\left[ N_n(t) = \frac{1}{n!} \frac{d^n}{dz^n} G_z(t) \right]_{z=0} \quad (1-15)$$

$$\frac{dG_z}{dt} = \lambda[M]_0 (z-1)G_z(t) \exp[-\lambda N_0 t] \quad (1-16)$$

or

$$G_z(t) = N_0 \exp\left[\frac{[M]_0}{N_0} (z-1)(1 - \exp[-\lambda N_0 t])\right] \quad (1-17)$$

which can undergo a Taylor expansion

$$P_n \equiv \frac{N_n(t)}{N_0} = \frac{e^{-a} a^n}{n!}; \quad (1-18)$$

where,

$$a \equiv \frac{[M]_0}{N_0} (1 - e^{-\lambda N_0 t}). \quad (1-19)$$

Note that

$$\sum_{n=0}^{\infty} n P_n(t) = e^{-a} \sum_{n=1}^{\infty} \frac{a^n}{(n-1)!} = e^{-a} \sum_{n=0}^{\infty} \frac{a^{n+1}}{n!} = a \quad (1-20)$$

and

$$a = \frac{[M]_0 - [M](t)}{N_0} \quad (1-21)$$

therefore, the monomer mass is conserved. Equation 1-20 is a form of a Poisson distribution.

Experimentally, most polymers made by anionic polymerization do not have Poisson distributions, but are somewhat broader due to the impurities contained within the reaction vessels, even with rigorous experimental procedures to try to remove them. The molecular weight distributions are thus approximated as Gaussian with low PDI.<sup>22</sup> It has also been found through MALDI TOF studies that, in some cases, Shultz-Zimm analysis will give an adequate description of the molecular weight distribution.<sup>23</sup> Although the distributions are broader than Poisson distributions, a typical anionic polymerization of styrene will give a PDI value less than 1.1. As an example of the different molecular weight distributions, Figure 1-4 contains molecular weight distributions created using a Poisson formula, and Gaussian formulas with varying PDI.

In each case the number average is 20 repeat units. It can be seen that as the PDI decreases the Gaussian distribution becomes more like the Poisson distribution.

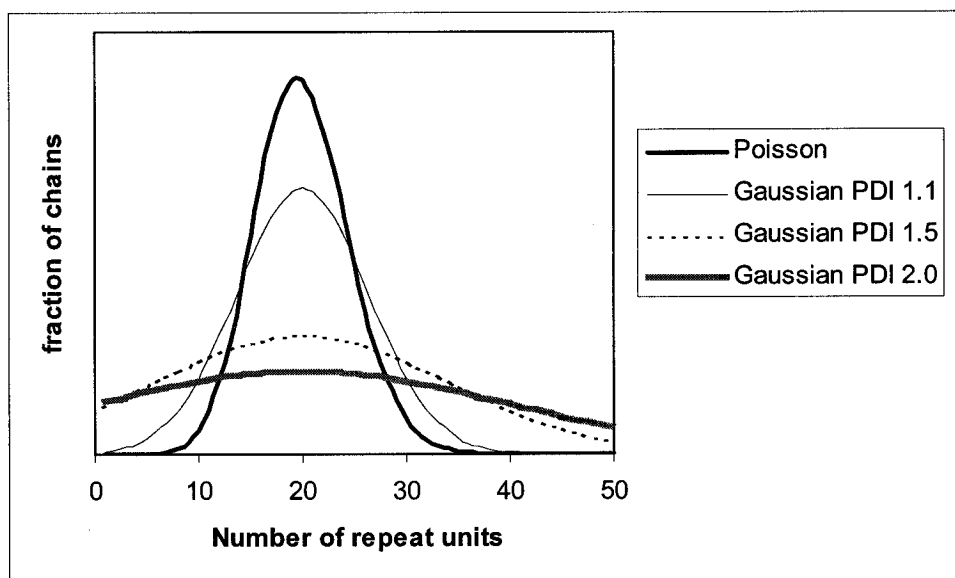


Figure 1-4: Molecular weight distributions of a sample with  $M_n = 20$  repeat units.

The living nature of anionic polymerizations allows us to prepare diblock copolymers; however, the method is successful only under some conditions.<sup>21</sup> The second carbanion must be a weaker nucleophile than the first one, i.e. the first anion has to be able to initiate the polymerization of the second monomer. The rate of initiation of the second monomer by the first must be faster than the rate of propagation of the second monomer in order to obtain a well-defined second block, and the second monomer must be free of oxygen, water or any other proton sources that will kill the reaction. Any such impurities in the second monomer will result in termination of the first block, and the presence of homopolymer.

An example of a diblock copolymer prepared by anionic polymerization is polystyrene-*block*-poly(*tert*-butyl acrylate).<sup>24</sup> The polymerization is initiated with *sec*-butyl lithium and styrene is polymerized first. In this case, the styrene carbanion is strong

enough to initiate the polymerization of the *tert*-butyl acrylate (*t*-BuA). The diblock must be made in this order as the *tert*-butyl acrylate carbanion is not able to polymerize styrene. The rate of initiation of the *t*-BuA is also higher than the rate of propagation of *t*-BuA. One last consideration is the fact that there are two double bonds in the second monomer. In order to have the carbanion attack the vinylic group instead of the carboxy group of the *t*-BuA, the temperature of the reaction is kept low. A ligand of the anionic species, such as LiCl, is also used to either control the dissociation of the active sites or create enough steric hindrance around them.<sup>24</sup>

### 1.2.3 Controlled Free Radical Synthesis

More recently, controlled free radical techniques have been developed.<sup>9-11</sup> The classical free radical polymerizations are very robust (i.e. they are possible in conditions that ionic polymerizations would fail in) and a number of monomers could be polymerized that cannot be through anionic synthesis.<sup>25</sup> Due to the nature of the free radical process, the production of block copolymers is not possible. Depending on the reactivity ratios of the two monomers, statistical or tapered copolymers can be formed, but a true diblock cannot be formed by classical free radical polymerization. This is due to the formal termination process of the free radical polymerization. In classical free radical polymerizations heat or light is added to activate the initiator. The initiator becomes active at a steady rate. Initially there are no growing chains, and then the concentration of growing chains gradually increases until a point is reached where the rate of termination (due to radical coupling or chain transfer or other processes) equals the rate of initiation of the initiators from the dormant state to the active state. In other words, there is a steady state concentration of active initiators. The steady state will

continue until the heat or light that is activating the initiator is removed, all of the initiator or monomer is used up, or something is added to terminate all of the radical species.<sup>25</sup> Since chains are terminated throughout the process, they cannot be extended to form diblock copolymers. Modifications of the free radical polymerizations have been achieved by using methods that keep the propagating species dormant for most of the time.<sup>9-11</sup> By capping the propagating species reversibly, the concentration of free radicals is kept very low and, therefore, two free radicals will rarely react in a formal termination step of a free radical polymerization. At the same time this reduces the rate of propagation. A reduction in the rate of propagation allows for the rate of initiation to be greater than the rate of propagation. This will allow all of the polymer chains to start growing at the same time, similar to the living anionic systems. The two main techniques used to perform controlled free radical synthesis are nitroxide mediated stable free radical<sup>9-10</sup> and atom transfer radical polymerizations (ATRP).<sup>11</sup>

In the nitroxide mediated stable free radical synthesis, a stable free radical source such as 2,2,6,6-tetramethylpiperidinoxy (TEMPO) is used to reversibly cap the growing end of the free radical chain.<sup>9-10</sup> The polymerization is initiated with regular free radical initiators such as benzoyl peroxide. The initiator is usually a chemical that will undergo homolytic cleavage to create two free radical species. The free radical will then be able to react with the double bond present in the monomer to propagate the polymerization. The free radical may also react with TEMPO to form a labile covalent bond. Cleavage of the labile C-O bond between the TEMPO and the propagating species will result in the free radical species being regenerated and, thus, allows one or more monomers to be added, before the TEMPO caps the free radical again. In other words, there is an equilibrium established between the polymer being capped with TEMPO and the polymer

and TEMPO present as free radicals. This equilibrium should be present throughout the polymerization. Once all of the monomer has been polymerized, a second monomer can be added to create diblock copolymers.<sup>9,10</sup>

ATRP utilizes reversible redox reactions of a transition metal catalyst to add a halogen atom to the growing free radical chain.<sup>11</sup> The catalyst usually has a ligand associated with it and the ligand can play many roles, for example it may help to solubilize the catalyst in the reaction media. Initiators for ATRP must contain a halogen atom in order to be effective. The transition metal complex is oxidized in the redox reaction and accepts the halogen atom from the initiator, resulting in the initiator containing a free radical. The free radical species can then react with the double bond of the monomer to propagate the reaction. The transition metal complex, however, can also donate a halogen atom to the propagating free radical in the reverse reaction of the initial initiation. This “caps” the propagating species until another redox reaction occurs. This process will continue until all of the monomer has been consumed.<sup>11</sup>

In both living free radical methods the concentration of the free radicals is kept low by reversibly capping the propagating free radical. There is still the possibility of termination in the same manner as that for regular free radical reactions, and termination will happen to a certain extent, resulting in chains that are incapable of further reaction. There is also the possibility of termination of the polymerization by chain transfer, such as that in classical free radical polymerizations. Both of these result in a slight broadening of the molecular weight distribution in the polymers prepared by living free radical techniques.



#### 1.2.4 Polymer Characterization

Once the polymer has been synthesized it must be characterized. One factor that must be ascertained is whether the functionality of the side chains of the monomers is still present in the polymer. For example, during the anionic polymerization of *t*-BuA, one wants to make sure that the anion has attacked the vinylic moiety of the monomer and not the carboxy ester (more specifically the carbonyl group) of the side chain. The stereochemistry or tacticity of the polymers needs to be characterized on occasion<sup>26</sup>, however, it was not in this thesis. Two of the most important properties of polymers are the molecular weight and the distribution of the molecular weights.

There are a variety of techniques for the characterization of polymers. To determine composition and the presence of functional groups, spectroscopic techniques such as nuclear magnetic resonance (NMR), infrared (IR), and ultraviolet light (UV) are used. Below are some of the techniques used for polymer characterization.

##### 1.2.4.1 Spectroscopic Techniques

Using NMR, information, such as the relative number of repeat units and the nature of the functional group (i.e. a phenyl group, tertiary butyl group, etc, ...) of the side chains of the repeating units of a polymer can be obtained in the same manner as that for small molecules.<sup>27</sup> <sup>1</sup>H has been the most commonly used NMR technique for the studies in this thesis. Because the polymers are such big molecules containing many different chemical environments within the same molecule, the <sup>1</sup>H signals are generally broad but can still be resolved. NMR was used to determine the functionality of side chains within the diblock copolymer and was used to determine the relative amount of phenyl moieties (styrene repeat units) to *t*-butyl groups (*t*-BuA repeat units).

IR was also used to determine the different functional groups present in the polymer chain by the characteristic absorption of energies corresponding to transitions between different energy states (i.e. different vibrational modes).<sup>28</sup> Quantitatively, IR is also useful in determining the relative number of repeating units in copolymers; however, a calibration curve is needed to do so. In the studies in this thesis, IR was used mainly to confirm post polymerization modification (the removal of the *t*-butyl group to give acrylic acid).

If the polymer contains a functional group that is UV active, then UV spectroscopy is a very useful, and sensitive analytical tool, which can be used to identify and quantify the amount of monomer present in the polymer.<sup>29</sup> This method was not used in the studies within this thesis.

#### 1.2.4.2 Molecular Weight Measurements

A wide range of instruments is available to determine the different molecular weights of polymer samples. Depending on the property of the polymer that is being probed, different average molecular weights are determined. For example, methods that depend on the number of molecules of the polymer (concentration of the analyte) will give the number average, while those that depend on the size of the polymer chain will give the weight average molecular weight.<sup>12,13</sup> Methods that measure the colligative properties of a polymer solution, such as osmometry, can be used to measure  $M_n$ , while static light scattering can be used to measure  $M_w$ . Size exclusion chromatography, which separates the copolymer by the size of the coil in solution, was used for the determination of the molecular weights and molecular weight distributions in the studies presented in this thesis. Since size exclusion chromatography was used extensively (because of its

relative ease and the information it gives on the molecular weight distributions), it is described in detail below; however, as this thesis is based on molecular weights and molecular weight distributions, the theory behind osmometry and static light scattering is covered in Appendix B.

#### **1.2.4.3 Size Exclusion Chromatography**

One technique that gives information not only on the average molecular weight but also on the distribution of the molecular weights is size exclusion chromatography (SEC), otherwise known as gel permeation chromatography (GPC).<sup>30</sup> As the name suggests, the polymer sample is separated by size and then is detected as it is eluted. A dilute sample is injected into the system, which consists of a solvent reservoir, a solvent pump, an injection port, separation columns and a detector all connected together in series. A porous material (usually an inert substance such as polystyrene cross-linked by divinyl benzene) is packed within the columns; the pores are similar size to the size of the macromolecules that will be separated. There is a range of sizes of the pores in each column.<sup>30</sup> Smaller macromolecules will be able to enter more of the pores and thus will be retained longer than larger molecules, which are excluded from most of the pores. Once the separation has occurred a suitable instrument is used to detect the fractions of polymer as they elute from the column.

Detectors can be split into two categories; 1) mass concentration (such as the differential refractometer, UV adsorption or IR detector) and 2) molecular weight (such as SLS or an inline viscometer in series with a mass concentration detector).<sup>30</sup> The most common detector is the differential refractometer. The detector measures the refractive index difference between a sample of pure solvent and the solution eluting from the

columns. As the polymer is eluted, the refractive index of the solution will change with respect to that of the pure solvent and an electronic signal is produced by the detector. The intensity of the signal is related to the number of polymer particles that are present in the field of detection. The refractometer is connected to a computer that monitors the output of the detector over time. The software plots the intensity of the signal over time and, therefore, produces the molecular weight distribution of the polymer sample.<sup>30</sup>

Calibration of the instrument is needed before the molecular weight of the sample can be determined.<sup>30</sup> Polymer samples (usually polystyrene) of low PDI and known molecular weight are run through the instrument and the values corresponding to the peak maxima in the chromatogram are used for the calibration curve. A universal calibration curve<sup>31</sup> can be used to obtain the molecular weight of polymers that are not made of styrene, but since this thesis deals with polystyrene, the universal calibration curve will not be discussed. From running a mixture of standard samples a calibration of the molecular weight at each peak maximum vs. time can be created. A semi log plot yields a linear calibration curve. The range of molecular weights available on a given calibration curve is dependent on the distribution of the sizes of the pores in the column used. Different columns can be added in series to increase the range of sizes of pores within the system and, therefore, the range of detection. Once the calibration has been performed, the sample is run. At each data point along the sample peak the molecular weight,  $M_i$ , is known from the calibration curve and the time at which the sample component eluted. Since the intensity of the signal is related to the number of polymer molecules eluted,  $n_i$ , the height of the measured point from the baseline of the chromatogram is related to the number of polymer molecules of that given molecular weight. Using each point in the chromatogram in equations 1-1, 1-2, and 1-3 will give

the number, weight average molecular weights, and the polydispersity of the sample, respectively.

The refractometer gives a linear response over a wide range of concentrations with minimum band broadening.<sup>30</sup> While it can be used at high temperature, it is an instrument that is very temperature sensitive and care must be taken to make sure that the samples investigated are at the same temperature as the sample in the solvent cell. Also since, a change in the temperature of the polymer mixture will change the dimensions of the polymer coil in solution, the unknown sample solutions must be run at temperatures close to those when the calibration samples were run.<sup>30</sup>

Care must be taken when using diblock copolymers in SEC. Copolymers that have different refractive indices, short blocks, or repeat units that behave differently in the solvent will yield a sample molecular weight that is not necessarily the true molecular weight but rather an apparent molecular weight. For instance, if a copolymer of styrene and acrylic acid is run through the SEC, the apparent molecular weight may be smaller than that of the styrene block by itself. This could be due to the possible affinity of the acrylic acid for the column, which retards its elution.

Asymmetric, incompatible diblock copolymers, such as those used in the studies presented in this thesis may also present a different problem. The two incompatible blocks may not form one spherical coil in solution. Instead a dumbbell shape may result. The smaller PAA block will have a smaller volume than the larger styrene block (in the case of an asymmetric block copolymer) so the diblock copolymer will have an asymmetric dumbbell shape. The smaller PAA block may enter a pore from which the large polystyrene block would have been excluded from had it not been covalently

attached, and thus the elution time of the diblock would be longer than that of the homopolymer precursor.

For the diblock copolymers used in this thesis, a mixture of analytical techniques was used to obtain information on the molecular weight and molecular weight distribution. SEC of the first block (as a homopolymer) gave the molecular weight of the first block; then, another quantitative method such as NMR or IR spectroscopy was used on the diblock to obtain the relative ratio of the two blocks. Once the relative ratio of the two blocks and the true molecular weight of one block were known, the copolymer was considered as characterized.

#### **1.2.4.4 MALDI TOF**

More recently, matrix assisted laser desorption and ionization time of flight mass spectrometry (MALDI TOF) has been used to obtain the molecular weight and molecular weight distributions of block copolymers.<sup>23</sup> This instrument works well for low molecular weight samples and the molecular weight and molecular weight distribution have been obtained for the second block in diblock copolymers of low molecular weight. One encounters problems deconvoluting all of the data with higher molecular weight samples and multiple blocks. There are so many possibilities of combinations of molecular weights that it is very hard to treat all of the data. Other problems present with this method include choosing the correct matrix for the sample preparation. Due to the large size of the polymers used in this thesis, MALDI TOF was not very useful for determining block lengths, but it is mentioned as another way to obtain information on smaller block copolymers.

### 1.3 Self-Assembly

Often, in polymer chemistry, mixtures, or blends, of two or more polymers are used to combine a specific property of one polymer with that of another. For example, golf balls consist of a butadiene and ionomer blend. The elasticity of the butadiene (allowing the balls to be hit further) is thus combined with the strength of the ionomer (so the cover of the ball does not split).<sup>32</sup> For many polymer mixtures, the incompatibility of the two homopolymers in the absence of specific additives results in large-scale phase separation, and therefore this method fails frequently. Methods of polymer syntheses that allow for the sequential addition of two monomers afford diblock copolymers. Most diblock copolymers consist of two incompatible blocks. Since the incompatible blocks are covalently attached macro-phase separation cannot occur; however, within the material, microphase separation will occur.<sup>33</sup> The behaviour of such incompatible copolymers has been studied extensively in bulk, as well as, to a lesser extent, in solution.

#### 1.3.1 Block Copolymers in the Bulk

Diblock copolymers such as those made of polystyrene and polyisoprene have been studied because of the interest in their morphology and bulk properties<sup>34-43</sup>. Since high molecular weight polystyrene and polyisoprene are immiscible, the bulk will consist of two different phases. Different morphologies of the microphases have been observed, including spheres, hexagonally packed cylinders, bicontinuous structures and lamellae.<sup>37</sup> A phase diagram generated from a self-consistent field theory is shown in figure 1-5.<sup>38</sup> The phase diagram can be seen to be symmetric around  $f = 0.5$ . The transitions from lamellae – bicontinuous – hexagonally packed cylinders – spheres – disordered state are found when moving from  $f = 0.5$  to 0 or 1.

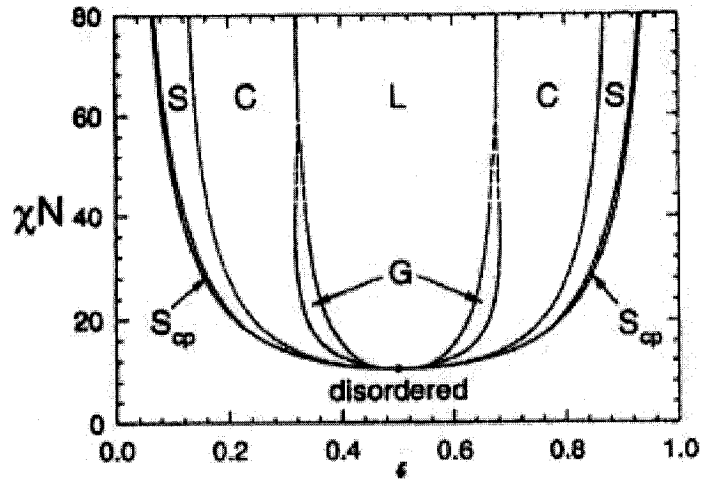


Figure 1-5: Theoretical phase diagram. S: Spheres, C: Cylinders, L: lamellae, G: Bicontinuous,  $S_{\phi}$ : close packed spheres.<sup>38</sup>

The morphology of diblock copolymers in the bulk phase depends on: 1) the overall degree of polymerization of the copolymer,  $N$ , 2) the Flory-Huggins parameter,  $\chi$ , which is a measure of the interaction between monomer A and B, and 3) the volume fraction of the components,  $f$ .<sup>44</sup> Since the entropic contribution is related to  $N$  and the enthalpic contribution to the free energy is related to  $\chi$ , the product  $N\chi$  is important. Three regions have been found depending on the  $N\chi$  product, i.e. the strong segregation, weak segregation and intermediate segregation. Leibler<sup>35</sup> and Semenov<sup>34</sup> have worked on mean field theories to describe the strong and weak segregation limits and have created phase diagrams. Their work shows that there is a competition between the interfacial energy and the loss of entropy associated with the stretching of the polymer chains. Matsen,<sup>38</sup> among other theorists, has worked with a self-consistent field theory for the intermediate segregation limit and, through his work, some morphologies that were thought to be stable in the strong and weak segregation limits were found not to be stable in the intermediate limit. Matsen's phase diagram is consistent with experimental



findings.<sup>45</sup> Earlier studies had suggested that the asymmetry in the diblock copolymer resulted in curvature of the interface, which caused the transitions in morphology. The curvature was thought to be due to a balance in the degree of stretching of each block.

In the past, studies of the dependence of the morphology on polydispersity have been made on polystyrene-*b*-polyisoprene mixtures in the bulk phase. Birshtein<sup>46</sup> has shown that the thermodynamic advantage of a mixture of polymers of different lengths grafted onto a planar surface ensures that a single lamella structure is thermodynamically stable. They also predicted that a morphological transition would result from mixing two copolymers, that made lamellar phases, resulting in the formation of cylindrical domains.<sup>47</sup> More recently, Court and Hashimoto have investigated the effect of chain organization on the stability of the microdomains.<sup>48</sup> Nguyen et al. have explored the effect of polydispersity of the ionic block on the size of the cores of inverse micelles of polystyrene-*b*-poly-4-vinylpyridinium methyl iodide and of polystyrene-*b*-poly(cesium methacrylate) in solution. They showed that the sizes of ionic microdomains varied linearly with the polydispersity of the ionic chain; however, if the copolymers micellized far from equilibrium, the polydispersity of the ionic group showed no effect on the sizes of the domains.<sup>22</sup> They did not see changes in morphology caused by polydispersity changes.

In solution, no studies had been published on the effect of the molecular weight distribution on the morphology of self-assembled copolymers. Following the earlier studies presented in this thesis,<sup>49,50</sup> Jain and Bates have used mixtures to artificially broaden the molecular weight distribution of poly(ethylene oxide)-*b*-poly(butadiene) copolymers in a strategy similar to the one used in these studies<sup>51</sup>. Their results show that

the average core composition, and the copolymer composition are important factors for their mixtures.

### **1.3.2 Micellization of Block Copolymers in Solution**

In solution, the incompatibility of the two blocks frequently remains. This is especially true of amphiphilic block copolymers that consist of at least one block that is hydrophobic and one or more that is hydrophilic. Therefore, in aqueous solution, the hydrophobic block(s) will drive the aggregation of the polymer chains. In the simplest case, the resulting structure has been shown to be one of a spherical micelle-like aggregate with the hydrophobic chains constituting the interior of the core and the hydrophilic chains providing a solvating shell around the core of the aggregate.<sup>52</sup> The behaviour of the amphiphilic copolymers is somewhat similar to that of small molecule surfactants in aqueous solution. The different physical properties of the copolymer result in different properties of the resulting micelles. As a simple example; in aqueous solutions, micelles made from copolymers with a long polystyrene block have much larger cores than those made from small molecule surfactants, such as sodium dodecyl sulfate. There is also more variability in the sizes of the hydrophobic or hydrophilic regions of the diblock copolymer than in those of the small molecule surfactants. Through control of the polymerization, diblock copolymers can be made with varying ratios of the insoluble to soluble block lengths. Both symmetric (both blocks are of the same length) and asymmetric (one block is longer than the other) block copolymers can be made. All of these types of diblock copolymers can aggregate in solution. In the case of asymmetric amphiphilic diblocks with longer hydrophilic blocks, the resulting star micelles, in aqueous solution, have large coronae and small cores. In the opposite case,

i.e. asymmetric diblock copolymers with longer hydrophobic blocks, aggregates are formed with relatively large cores and small coronae, called “crew cut” micelles.<sup>52</sup> While the star micelles are also of interest, this thesis concentrates on the crew cut aggregates. Many groups are working in the field of block copolymers in solution<sup>45, 53-71</sup> and many different morphologies of the crew cut aggregates in aqueous solution have been observed. Figure 1-6 displays some of the observed morphologies. Simple architectures, such as spherical micelles, rods, bilayers, vesicles and mixtures of two or more morphologies are readily observed by tuning the solution conditions.<sup>53, 55-57</sup> Other more complex morphologies, such as large compound micelles, large compound vesicles, hexagonally packed hollow hoops and branched rods have also been observed.<sup>53, 55-57</sup>

Before discussing how the copolymer chains aggregate to form the more complex morphologies, a brief summary of the aggregation process of single chains into a simple spherical architecture is presented. The critical micelle concentration is discussed first, followed by discussions of the thermodynamic considerations of the morphological transitions, factors that can be used to control the morphology of the aggregates and finally the kinetics of the transitions.

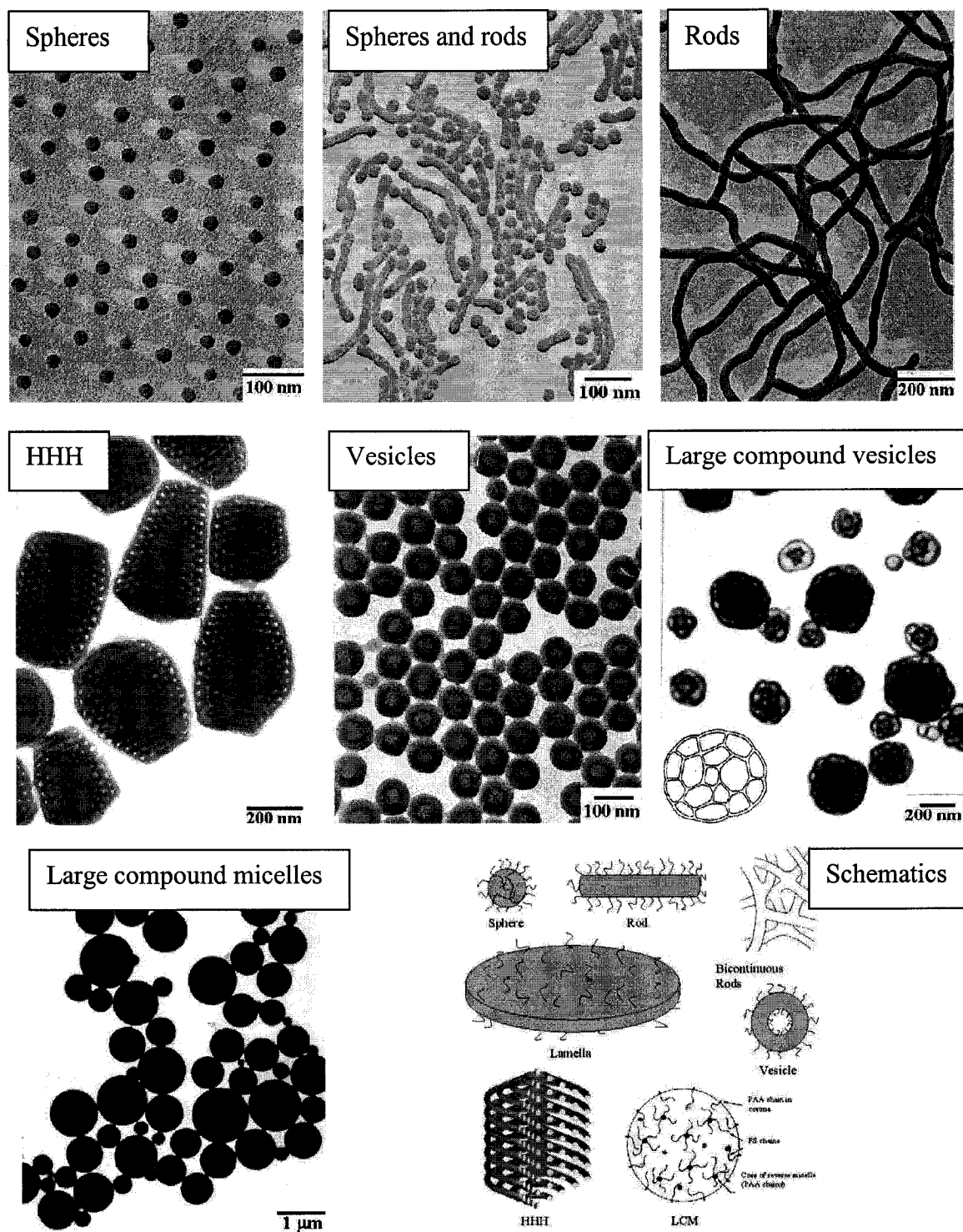


Figure 1-6: Morphologies of crew-cut aggregates of amphiphilic diblock copolymers in solution. (HHH: Hexagonally packed hollow hoops)<sup>55</sup>

### 1.3.2.1 Critical Micelle Concentration

Aggregation of diblock copolymer chains in solution occurs only above a certain concentration known as the critical micelle concentration (cmc). At concentrations below the cmc, the single chains, called unimers, are dissolved in the solution. The nature of the copolymer, relative block length and the overall molecular weight all determine the cmc of a block copolymer in a given solvent.<sup>72</sup> The difference in the  $\chi$  parameters between each block and the solvent also play important roles in determining the cmc.

As an example of how block length can affect the cmc, let us consider the insoluble block. In the case of a homopolymer, the higher the molecular weight the lower the limit of solubility of the polymer due to the presence of more insoluble repeat units within the polymer chain. The interaction between the repeat units and the solvent is increased because of the increase in the number of repeat units. Since the increased interaction is even more unfavourable, at some critical point, the polymer precipitates. An analogous effect is seen in diblock copolymers, where the higher the molecular weight of the insoluble block (keeping the soluble block fixed), the lower the cmc. The difference is the insoluble block is covalently attached to the soluble block, so micellization occurs instead of precipitation.<sup>72</sup>

### 1.3.2.2 Thermodynamic Considerations

The micellization process, and the resulting morphology are frequently driven by thermodynamics, and in some cases thermodynamic equilibrium can be reached. The kinetics of chain exchange in the system may get in the way of obtaining the thermodynamically most stable morphology. So, while the driving force is

thermodynamic, the structure that is obtained may not be the thermodynamically most stable structure due to the kinetics.<sup>55</sup> Therefore, the way the aggregates are made may affect whether or not the system reaches equilibrium. The two most used methods to form the block copolymer aggregates are the direct dissolution method or the water addition method.<sup>55</sup> In the direct dissolution method the polymers can be directly dissolved into a mixture of a common solvent and a solvent selective for one block (the selective solvent). On the other hand, the copolymer can be dissolved in the common solvent and then the selective solvent is added (water addition method). The water addition method was used extensively in the research presented in this thesis. The addition of the selective solvent decreases the solvent quality for the insoluble block and causes the microphase separation, or the aggregation of chains into concentrated domains within the solvent. This can result in the collapse of a single chain or the formation of multi-chain micelles.<sup>65</sup> The whole process occurs as the system tries to achieve its lowest possible free energy state (i.e. lowest value of the Gibbs free energy,  $G$ ).

When dealing with amphiphilic block copolymers, dioxane, DMF, or THF can usually be used as common solvents and water as a selective solvent. As water is added to the copolymer solution, the polymer-solvent parameter,  $\chi$ , changes for both blocks. At a given concentration of water (the critical water concentration,  $cwc$ ) the copolymer will start to aggregate resulting in the formation of phase-separated regions. A further increase in the water concentration will increase the interfacial energy between the phases of the system. The system will react by decreasing the interfacial surface by increasing in radius, with a coupled decrease in the number of micelles. The rate of single chain exchange of the micelles will determine if the system reaches equilibrium. Due to the

large size of the polymer chains, it will take time for chain exchange between two micelles. For core-forming blocks such as polystyrene, the situation is further complicated because of the glass transition temperature,  $T_g$ . At room temperature, PS is below its  $T_g$ . At low water contents there is a lot of common solvent present in the core, which acts as a plasticizer, and therefore lowers the  $T_g$  of the PS. The common solvent will partition between the core and the solution. The addition of water to the solution will result in the concentration of the common solvent decreasing. Consequently, some of the common solvent will leave the core. As the amount of solvent in the core decreases, the  $T_g$  of the polystyrene will increase. Once the  $T_g$  is above room temperature, the core will become glassy and freeze its morphology and size. Once this has happened, the system freezes in and thermodynamic considerations are no longer operative. It has been found that the polymer chains within the aggregates are dynamic for water concentrations up to ~12% for DMF, but ~50% for THF or dioxane.<sup>73</sup>

For systems that are still dynamic, the standard thermodynamic quantities are measurable. In order to determine the entropy, enthalpy and free energy of the micelle system the cmc has to be measured. A closed association model (assuming an equilibrium between the unimers in solution and the aggregates) is assumed for such systems and the standard Gibbs free energy of micellization has been calculated by<sup>74</sup>

$$\Delta G^0 = RT \ln (cmc) \quad (1-22)$$

The temperature dependence of the cmc can be used to determine the standard enthalpy of micellization,  $\Delta H^0$ , using the Gibbs-Helmholtz equation<sup>75</sup>

$$\Delta H^0 = R \frac{d \ln (cmc)}{d (T^{-1})}. \quad (1-23)$$

Finally the standard entropy of micellization,  $\Delta S^0$ , can be determined using<sup>75</sup>

$$\Delta G^0 = \Delta H^0 - T\Delta S^0. \quad (1-24)$$

Another variable that can be more easily measured is the critical micelle temperature (cmT). Using an instrument, such as SLS, to measure the turbidity of the solution, while keeping the copolymer concentration constant and changing the temperature of the micelle solution, the specific temperature at which micellization occurs can be found. Once the cmT is found it can be used in<sup>75</sup>

$$\frac{d \ln( cmc )}{d (T^{-1})} = \frac{d \ln c}{d (cmT^{-1})}. \quad (1-25)$$

Equation 1-25 can be substituted into Equation 1-23 to achieve

$$\Delta H^0 = R \frac{d \ln c}{d (cmc^{-1})}. \quad (1-26)$$

The standard free enthalpy of micellization can be determined by finding the cmT or cmc whichever is more convenient, experimentally. However, it should be noted that Equation 1-25 only holds for linear block copolymers.<sup>75</sup>

The enthalpy has been found to be solely responsible for the micellization of block copolymers such as PS-*b*-Poly(ethylene/propylene), and PS-*b*-polyisoprene in organic solvents.<sup>76</sup> On the other hand, the entropy was found to drive the micellization of amphiphilic Pluronic copolymers, poly(ethylene oxide)-*b*-poly(propylene oxide)-*b*-poly(ethylene oxide), in aqueous solution.<sup>77</sup>

Since the method of preparation of the aggregates used in this thesis involves both organic solvents and aqueous solutions, it is interesting to know whether the process is enthalpically driven, similar to the PS-*b*-polyisoprene in organic solvents, or entropically driven, like the Pluronics in water. Shen et al measured the thermodynamic properties for PS-*b*-PAA micelles in N,N-dimethylformamide (DMF) and water mixtures under



different conditions.<sup>74</sup> They used static light scattering and the equations above to determine thermodynamic functions incorporating the dependence of these quantities ( $\Delta G$ ,  $\Delta H$ ,  $\Delta S$ ) on water content, block length and salt concentration at different DMF/water mixtures. They found, for all of the copolymers that they studied, that at low water contents all three thermodynamic parameters ( $\Delta G$ ,  $\Delta H$ ,  $\Delta S$ ) are negative. This shows that the enthalpy has to be more influential than the entropy during the micellization process.<sup>74-75</sup> However, Shen et al also show that one can make the process entropically driven by increasing the water content or increasing the block length of the insoluble block, which forms the micelle core (polystyrene).<sup>74</sup> At first, one might think that the entropy would decrease as more single chains aggregate (i.e. form a more ordered structure); however, the unimers in solutions containing water will have a hydrophobic hydration associated with them. The water molecules are ordered around the hydrophobic tail of the copolymer. When the unimer joins an aggregate, the order in the structure of the water molecules is broken, thereby increasing the entropy. The longer the hydrophobic chain, the more water molecules will be ordered around the hydrophobic block of the unimer. Therefore, more water molecules will be released when a longer chain aggregates and there will be a bigger increase in the entropy.

The morphology of the micelles is also determined by the thermodynamic parameters. While there are many parameters that enter into the micellization process, (such as the entropy associated with the junction point of the diblock copolymer being at the interface of the core and the corona of the micelle, or the entropy increase by the breaking of the order of the water molecules surrounding the hydrophobic block) the three which determine the morphology are: 1) the decrease in entropy due to core-chain stretching, 2) interfacial energy, and 3) inter-coronal chain interactions.<sup>78</sup>

As an example of how these three parameters are related, let us resume the discussion (from section 1.3.2.1) of the spherical aggregates formed at water contents just above the critical water content (cwc). The cwc is the point at which enough selective solvent has been added to the polymer solution to induce aggregation. Further addition of water will result in an increase of the interfacial energy. In response, the system will act to decrease the total interfacial area. As mentioned above (in section 1.3.2.1), to decrease the surface area, the number of particles is decreased but the particle size is increased. Each particle thus contains more chains. The aggregation of more chains results in a stronger repulsion among the corona chains and an increase in the core size. A bigger core, in turn, means that the average degree of core block stretching increases. The increased stretching is not favoured entropically. The free energy of the system will increase. At some critical point the aggregate will change shape from a sphere to a rod. The rod will have a smaller diameter than the sphere and, therefore, the degree of stretching of the chains will be lower in the rod than in the large sphere.<sup>55</sup>

The three contributions to the free energy are equally important when dealing with morphology changes. The overall free energy must be lower (the sum of all three contributions) in the new morphology for the transition to occur.

### **1.3.2.3 Factors Affecting Morphologies of Block Copolymer Aggregates in Solution**

The specific morphology of block copolymer aggregates is determined by a balance of three contributions to the free energy of the system; chain stretching in the core, the interfacial energy, and repulsion among corona chains.<sup>78</sup> Factors that affect the balance of these three forces will affect the morphology of the resulting aggregates. To date, a number of factors have been shown to effect morphology, including the relative

block lengths of the copolymer<sup>79</sup>, the concentration of the polymer<sup>80</sup>, the composition and nature of the solvent system<sup>81</sup>, additives, and temperature<sup>82</sup>. The following explains how these factors can be used to control the aggregate morphology.

For PS-*b*-PAA copolymers in solution, where the corona consists of PAA, additives such as salts,<sup>83-85</sup> acids,<sup>83-87</sup> bases,<sup>83-85</sup> or homopolymer,<sup>79,87</sup> can affect the morphology of the self-assembled copolymer. Salts, acids and bases all act to change the effective charge of the corona chains and, therefore, the repulsion among corona chains. Adding salts causes electrostatic shielding in the corona while adding acids protonates (and thus also shields the corona charges) the corona; both of these reduce the repulsion among corona chains and allow more chains to assemble in the same aggregate. The increase in the number of chains in the core increases its size and, therefore, the degree of stretching. A change in morphology from sphere to rod is favoured, and, as still more salt or acid is added, the rod changes to a vesicle. Bases, on the other hand, deprotonate the corona, causing increased repulsion in the corona chains, leading to a lower aggregation number and, therefore, less stretching in the core. The addition of bases has the opposite effect of adding acids or salts.

Addition of even 5% (w/w) homopolystyrene to aggregates of PS-*b*-PAA has been shown to increase the size of spherical micelles and cause a morphological change from vesicles or rods to spheres.<sup>79</sup> As the aggregate is forming, the homopolymer is incorporated into the core of the aggregate and can fill the centre of the micelle. Therefore, the chains of the hydrophobic block will not have to stretch as much as in the absence of homopolymer. While the entropy of localization of the homopolymer in the middle of the core will be negative, there is not as much of a loss in entropy due to core chain stretching and, therefore, the addition of more diblock copolymer chains to the

aggregate does not change the free energy of the system enough to cause a change in morphology. The homopolymer should have a lower degree of polymerization than the hydrophobic block, so it does not precipitate before the onset of micellization, otherwise it might not be incorporated into the micelle.

The addition of small molecule surfactants to solutions of block copolymer aggregates can also affect the resulting morphology. Burke et al showed that addition of sodium dodecyl sulfate (SDS) to solutions of PS-*b*-PAA caused morphological changes at lower water contents than they would have occurred in the absence of the surfactant.<sup>88</sup> The SDS was found to interact with the aggregates in two ways: the hydrophobic tails can penetrate into the core of the micelle, which increases the distance between PAA chains, and, also, the counter ions screen the electrostatic charges of the partially ionized PAA. Screening of the PAA chains creates less repulsion among the corona chains. This allows for more chains to aggregate. Once more chains have aggregated, the core becomes larger and the corona repulsions increase. The core chain stretching will dominate and the resulting morphological transition will occur, without an increase in amount of water present.

The relative lengths of the corona and core forming blocks of the copolymer can influence the morphology of the resulting aggregates in solution.<sup>79</sup> For spherical micelles made from PS-*b*-PAA copolymers, the degree of stretching has been found to scale as  $N_{PS}^{-0.1} N_{PAA}^{-0.15}$ , where  $N_{PS}$  and  $N_{PAA}$  are the respective degrees of polymerization of the PS and the PAA blocks. Therefore, it can be seen that increasing either block will lead to a decrease in the degree of stretching. The degree of stretching has also been found to change when the aggregate changes morphology. For example, in PS-*b*-PAA systems,

spherical micelles were found to have a higher degree of stretching than that of rods, which, in turn, had a higher degree of core chain stretching than vesicles.

The area per corona chain,  $A_c$ , is also affected by the length of the two blocks and can be related by;<sup>79</sup>

$$A_c = N_{PS}^{0.6} N_{PAA}^{0.15} \quad (1-27)$$

Since intercorona repulsions are inversely proportional to  $A_c$ , increasing either block will result in a lowering of the intercorona repulsions. As an example consider the core block. Increasing the PS block length, with constant PAA length, will result in a bigger core due to the longer core chains. Since the core radius has increased and the corona chains have not, the surface area per corona chain will have increased. The increase in surface area per corona chain leads to less repulsion. Because there is less repulsion, more chains can aggregate, causing a bigger increase in the core size. As more chains aggregate the degree of stretching of the core chains increases. This is not favoured entropically, and, if the conditions are proper, a transition in morphology will occur.

The concentration of the precipitant<sup>80</sup> (i.e. water) and of the copolymer<sup>80</sup> are also morphogenic factors. Phase diagrams have shown that as the water content increases, the morphologies change from spheres, to rods, followed by lamellae or vesicles. This occurs because, with increasing water content, the solvent becomes worse for the core block; therefore, there is a change in interfacial energy, leading to more extensive aggregation. As in the case of the increased aggregation by addition of bases, the volume of the core increases while at the same time the repulsion of the corona chains increases. These two forces will oppose one another; however, the core stretching becomes more important and eventually, as more water is added, a morphology change occurs from sphere to rod.

The aggregation number ( $N_{\text{agg}}$ ) of chains has been found to be proportional to the concentration of the polymer; therefore, as the concentration of the polymer increases  $N_{\text{agg}}$  increases, causing higher repulsion in the corona and a higher degree of stretching in the core. Once again, the transition from sphere, to rod, and eventually to vesicle is observed with increasing polymer concentration.

The common solvent used<sup>81</sup> to dissolve the copolymers can affect the resulting morphology. Changing the polymer-solvent parameter by changing the solvent results in the copolymer chains having different relative coil dimensions. Also the rate of change of the coil dimensions with an increase in the water concentration. An example of the common solvent effect was seen with PS<sub>420</sub>-*b*-PAA<sub>26</sub>, which gave spheres in DMF, vesicles in dioxane, and large compound micelles in THF<sup>81</sup>.

Temperature<sup>82</sup> can also cause changes in morphology. Much like adding water to an aggregate system, changing the temperature of the system also changes the polymer-solvent parameter. Studies have been performed using low molecular weight alcohols (i.e. methanol, ethanol, 2-propanol, and *n*-butanol). The systems were heated to temperatures greater than 140°C under increased pressure. As the temperature increases the solubility of the hydrophobic block increases; this leads to well-defined aggregates at a given temperature. As the temperature is cooled back down, the morphologies freeze. As an example of temperature effects, PS<sub>386</sub>-*b*-PAA<sub>79</sub> produced spherical micelles when it was heated in butanol to 160°C but produced a mixture of spheres and vesicles when heated to only 115°C.<sup>82</sup>

### 1.3.2.4 Kinetics of Morphological Transitions

While this thesis does not deal with the kinetic aspects of the systems involved, it is important to know the kinetic aspects to make sure that the experimental procedures result in aggregates that were in thermodynamic equilibrium prior to being kinetically trapped. The trapping procedure has to be done under conditions where the kinetics are slow enough so that further changes in morphology do not occur. While the specific morphology of a copolymer system has been found to be dependent on thermodynamics, the rate of a transition between morphologies is dependent on the kinetics of the process, under a given set of conditions. Transition kinetics are believed to be dependent on the position of the system with respect to the location of the phase boundaries and the degree of plasticization of the core block.<sup>89</sup> If the dynamics are too slow, an equilibrium morphology will not be reached.

The kinetics of the sphere to rod, rod to sphere<sup>89</sup>, rod to vesicle<sup>90</sup>, and vesicle to rod<sup>91</sup> transitions of PS<sub>310</sub>-*b*-PAA<sub>52</sub> have been studied. This was done by starting at a location close to a morphological boundary in the phase diagram of the copolymer, and then adding water (or dioxane) to make the system cross the morphology boundary. The studies have shown that the rate of the morphological transition depends on the initial solvent composition, the polymer concentration and the size of the solvent jump.<sup>89-91</sup> In general as the initial water content increases, the relaxation time,  $\tau$ , of the transition increases (i.e. a longer time is needed to reach equilibrium). An increase in the polymer concentration was found to decrease the relaxation time for the sphere-to-rod and rod-to-sphere transitions, while it increased that of the rod-to-vesicle and vesicle-to-rod transitions. The magnitude of the water jump was found to have little influence on the

kinetics of the transition from rods to vesicles,<sup>90</sup> and vesicles to rods<sup>91</sup> but did influence the kinetics of the sphere-to-rod transition<sup>89</sup>. It has also been discovered that if the water jump is too large (i.e. greater than 2% H<sub>2</sub>O w/w) then the initial morphology may be kinetically frozen. The relaxation rates of the sphere-to-rod transition, for systems that were close to the sphere-rod boundary have been found to be of the same order of magnitude to those of the rod-to-sphere transition ( $\tau \sim 20\text{-}30$  minutes).<sup>89</sup> This is in contrast to the transition from rods to vesicles, for samples close to the rod-vesicle boundary ( $\tau \sim 5\text{-}15$  seconds), which has been found to be much slower than the transition from vesicles to rods ( $\tau \sim 10\text{-}15$  minutes).<sup>90,91</sup> Conceivably, the slower kinetics for the vesicle to rod transition could be due to the starting solvent composition. The vesicle to rod transition had to start at higher water contents where the core would not have contained as much plasticizer as it would for lower water contents. The mechanisms of the transitions were also determined by the coupled analysis of the kinetic data and TEM pictures.

Studies of the kinetics of vesicle fusion have also been reported. While not dealing with morphological changes, the change in the size of vesicles as water is added also takes time. Since the initial water content is higher, the dynamics of chain exchange may be slower; however, Choucair et al showed that the relaxation time for the increase in vesicle size with an increase in water content is of the order of 30 ~ 60 seconds.<sup>92</sup>

In the above studies, the relaxation rates are found to be on the order of minutes; these are important results for the studies presented in this thesis since they provide a lower limit on the times required for the polymer solutions to go through morphological changes. The conditions used in the research presented in this thesis are similar to those used in the kinetic studies discussed above. Since the relaxation times have been found to



be on the order of minutes and the samples in the present studies have been allowed to stir for hours, the present systems should be at or near equilibrium.

### **1.3.2.5 Aggregate Characterization**

There are many ways to characterize the aggregates formed by the diblock copolymers. Sedimentation velocity<sup>93</sup>, intrinsic viscosity<sup>94</sup>, and SEC<sup>95</sup> have been used by others to measure properties such as the mass ratio of unimers to micelles, among other thermodynamic and hydrodynamic properties. Dynamics and morphologies of micelles, especially in thin films, have been studied using complex techniques of small angle X-ray<sup>96-98</sup> and neutron<sup>99-101</sup> scattering. In this thesis transmission electron microscopy (TEM) and light scattering were used extensively for characterization of the morphology and size of the block copolymer aggregates.

The principles of TEM are similar to those of light microscopy except that TEM uses the wave properties of electrons instead of light to produce an image.<sup>102</sup> The electron beam is passed through the specimen (solid micelles on a copper grid) and then focused by the objective lens (which consists of a magnet) into a magnified intermediate image. A projector lens further enlarges the intermediate image into the final image that is displayed on a fluorescent screen. The final image can also be displayed on a photographic film, or captured by a digital camera, allowing for easy picture taking of the magnified image.

Figure 1-7 shows a schematic of a two-stage transmission electron microscope. The electron lenses used in the transmission electron microscope can be made to magnify 50–200 times and a simple two-stage TEM would have a magnification of 10,000 times

allowing resolution down to 5nm.<sup>102</sup> Since micelle diameters are 10-100 nm they can easily be resolved in the TEM image.

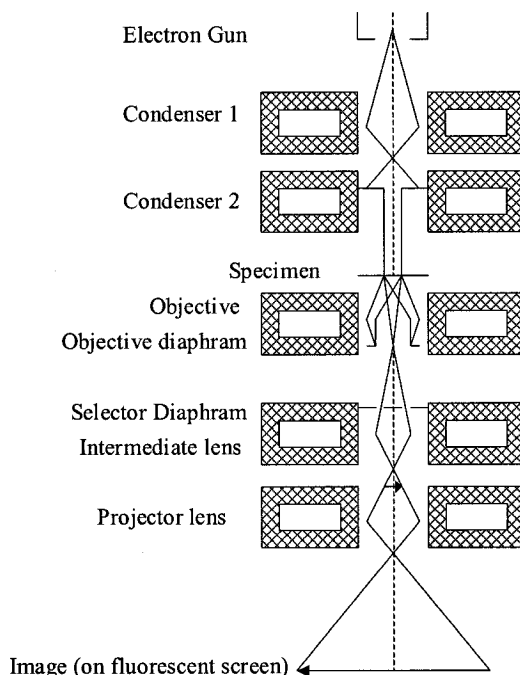


Figure 1-7: Schematic of 2-stage transmission electron microscope.<sup>102</sup>

Static light scattering methods allow the determination of radius of gyration and the second virial coefficient of the polymer chains.<sup>103</sup> As well, the molecular weight of the copolymer chains and the size and molecular weight of the aggregates formed by self-assembly can be determined. Dividing the measured molecular weight of the aggregate by the molecular weight of the single chain gives the aggregation number. It should be remembered; however, that in the case of diblock copolymers, the real molecular weight is not obtained by light scattering, but rather an approximate average is found.<sup>79</sup> Since the molecular weights are approximate, the aggregation number is also an approximate number when obtained in this method. Observing the scattering of light by the particles over time can be used to obtain physical properties of the particles such as the hydrodynamic radius, the polydispersity of the particle size and the diffusion coefficient.

This technique, known as dynamic light scattering,<sup>104</sup> relies on the same scattering principles as that of static light scattering, described in Appendix B. The difference is the scattered light is measured as a function of time. The fluctuations in the intensity of the scattered light are a result of changes in the number of scattering particles within the laser beam. The movement of the particles in the solution is due to Brownian motion. For a system consisting of small, identical, spherical, non-interacting particles, the normalized electric field time-correlation function,  $g^{(1)}(t)$ , can be expressed as;<sup>104</sup>

$$g^{(1)}(t) = A + Be^{-\Gamma t} = A + Be^{-Dq^2 t}. \quad (1-28)$$

A and B are constants dependent on the experimental set up,  $q$  is the scattering vector ( $q = 4\pi/\lambda \sin(\theta/2)$ ),  $D$  is the translational diffusion coefficient,  $\Gamma$  is the decay rate, and  $\theta$  is the angle of detection. Since the decay rate can be determined by an appropriate analysis, the diffusion constant, which is related to the hydrodynamic radius, can be evaluated directly from the correlation function.

For ideal systems, (i.e. spherical, identical, non-interacting particles) the correlation function is straightforward and can be expressed as a single exponential function. For real systems, such as those found within the studies presented in this thesis, there is polydispersity within the size of the aggregates, and the particles may not be totally spherical. Therefore, the correlation function is a sum of two or more exponential decay functions, and a more sophisticated algorithm such as CONTIN must be used. Each particle has its own diffusion coefficient,  $D_i$ . The correlation function is thus evaluated as a sum of exponentials;<sup>104</sup>

$$g^{(1)}(t) = A + B \sum [N_i a_i^2 P_i e^{-D_i q^2 t}] \quad (1-29)$$

$N_i$  is the number,  $a_i$  is the polarizability and  $P_i$  is the form factor for each particle.

The measured correlation function from the intensity of the scattered light is the actually unnormalized intensity time correlation function  $G^{(2)}(t)$ . Through the Siegert relationship,  $g^{(1)}(t)$  can be determined by  $G^{(2)}(t)$ :

$$G^{(2)}(t) = B \cdot \left( 1 + f^2 \left| g^{(1)}(t) \right|^2 \right) \quad (1-30)$$

The CONTIN algorithm attempts to obtain an inverse Laplace transform of the correlation function to determine the different Gamma values that go into the correlation function. This is similar to the way modern NMR uses Fourier transforms to determine the frequencies that go into an FID.

Since the particles are in solution, the diffusion coefficient is concentration dependent.

$$D = D_0(1 + k_D c + \dots) \quad (1-31)$$

where  $D_0$  is the diffusion coefficient at infinite dilution and  $k_D$  is a constant that takes into account the temperature dependent polymer-solvent interactions of the system.

$$k_D = 2A_2M - k_f(N_a V/M) = 2A_2M - k_f v \quad (1-32)$$

where  $A_2$  is the second virial coefficient,  $M$  is the molecular weight,  $V$  is the volume of the particle,  $v$  is the partial specific volume and  $k_f$  is the proportionality constant of the concentration dependence of the friction coefficient.

$D_0$  can be related to the hydrodynamic radius through the Stokes-Einstein relation;<sup>104</sup>

$$R_h = kT/6\pi\eta D_0 \quad (1-33)$$

where  $k$  is the Boltzman constant,  $T$  is the absolute temperature, and  $\eta$  is the solvent viscosity. For diblock copolymers  $R_h$  and  $D_0$  are apparent values due to the presence of two blocks. They are closer to real values if the polydispersity of the system is low and

both blocks have a high refractive index change with concentration ( $dn/dc$ ). A method similar to the Zimm plot used in SLS can be used for polydisperse samples.<sup>105</sup>

#### 1.4 Summary of Purpose and Scope

The purpose of the research presented in this thesis is to see whether block polydispersity is a parameter that can control the morphology of block copolymer aggregates in solution. With new polymerization techniques<sup>9-11</sup> giving rise to the production of block copolymers with varying polydispersities, the effect of polydispersity on self-assembly needs to be explored.

An extended series of studies was performed to elucidate the effect of polydispersity on the self-assembly of block copolymer aggregates in solution. Because of the major differences (i.e. in the solubility) of the two blocks of the amphiphilic diblock copolymers, the effect of each block was studied separately. This was not a simple task. One cannot easily control a polymerization to obtain both a desired polydispersity and a selected average molecular weight at will. Anionic polymerizations will give polymers of low polydispersity<sup>21</sup> and there will be a slight variation depending on the experimental conditions of the day (i.e. the rate of stirring in the flask), some of which are very hard to control (i.e. the humidity in the laboratory). However, anionic synthesis can be used to produce a series PS-*b*-Pt-BuA copolymers with identical PS blocks and different Pt-BuA block lengths. Each copolymer has a narrow molecular weight distribution, but mixing the copolymers allows one to artificially increase the PDI of the corona block. Because of the nature of anionic synthesis, a series of polymers with an identical Pt-BuA block and increasing PS block length in one batch is not possible. To increase the PDI of the core-forming block, separate syntheses needed to be performed,

and by careful control of the ratio of initiator to styrene to *t*-BuA, the *Pt*-BuA blocks were all of a similar length (Fortunately, the Eisenberg lab contains a library of samples from past members of the group and enough samples were present to perform the self-assembly experiments without many extra polymerizations). These polymers could be mixed to artificially increase the PS PDI with minimal change in the PAA block length and polydispersity.

Due to the recent interest in vesicles, for their potential use in fields such as drug delivery,<sup>57</sup> the first experiments, presented in Chapter 2, explored the effect of the corona block PDI on the sizes of vesicles. The general trend was a decrease in the size of the vesicle as the PAA PDI increased. During this study, at high PAA PDI, spherical micelles were found under conditions where they were not found for narrow distribution samples. This morphology change prompted further investigation into the effects of PAA PDI on other morphologies.

In Chapter 3 a partial phase diagram of morphologies as a function of water content and PAA PDI is presented. The phase boundary between vesicles and lower order structures such as rods and spherical micelles was found to move to lower water contents with an increase in the PAA PDI.

In the studies discussed in both Chapters 2 and 3, mixtures of copolymers were used to artificially broaden the molecular weight distribution. This resulted in distributions that were bi- or trimodal. Chapter 4 presents results from a study, which addressed the issue of multimodal distributions. The polymodal nature of the molecular weight distribution was found to be very important to the PAA PDI effects described in chapters 2 and 3. Chapter 4 also reports on the studies dealing with the molecular weight distribution effect and its relation to the average relative molecular weights of the blocks

in the copolymer. It was found that the PAA molecular weight distribution effect is only observed when the average PAA block length was below a certain length relative to that of the PS block.

Chapter 5 completes the study of the effect of molecular weight distributions by reporting the findings of the study involving changing the core block polydispersity. Increasing the PS PDI was found to have the opposite effect of increasing the PAA PDI. At a given water content that resulted in the formation of vesicles in the low PS PDI sample, only spherical micelles were found at high PS PDI.

The final Chapter summarizes the results of the studies of the effect of the molecular weight distribution on aggregates of PS-*b*-PAA in solution. Through the presentation of this research it is hoped that the reader will obtain new insights into the self-assembly of diblock copolymers, and a new way to control morphologies. Also, these studies may give an idea of how copolymers made by syntheses that result in larger molecular weight distributions will behave in solution.

## REFERENCES

1. Stix, G. *Scientific American* **2001**, 285, 32-37.
2. Lim Soo, P.; Luo, L.; Maysinger, D.; Eisenberg, A. *Langmuir* **2002**, 18, 9996-10004.
3. Gebhart, C. L.; Kabanov, A. V. *Journal of Controlled Release* **2001**, 73, 401-416.
4. Harada-Shiba, M.; Yamauchi, K.; Harada, A.; Takamisawa, I.; Shimokado, K.; Kataoka, K. *Gene Therapy* **2002**, 9, 407-414.
5. Wang, G.; Henselwood, F.; Liu, G. *Langmuir* **1998**, 14, 1554-1559.

6. Henselwood, F.; Wang, G.; Liu, G. *J. Appl. Polym. Sci.* **1998**, *70*, 397-408.
7. Wang, Wang, *J. Am. Chem. Soc.* **2000**, *122*, 6855.
8. Bronstein, L. M.; Chernyshov, D.M.; Karlinsey, R.; Zwanziger, J.W.; Matveeva, V.G.; Sulman, E.M.; Demidenko, G.N.; Hentze, H.-P.; Antonietti, M. *Chemistry of Materials* **2003**, *15*, 2623-2631.
9. Georges, M.K; Hamer, G.K; Listigovers, N.A. *Macromolecules* **1998**, *31*, 9087-9089.
10. Barclay, G. G.; Hawker, C. J.; Ito, H.; Orellana, A.; Malenfant, P. R. L.; Sinta, R. F. *Macromolecules* **1998**, *31*, 1024-1031.
11. Matyjaszewski, K.; Xia, J. *Chem. Rev.* **2001**, *101*, 2921-2990.
12. Allcock, H.R.; Lampe, F.W. *Contemporary Polymer Chemistry* 2<sup>nd</sup> ed.; pp. 3, Prentice Hall Inc, Toronto, **1990**.
13. Cowie, J.M.G. *Polymers: Chemistry & Physics of Modern Materials* 2<sup>nd</sup> ed.; pp. 8-10, Blackie Academic & Professional, New York, **1996**.
14. Moran, L.; Scrimgeour, K.G.; Horton, H.R.; Ochs, R.S.; Rawn, J.D. *Biochemistry* Chapter 25, Prentice Hall Canada Inc., Toronto, **1994**.
15. Boor, J. Jr *Ziegler-Natta catalysts and polymerizations* Academic Press, New York, **1978**.
16. Allcock, H.R.; Lampe, F.W. *Contemporary Polymer Chemistry* 2<sup>nd</sup> ed.; pp. 64-91, Prentice Hall Inc, Toronto, **1990**.
17. Grubbs, R.H.; Khosravi, E. *Materials Science and Technology* **1999**, *20* (Synthesis of Polymers), 65-104.
18. Feldermann, A.; Toy, A.A.; Phan, H.; Stenzel, M.H.; Davis, T.P.; Barner-Kowollik, C. *Polymer* **2004**, *45*, 3997-4007.



19. Faust, R.; Shaffer, T.D. eds. *Cationic polymerization: fundamentals and applications* Washington, DC: American Chemical Society, **1997**.
20. Hsieh, H.L.; Quirk, R.P. eds. *Anionic polymerization: principles and practical applications* New York: Marcel Dekker, **1996**.
21. Cowie, J.M.G. *Polymers: Chemistry & Physics of Modern Materials* 2<sup>nd</sup> ed.; pp. 97-100, Blackie Academic & Professional, New York, **1996**.
22. Nguyen, D.; Zhong, X.F.; Williams C.E.; Eisenberg, A. *Macromolecules* **1994**, 27, 5173-5181.
23. Wilczek-Vera, G.; Yu, Y.; Waddell, K.; Danis, P. O.; Eisenberg, A. *Macromolecules* **1999**, 32, 2180-2187.
24. Hautekeer, J. P.; Varshney, S. K., Fayt, R.; Jacobs, C.; Jerome, R.; Teyssie, P. *Macromolecules* **1990**, 23, 3893-3898.
25. Allcock, H.R.; Lampe, F.W. *Contemporary Polymer Chemistry* 2<sup>nd</sup> ed.; pp. 46-59. Prentice Hall Inc, Toronto, **1990**.
26. Bovey, F.A. *Polymer Conformation and Configuration* Academic Press, **1969**.
27. Cheng, H.N. in *Modern Methods of Polymer Characterization* Barth, H.G.; Mays, J.W. eds. Chapter 11, Wiley Interscience, **1991**.
28. Williams, D.; Flemming, I. *Spectroscopic Methods in Organic Chemistry*, 4<sup>th</sup> ed. McGraw-Hill Book Co., Montreal, **1987**.
29. Meehan, J. *J. Polym. Sci.* **1946**, 1, 175-182.
30. Provder, T. ed., *Size Exclusion Chromatography: Methodology and Characterization of Polymers and Related Materials* Washington DC, American Chemical Society, **1984**.

31. Grubisic, Z.; Rempp, P.; Benoit, H. *J. Polym. Sci. Polym. Lett. Ed.B* **1967**, *5*, 753-759.
32. Farrell, V.; Grady, P. *Macromolecules* **2001**, *34*, 7108-7112.
33. Brown, R.A.; Masters, A.J.; Price, C.; Yuan, X.F. in *Comprehensive Polymer Science: Polymer Properties* Allen, S.G.; Bevington, J.C.; Booth, C.; Price, C. Eds. Vol2, pp 155, Pergamon, Oxford. **1989**.
34. Semenov, A.; Likhtman, A. *Macromolecules* **1998**, *31*, 9058-9071.
35. Liebler, L. *Macromolecules* **1980**, *13*, 1602-1617.
36. Helfand, E. Wasserman, Z.R. *Microdomain Structure and the Interface in Block Copolymers: Applied Science*; Essex, England; **1982**.
37. Matsen, M.W.; Bates, F.S. *Macromolecules* **1998**, *31*, 3498-3508.
38. Matsen, M.W.; Schick, M. *Phys. Rev. Lett.* **1994**, 2660-2663
39. Matsen, M.W. Bates, F.S. *J. Phys Chem.* **1997**, *106*, 2436-2448.
40. Hadziioannou, G.; Skoulios, A.; *Macromolecules*, **1982**, *15*, 267-271.
41. Dan, N.; Safran, S.; *Macromolecules* **1994**, *27*, 5766-5772.
42. Koneripalli, N.; Levicky, R.; Bates, F.S.; Matsen, M.W.; Satija, S.K.; Ankner, J.; Kaiser, H. *Macromolecules* **1998**, *31*, 3498-3508.
43. Park, S.; Cho, D.; Ryu, J.; Kwon, K.; Lee, W.; Chang, T. *Macromolecules* **2002**, *35*, 5974-5979.
44. Bates, F.S.; Frederickson G.H. *Annu. Rev. Phys. Chem.* **1990**, *41*, 525-557.
45. Hadjichristidis, N.; Pispas, S.; Floudas, G.A. *Block Copolymers: Synthetic Strategies, Physical Properties and Applications*. pp. 255-267, Wiley-Interscience, Hoboken, New Jersey, **2003**.
46. Zhulina, E.B.; Birshtein, T.M. *Polymer* **1991**, *32*, 1299-1308.

47. Lyatskaya, J.V.; Zhulina, E.B.; Birshstein, T.M. *Polymer* **1992**, *33*, 343-351.
48. Court, F.; Hashimoto, T. *Macromolecules* **2002**, *35*, 2566-2575.
49. Terreau, O.; Luo, L.; Eisenberg, A. *Langmuir* **2003**, *19*, 5601-5607.
50. Terreau, O.; Bartels, C.; Eisenberg, A. *Langmuir* **2004**, *20*, 637-645.
51. Jain, S.; Bates, F.S. *Macromolecules* **2004**, *37*, 1511-1523.
52. Halperin, A.; Tirrell, M.; Lodge, T.P. *Adv. Polym. Sci.* **1992**, *100*, 31-71.
53. Zhang, L.; Eisenberg, A. *Science* **1995**, *268*, 1728-1731.
54. Yu, K.; Zhang, L.; Eisenberg, A. *Langmuir* **1996**, *12*, 5980-5984.
55. Cameron, N. S.; Corbierre, M. K.; Eisenberg, A. *Can. J. Chem.* **1999**, *77*, 1311-1326.
56. Choucair, A.; Eisenberg, A. *Eur. Phys. J. E.* **2003**, *10*, 37-44.
57. Lim Soo, P.; Eisenberg, A. *J. Polym. Sci. B: Polym. Phys.* **2004**, *42*, 923-938.
58. Liu, F.; Liu, G. *Macromolecules* **2001**, *34*, 1302-1307.
59. Kukula, H.; Schlaad, H.; Antonietti M.; Forster S. *J. Amer. Chem. Soc.* **2002**, *124*, 1658-1663.
60. Bendejacq, D.; Ponsinet, V.; Joanicot, M.; Loo, Y.-L.; Register, R. A. *Macromolecules* **2002**, *35*, 6645-6649.
61. Nardin, C.; Hirt, T.; Leukel, J.; Meier, W. *Langmuir* **2000**, *16*, 1035-1041.
62. Kalinina, O.; Kumacheva, E. *Macromolecules* **1999**, *32*, 4122-4129.
63. Raez, J.; Manners, I.; Winnik, M. *J. Am. Chem. Soc.* **2002**, *124*, 10381-10395.
64. Discher, B.M.; Won, Y.-Y. Ege, D.S.; Lee, J.C.M.; Bates, F.S.; Discher, D.E.; Hammer, D.A. *Science* **1999**, *284*, 1143-1146.
65. Webber, S.E.; Munk, P.; Tuzar, Z.; Eds. *Solvents and Self-Organization of Polymers. (Proceedings of the NATO Advanced Study Institute on Solvents*

*and Self-Organization of Polymers, held in Belek, Antalya, Turkey, July 31-August 11, 1995.)* **1996.**

66. Weaver, J. V. M.; Armes, S. P.; Liu, S. *Macromolecules* **2003**, *36*, 9994-9998.
67. Jungmann, N.; Schmidt, M.; Maskos, M.; Weis, J.; Ebenhoch, J. *Macromolecules* **2002**, *35*, 6851-6857.
68. Discher, D.E.; Eisenberg, A. *Science* **2002**, *297*, 967-973.
69. Riegel, I.C.; de Bittencourt, F.M.; Terreau, O.; Eisenberg, A.; Petzhold, C.L.; Samios, D. *J. Pure Appl. Chem.* **2004**, *76*, 123-131.
70. Booth, C.; Attwood, D. *Macromol. Rapid Commun.* **2000**, *21*, 501-527.
71. Stepanek, M.; Podhajecka, K.; Tesarova, E.; Prochazka, K.; Tuzar, Z.; Brown, W. *Langmuir* **2001**, *17*, 4240-4244.
72. Allen, C.; Eisenberg, A.; Maysinger, D. *S.T.P. Pharma Sciences* **1999**, *9*, 139-151.
73. Zhang, L.; Eisenberg, A. *Macromolecules* **1999**, *32*, 2239-2249.
74. Shen, H.; Zhang, L.; Eisenberg, A. *J. Phys. Chem. B.* **1997**, *101*, 4697-4708.
75. Hiemenz, P.C. *Principles of Colloid and Surface Chemistry* 2<sup>nd</sup> ed.; Marcel Decker: New York, **1986**.
76. Deng, Y.; Price, C.; Booth, C. *Euro Polym. J.* **1994**, *30*, 103-111.
77. Alexandridis, P.; Holzwarth, J.F.; Hatton, T.A. *Macromolecules* **1994**, *27*, 2414-2425.
78. Zhang, L.; Eisenberg, A. *Polym. Adv. Technol.* **1998**, *9*, 677-699.
79. Shen, H.; Eisenberg, A. *Macromolecules*, **2000**, *33*, 2561-2572.
80. Shen, H.; Eisenberg, A. *J. Phys. Chem. B.* **1999**, *103*, 9473-9487.

81. Yu, Y.; Zhang, L.; Eisenberg, A. *Macromolecules*, **1998**, *31*, 1144-1154.
82. Desbaumes, L.; Eisenberg, A. *Langmuir* **1999**, *15*, 36-38.
83. Zhang, L.; Yu, K.; Eisenberg, A. *Science* **1996**, *273*, 1777-1779.
84. Zhang, L.; Eisenberg, A. *Macromolecules* **1996**, *29*, 8805-8815.
85. Shen, H.; Zhang, L.; Eisenberg, A. *J. Amer. Chem. Soc.* **1999**, *121*, 2728-2740.
86. Zhang, L.; Shen, H.; Eisenberg, A. *Macromolecules* **1997**, *30*, 1001-1011.
87. Zhang L.; Eisenberg, A. *J. Polym. Sci. B.: Polym. Phys.* **1999**, *37*, 1469-1484.
88. Burke, S. E.; Eisenberg, A. *Langmuir* **2001**, *17*, 8341-8347.
89. Burke, S.E.; Eisenberg, A. *Langmuir* **2001**, *17*, 6705-6714.
90. Chen L.; Shen, H.; Eisenberg, A. *J. Phys. Chem B.* **1999**, *103*, 9488-9497.
91. Burke, S.E.; Eisenberg, A. *Polymer* **2001**, *42*, 9111-9120.
92. Choucair, A.; Kycia, A.; Eisenberg, A. *Langmuir* **2003**, *19*, 1001-1008.
93. Tian, M, Qin, A.; Ramireddy, C.; Webber, S.E.; Munk, P.; Tuzar, Z. *Langmuir* **1993**, *9*, 1741-1748.
94. Antonietti, M.; Heinz, S., Schmidt, M.; Rosenauer, C. *Macromolecules* **1994**, *27*, 3276-3281.
95. Prochazka K.; Bednar, B.; Tuzar, Z.; Kocirik, M. *J. Liq. Chromatogr.* **1989**, *12*, 1023-1041.
96. Mochrie, S. Mayes, A.; Sandy, A.; Sutton, M. Brauer, S. Stephenson, G.; Abernathy, D.; Grubel, G. *Phys. Rev. Lett.* **1997**, *78*, 1275-1278.
97. Bluhm, T.L.; Whitmore, M.D. *Can. J. Chem.* **1984**, *63*, 249-252.
98. Plestil, J. Hlavata, D.; Hrouz, J.; Tuzar, Z. *Polymer* **1990**, *31*, 2112-2117.

99. Londonono, J.; Dharmapurikar, R.; Cochran, H.; Wignal, G.; McClain, J.; Betts, D.; Canelas, D.; DeSimone, J.; Samulski, E.; Chillura, D.; Triolo, R. *J. Appl. Cryst.* **1997**, *30*, 690-695.
100. Moffitt, M. Yu, Y., Nguyen, D.; Graziano, V.; Schneider, D.K.; Eisenberg, A. *Macromolecules* **1998**, *31*, 2190-2197.
101. Liu, Y.; Chen, S.H.; Huang, J.S. *Macromolecules* **1998**, *31*, 2236-2244.
102. Reimer, L.; *Transmission Electron Microscopy Physics of Image Formation and Microanalysis* 4<sup>th</sup> ed, Chapter 1, Springer, Germany, **1997**.
103. Allcock, H.R.; Lampe, F.W. *Contemporary Polymer Chemistry* 2<sup>nd</sup> ed.; pp. 348-363, Prentice Hall Inc, Toronto, **1990**.
104. Chu, B. *Laser Light Scattering* 2<sup>nd</sup> ed; Chapter 6, Academic Press **1991**.
105. Schmidt, M. *Macromolecules* **1984**, *17*, 553-560.

## CHAPTER 2

---

### **EFFECT OF POLY(ACRYLIC ACID) BLOCK LENGTH DISTRIBUTION ON POLYSTYRENE-*b*-POLY(ACRYLIC ACID) AGGREGATES IN SOLUTION. 1. VESICLES.**

---

#### ABSTRACT

The effect of polydispersity on the self-assembly of block copolymer aggregates in solution was studied under two sets of conditions. A series of polystyrene-*block*-poly(acrylic acid) copolymers of an identical polystyrene length of 310 units but of varying degrees of polymerization of the poly(acrylic acid) (PAA) was synthesized. Mixtures of the copolymers were made to artificially broaden the molecular weight distribution of the PAA at a constant number average of 28 repeat units, in the polydispersity index (PDI) range of 1.1-2.1. The samples were dissolved in two different solvent systems (dioxane and a mixture of tetrahydrofuran (THF)/*N,N*-dimethyl formamide (DMF)), and self-assembly was induced by the slow addition of water. The samples were quenched at a predetermined water content. Transmission electron microscopy and dynamic light scattering were used to measure sizes and size distributions of the aggregates. At a low PAA polydispersity index (PAA PDI  $\sim 1.1$ ), in the THF/DMF system, large polydisperse vesicles of a diameter of  $270 \pm 220$  nm were seen. Generally the size of the vesicles decreased with increased PAA polydispersity. For example, in the THF/DMF system, at a PAA PDI of 1.8, the average vesicle size was  $80 \pm 20$  nm. The trend is explained qualitatively by the length segregation of the PAA chains (large chains segregate to the outer surface while smaller chains prefer the inner surface of the vesicle)

and the ratio of short chains to long chains in the mixtures. The presence of only vesicles in mixtures containing polymers that do not form vesicles by themselves, but rather spheres and large compound micelles, suggests that there is no significant segregation of chains between aggregates, but only segregation of chains within individual vesicular aggregates.

## **2.1 INTRODUCTION**

The self-assembly of amphiphilic diblock copolymers in selective solvents can result in the formation of a wide variety of aggregates.<sup>1</sup> When aggregation is primarily under thermodynamic control, a spectrum of morphologies including spheres, rods and bilayers (lamellae or vesicles) is observed.<sup>2</sup> It is also possible to prepare aggregates of more complex architecture such as large compound micelles (LCMs), large compound vesicles (LCVs), hexagonally packed hollow hoops (HHH), tubules and branched tubules, to name just a few. There has been a high level of activity in this field including work in the groups of Eisenberg,<sup>1,2,10-18</sup> Liu,<sup>3</sup> Antonietti,<sup>4</sup> Wooley,<sup>5</sup> Bates,<sup>6</sup> Manners and Winnik,<sup>7</sup> and Li.<sup>8</sup>

The specific morphology of the aggregate can be attributed to a balance of three contributions to the free energy of the system: chain stretching in the core, the interfacial energy, and repulsion among corona chains.<sup>9,10</sup> There are many factors that affect the above three terms, and by variation of one or more of these, the morphologies can, in principle, be fine-tuned. Examples of such factors that have been studied previously include the block length of the copolymer,<sup>11</sup> the concentration of the precipitant,<sup>12</sup> the initial concentration of polymer,<sup>13</sup> the presence of additives such as salts,<sup>14</sup> acids,<sup>15</sup>



bases,<sup>16,17</sup> or homopolymer,<sup>11,17</sup> the common solvent used,<sup>18</sup> and, to a lesser extent, the temperature.<sup>19</sup> All of the above studies have been performed using block copolymers of narrow molecular weight distributions.

Aggregates of block copolymers in solution have potential industrial applications in fields such as drug delivery, the cosmetic industry, catalysis, separations, microelectronics, and others. To date, the vast majority of studies of block copolymer self-assembly were performed using materials synthesized by anionic polymerization. The cost of anionic polymerization, however, is high, which might hinder the exploration of block copolymer aggregates in some of these fields.

Living free radical polymerizations are now available to synthesize block copolymers.<sup>20, 21</sup> These techniques may be much more suitable for low-cost production of such materials; however, the resulting copolymers frequently have somewhat broader molecular weight distributions (polydispersities) than those made by anionic techniques.

Only a few studies have been devoted to the effect of polydispersity on block copolymer self-assembly. The effect of polydispersity on critical micelle concentrations (cmc's) and on self-assembly of Pluronics has been investigated by Linse,<sup>22</sup> while Sommerdijk has shown that multiblock copolymers containing polydisperse ( $M_w/M_n=1.6$ ) hydrophobic blocks do, indeed, form aggregates in solution.<sup>23</sup> Also, Meier has used a triblock copolymer with a polydispersity index of 1.7 to form vesicles.<sup>24</sup> Several workers have explored the effect of binary mixtures of polystyrene-*b*-polyisoprene block copolymers in the bulk phase.<sup>(25-29)</sup> Nguyen et al. have explored the effect of polydispersity of the ionic block on the size of the cores of inverse micelles of polystyrene-*b*-poly-4-vinylpyridinium methyl iodide and of polystyrene-*b*-poly(cesium methacrylate). They showed that the sizes of ionic microdomains varied linearly with the

polydispersity of the ionic chain; however, if the copolymers micellized far from equilibrium, the polydispersity of the ionic group showed no effect on the sizes of the domains.<sup>30</sup> It is also known that the balance of forces involved in the formation of aggregates of various morphologies is very delicate. Therefore, in the absence of a comprehensive theory of self-assembly of amphiphilic block copolymers in solution, which includes the effect of polydispersity that allows quantitative predictions of the results, it is necessary to systematically explore the effects of molecular weight distributions experimentally. The present study investigates the effect of corona chain polydispersity on block copolymer aggregation in solution. Since vesicles are possibly the most interesting morphology<sup>31-33</sup> from the point of view of potential applications, vesicles were chosen for the first such study.

To carry out this investigation, a series of block copolymers of narrow molecular weight distribution was synthesized by anionic techniques. The copolymers were then mixed to broaden artificially the molecular weight distribution of the corona-forming (poly(acrylic acid)(PAA)) block while keeping its number average molecular weight constant. The copolymer mixtures were dissolved, in either dioxane or a mixture of tetrahydrofuran (THF) and *N,N*-dimethyl formamide (DMF), and water was added to induce self-assembly. Slow water addition was continued until a predetermined amount had been added, at which point the samples were quenched. These two solvent systems were chosen because they yield different vesicle sizes for the same block copolymer under otherwise identical conditions. Direct observation of the morphologies and measurements of the sizes of the aggregates were made by transmission electron microscopy (TEM). Dynamic light scattering (DLS) was also used to measure the sizes of the aggregates in solution, and the results of the two methods are compared.

## 2.2 EXPERIMENTAL

### 2.2.1 Anionic Synthesis

The polystyrene-*b*-poly(*tert*-butyl acrylate) block copolymers were synthesized by sequential anionic polymerization of styrene followed by *tert*-butyl acrylate (*t*-BuA) using *sec*-butyllithium as the initiator.<sup>34</sup> Lithium chloride (LiCl) and  $\alpha$ -methyl styrene were used to prevent side reactions during the *t*-BuA polymerization.<sup>34</sup> The polymerization was performed in tetrahydrofuran (THF) at  $-78\text{ }^{\circ}\text{C}$  under UHP nitrogen in a round-bottom flask equipped with a rubber septum. Solvents, initiators, and monomers were transferred via a stainless capillary and syringe to the reactor. *sec*-Butyllithium was added to a round-bottom flask containing LiCl and  $\alpha$ -methyl styrene in THF; a dark red color appeared. After the temperature was decreased to  $-20\text{ }^{\circ}\text{C}$ , the styrene was added, turning the color to yellow; the polymerization of styrene was completed in a few minutes, and the dark red color returned. An aliquot of the reaction mixture was withdrawn for characterization by gel permeation chromatography (GPC). The polymerization flask was cooled to  $-78\text{ }^{\circ}\text{C}$ , and *t*-BuA was added. As soon as the *t*-BuA was added to the solution, the red color disappeared completely; the polymerization of *t*-BuA was carried out for 90 min. An aliquot of the mixture was then removed. A second aliquot of *t*-BuA was then transferred to the reactor and allowed to polymerize for 90 min. By this method, a series of diblock copolymers all with the same polystyrene (PS) block but varying degrees of polymerization of poly(*t*-BuA) was synthesized. Each polymerization was terminated by the addition of methanol. The diblock copolymers were refluxed in toluene along with *p*-toluenesulfonic acid (catalyst) to convert the poly(*t*-BuA) into poly(acrylic acid).

The degree of polymerization of the homopolystyrene and the polydispersity of the polymers were determined by GPC. The degree of polymerization of the poly(*t*-BuA)

block was calculated from the polymer composition, which had been determined by NMR. The homopolymer and the copolymers had narrow and monomodal molecular weight distributions. The molecular parameters of the polymers are listed in Table 2-1. The polymers are denoted as  $PS_x-b-PAA_y$  where  $x$  and  $y$  stand for the number average degrees of polymerization of the PS and PAA blocks, respectively. For example,  $PS_{300}-b-PAA_{11}$  represents a copolymer containing 300 styrene units and 11 acrylic acid units.

Table 2-1: Characteristics of the individual block copolymers

Polymer	PDI of PS block	PDI of copolymer	PDI of PAA block*
$PS_{300}-b-PAA_{11}$	1.07	1.04	1.14
$PS_{310}-b-PAA_{28}$	1.03	1.03	1.10
$PS_{310}-b-PAA_{36}$	1.03	1.03	1.08
$PS_{310}-b-PAA_{45}$	1.03	1.03	1.07
$PS_{300}-b-PAA_{74}$	1.07	1.09	1.05

\* assuming that the polydispersity of the second block of the diblock is equal to the polydispersity of a homopolymer of comparable length prepared under similar conditions.

### 2.2.2 Molecular Weight Distributions

GPC could not measure independently the polydispersity of the PAA blocks. In principle, if one knows the molecular weight and the polydispersity of the PS and of the copolymers, it should be possible to calculate the polydispersity of the PAA block, but only if the block lengths are comparable. However, in our case, the PAA chain lengths were too short. Thus, to evaluate the polydispersity of the PAA block, a previously developed approximate method was followed.<sup>30</sup> It was assumed that the short chains of PAA had molecular weight distributions that were similar to those of chains of PS of the

same length polymerized under similar conditions. Using the polydispersity of low molecular weight PS data from a previous study,<sup>30</sup> the polydispersity of the PAA chains was estimated. (This data is contained in Appendix D). For each PS-*b*-PAA copolymer the molecular weight distribution of the PAA block was assumed to follow Gaussian statistics:

$$f(x) = \frac{1}{(\sigma_n) * (2\pi)^{0.5}} \exp \left[ -\frac{(x - x_n)^2}{2\sigma_n^2} \right] \quad (2-1)$$

where

$$\sigma_n = x_n (PDI - 1)^{0.5}$$

where  $x_n$  is the average number of units in the PAA block, and PDI is the estimated polydispersity of the PAA block. Figure 1 shows the molecular weight distributions of PAA in the family of PS-*b*-PAA copolymers.

Blends were then mixed keeping  $M_n$  constant but varying  $M_w$  and thus the polydispersity index. Using the estimated polydispersity indexes of PAA from Table 2-1, the compositions of the mixtures were calculated. The molecular weight distribution curves for the blends were obtained by taking the sum of all the distributions of the components in proportion to their ratio in the mixture. From these distributions,  $M_n$  and  $M_w$  of the blends could be calculated using standard formulas, and their ratio gave the PAA polydispersity of the blend. Figure 2-2 shows PAA molecular weight distributions of different blends of PS-*b*-PAA copolymers with a constant  $M_n$  of 28 acrylic acid units.

### 2.2.3 Preparation of vesicles

Two solvent systems were used for the preparation of vesicles. The first system used a mixture of DMF/THF as a common solvent for both the PS and PAA blocks; the second system used dioxane as the common solvent. Water was used as the precipitant in both systems.

#### 2.2.3.1 DMF/THF System

A mixture of DMF and THF (39% DMF w/w) was used to dissolve the PS-*b*-PAA copolymer mixtures (2 % w/w). Water was added slowly ( $\sim 0.7\%$  (w/w)/ min) to obtain a final concentration of 50% w/w. The samples were then quenched by adding them into an excess of water. After quenching, the samples were dialyzed against Milli-Q water to remove the organic solvents, leaving a dilute aqueous solution of the aggregates.

#### 2.2.3.2 Dioxane System

The PS-*b*-PAA copolymer mixtures (0.5% w/w) were dissolved in dioxane and stirred overnight. Water was then added slowly ( $\sim 0.7\%$  (w/w)/min) to a final concentration of 15% w/w. The samples were then brought to liquid nitrogen temperature and the water/dioxane was sublimed in order to quench the morphology.

### 2.2.4 Transmission Electron Microscopy

A JEOL 2000FX microscope was used for the transmission electron microscopy (TEM) studies. The dilute water quenched samples were deposited on EM grids that had been precoated with a thin film of Formvar (poly(vinylformaldehyde) plastic) and then coated with carbon. The water evaporated at room temperature overnight leaving the solid aggregates on the grids.

### **2.2.5 Dynamic Light Scattering**

DLS experiments were performed on a Brookhaven Instruments photon correlation spectrophotometer equipped with a BI-9000AT digital correlator and compass 315M-150 laser (532 nm) from Coherent Technologies. All measurements were made in water at 20°C. The dilute aqueous vesicle solutions were added to dust free vials. The angle of detection was 90° for all measurements. The Contin algorithm was used to analyze the data.

## **2.3 RESULTS AND DISCUSSION**

### **2.3.1 Molecular Weight distributions of blends**

Once the polymers were synthesized, they were mixed to give different PAA polydispersities. Table 2 shows the contents of each mixture and the resulting polydispersity index. In order to calculate the polydispersity of the PAA blocks in the mixture, the polydispersity index of the PAA block of each individual copolymer was needed. This was not measurable by GPC. Two approaches were taken to approximate the PAA PDI of the blends. The first approximation was made by assuming that the copolymers were unimodal and that their polydispersity was equal to 1.0, an idealized polydispersity of the mixture could thus be obtained. The next to last column of table 2-2 contains these values. However, the copolymers used in the study do have a distribution of block lengths, thus, in the second approximation, the assumption was made that the polydispersity index of the PAA block of the copolymers in the mixture was the same as that of a homopolymer of similar length synthesized by anionic polymerization. These values of assumed polydispersities are found in table 2-1, and the results of the polydispersity calculations using these assumed values are found in the last column of

table 2-2. It can be seen that the polydispersity of the components does make a difference in determining the overall PAA PDI of the mixture; it is important to note, however, that the differences between the two values are not large, especially at high polydispersities. The assumed polydispersities of the second block are similar to those found experimentally by MALDI TOF analysis of diblocks with comparable block lengths.<sup>35</sup>

Figure 2-1 shows the molecular weight distributions (based on the polydispersities given in table 1) of the PAA block of each of the copolymers synthesized. Figure 2-2 contains plots of the molecular weight distributions for the different mixtures. It should be noted that the distributions of the mixtures are not unimodal. The effect of the shape of the distribution will be explored in further studies.

Table 2-2: Blends and resulting PDIs of the PAA blocks

Mixture	PS <sub>300</sub> - <i>b</i> - PAA <sub>11</sub>	PS <sub>310</sub> - <i>b</i> - PAA <sub>28</sub>	PS <sub>310</sub> - <i>b</i> - PAA <sub>36</sub>	PS <sub>310</sub> - <i>b</i> - PAA <sub>45</sub>	PS <sub>300</sub> - <i>b</i> - PAA <sub>74</sub>	PDI of PAA in mixture assuming monodisperse components in mixtures	PDI of PAA in mixture taking PDIs from the last column of table 1.
1	-----	100 %	-----	-----	-----	1.00	1.10
2	30 %	-----	70 %	-----	-----	1.15	1.27
3	34 %	-----	56 %	10 %	-----	1.25	1.36
4	45 %	-----	44 %	-----	11 %	1.49	1.59
5	48 %	-----	40 %	-----	12 %	1.54	1.64
6	57 %	-----	23 %	-----	12 %	1.75	1.85
7	73 %	-----	-----	-----	27 %	2.00	2.13



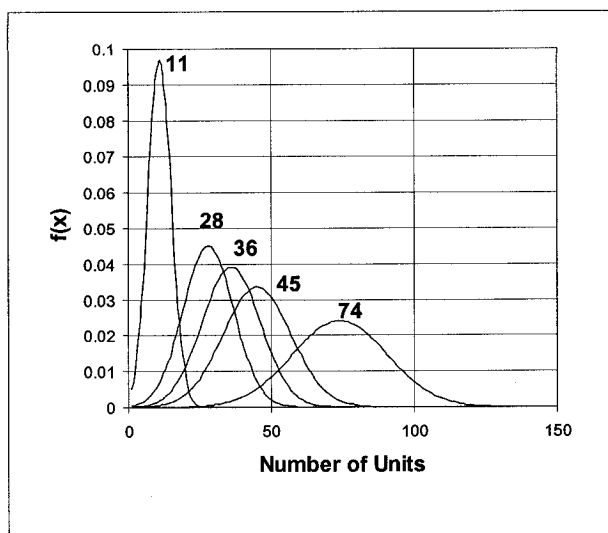


Figure 2-1: Molecular weight distributions of PAA blocks of the individual copolymers assuming that the polydispersity of the block is the same as that of a homopolystyrene of similar length prepared under identical conditions.

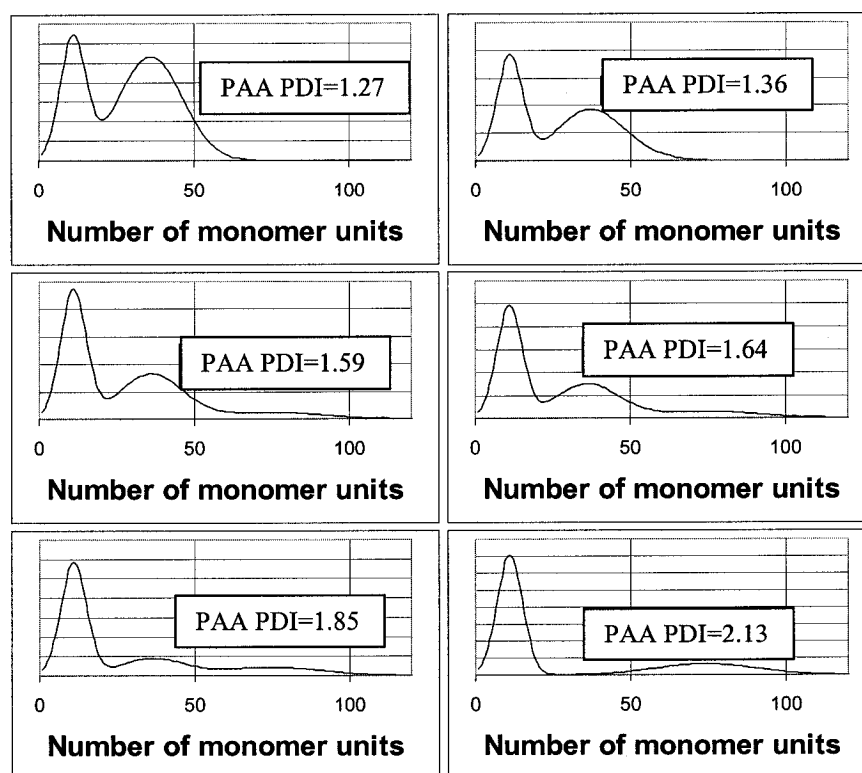


Figure 2-2: Molecular weight distributions of the PAA blocks in the mixtures.

### 2.3.2 THF/DMF System

The first system that was investigated was prepared using a THF/DMF mixture as the common solvent. It had been shown previously<sup>36</sup> that the narrow molecular weight distribution polymer (PS<sub>310</sub>-*b*-PAA<sub>28</sub>) aggregated to form large, polydisperse vesicles in that solvent mixture, and therefore the THF/DMF solvent mixture was used to see the effect of PAA polydispersity on large vesicles. After self-assembly of the polymers was induced by addition of water, the morphology of the aggregates was frozen by quenching them into an excess of water, the solution was dialyzed and a small amount deposited onto TEM grids. Analysis of the TEM data showed an initial rise in the average vesicle diameter followed by a decrease as the PAA PDI became larger; eventually, at a high enough PAA PDI, spheres were also observed. Figure 2-3 shows comparison micrographs of aggregates formed from the samples of four different polydispersity indexes. As the polydispersity of the sample increased from 1.10 (figure 2-3a) to 1.37 (not shown) there was an increase in the average diameter of the vesicles from 270±220 nm to 370±230 nm. A further increase in PAA polydispersity to 1.64 (figure 2-3b) resulted in a decrease in the average vesicle radius to a value of 150±110 nm. Increasing the PAA polydispersity of the sample further to 1.85 (figure 2-3c) showed a further decrease in average vesicle radius to 80±20 nm, accompanied by the appearance of spheres. The sample with a PAA polydispersity of 2.13 (figure 2-3d) also showed vesicles and spheres, similar to those in the sample with a polydispersity of 1.85. Figure 2-4 is a graph of average vesicle diameter as a function of polydispersity as measured by both TEM and DLS (see below for comments on the DLS data) for five samples of different polydispersities. The bars on figure 2-4 indicate the population standard deviations of the samples, and are very large at low PAA PDI indicating a broad

distribution of sizes while they are small at higher PAA PDI. This is a common phenomenon among vesicles; large vesicles have a broader size distribution than small vesicles.<sup>36</sup> The average wall thickness of the vesicles at each PAA PDI was measured from the TEM pictures and is included in table 2-3. There was no significant change in the wall thickness. This was expected because the styrene block was identical in all of the mixtures.

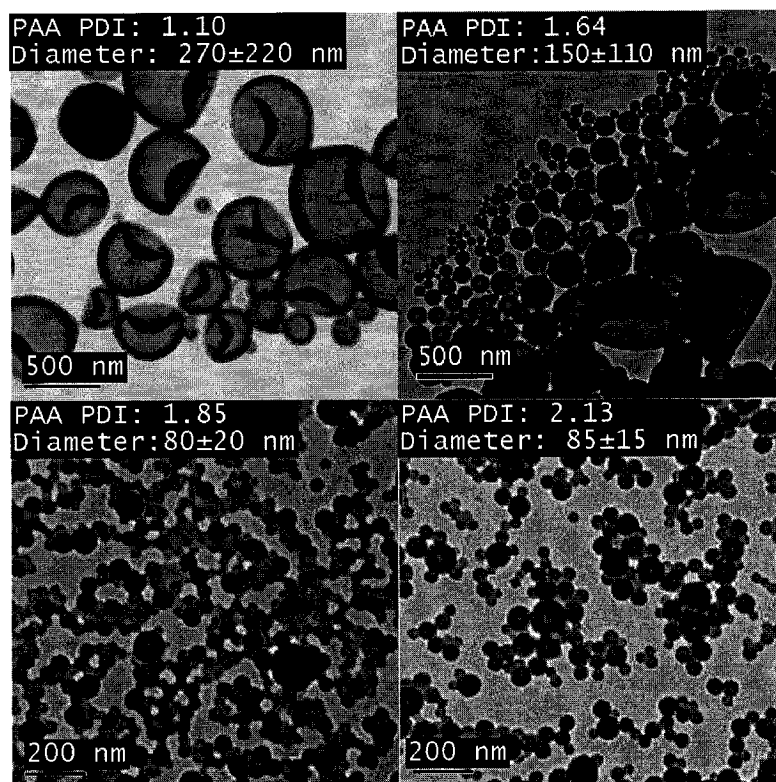


Figure 2-3: Comparison TEM photos of vesicles made from different mixtures of copolymers in the THF/DMF system. The number at the top left corner refers to the polydispersity index of the PAA block.

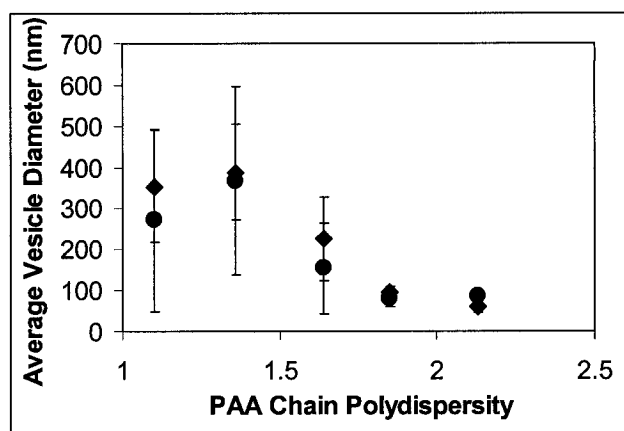


Figure 2-4: Size as a function of polydispersity of vesicles in the THF/DMF system. ● TEM data, ◆ DLS data.

DLS was also used to measure the size of the aggregates formed in the DMF/THF system. The results showed the same general effect of PAA chain polydispersity on the size of vesicles, i.e. an initial increase followed by a decrease in particle size with increasing polydispersity, as shown in figure 2-4. DLS also showed a distribution of vesicle sizes at all polydispersities; however, the average vesicle size for each PAA PDI, as measured by TEM, was not significantly different (at the 90% confidence limit) from the size as measured by DLS. This is due to the large population standard deviations of the samples and the number of particles counted. It is interesting to note that although, statistically, the averages are not different, the average vesicle size as measured by DLS was always slightly higher (except for the PAA PDI sample that contained a lot of spherical micelles) than that obtained for the TEM measurements as shown in figures 2-4 and 2-5. The DLS measurements were made on the aggregates in solution where the coronae would not have been collapsed because of the solubility of the acrylic acid in the water, while the TEM measurements were made on solid aggregates in which the coronae were collapsed. As a first approximation of the effect of the corona stretching, the size of

a fully stretched planar zigzag corona chain can be compared to the size of the collapsed corona chain. This would be the maximum possible difference in size due to corona stretching, as a planar zigzag conformation would embody the largest extension possible for a polymer chain. The calculated (see Appendix E) expected difference in average size, between a fully extended corona and a collapsed corona, was 20 nm, which was close to the observed difference for the PAA PDI 1.36 and 1.85 samples; however, it is not reasonable to expect that the corona chains are completely stretched in these situations. There will be some extension due to increased repulsion from the corona chains being close together near the core, as well as from electrostatic repulsion since the PAA is expected to be partially ionized; and, this can account for some of the difference. With both methods the trend of an increase followed by a decrease in vesicle size with increasing PAA PDI was parallel.

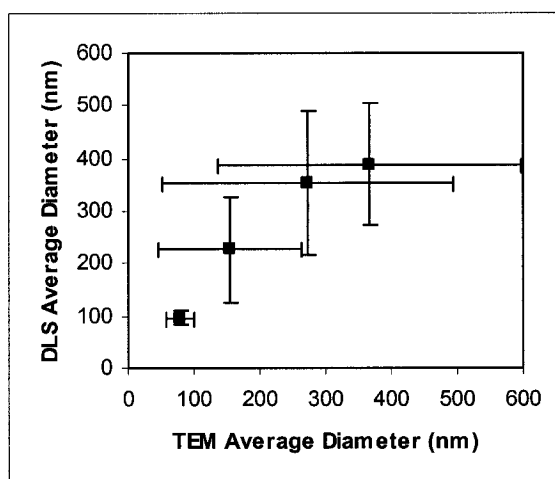


Figure 2-5: Vesicle sizes as measured by DLS and TEM

Table 2-3: Dimensions of aggregates of varying PAA PDI in the THF/DMF/H<sub>2</sub>O mixtures

PAA PDI	Average Vesicle Size (TEM) (nm)	Average Vesicle Diameter (DLS) (nm)	Average Wall Thickness (nm)	Average Sphere Diameter (nm)	Apparent Mass Fraction of Vesicles (%)
1.10	270 ± 220	355 ± 135	32 ± 7	N/A	100
1.37	365 ± 230	390 ± 115	37 ± 7	N/A	100
1.64	155 ± 110	225 ± 100	41 ± 8	N/A	100
1.85	80 ± 20	96 ± 15	36 ± 8	38 ± 8	50
2.13	85 ± 15	60 ± 15	35 ± 4	37 ± 9	63

One can speculate on the origin of the two trends observed. First, the decrease in average vesicle size with increasing PAA PDI at high PAA PDI will be addressed, then, the slight vesicle size increase at an intermediate value of the PAA PDI will be discussed. The decrease in vesicle diameter with increased polydispersity can be explained as follows: As the polydispersity of the PAA increases, there are more long chains (chains longer than 28 units) and more short chains (chains less than 28 units). The long and short chains segregate in the aggregate; the short chains preferentially segregate to the inner surface of the wall, while the long chains prefer the outer surface.<sup>36,37</sup> When looking at the compositions of the mixtures, it is seen that as the PAA polydispersity increases, there is more of the PS<sub>300</sub>-b-PAA<sub>11</sub> copolymer. Since there are more short chains, which can be placed on the inside of the vesicle, the radius becomes smaller, as shown schematically in figure 2-6. As the outside surface of the vesicle contains more longer chains, the repulsions among them increase which favors a reduction in the vesicle radius. The presence of the shorter chains on the inside allows this to happen. Both of these factors combine to lead to a decrease in the size of the vesicle.

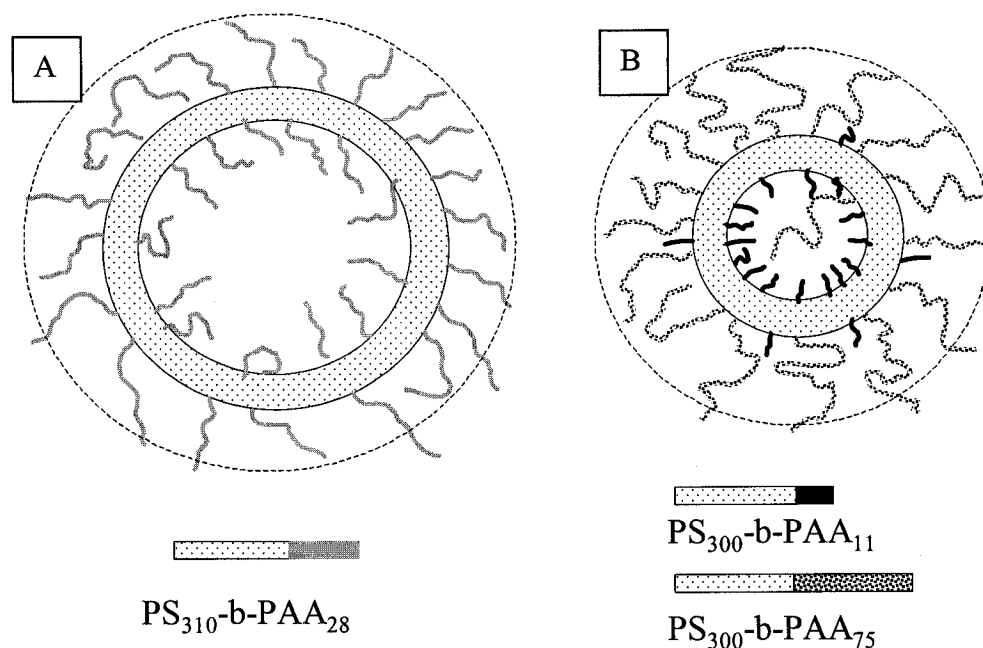


Figure 2-6 Schematic illustration of why an increase in polydispersity of the PAA block results in smaller vesicles. A) A vesicle made with a narrow molecular weight distribution of  $\text{PS}_{310}\text{-}b\text{-PAA}_{28}$  lengths. B) A vesicle made from a mixture of two different blocks with different PAA chain lengths. The smaller  $\text{PS}_{310}\text{-}b\text{-PAA}_{11}$  chains segregate preferentially to the inside surface of the vesicle and therefore the hollow core of the vesicle can become smaller. The dotted lines are meant as guides for the eye to indicate the vesicle size.

As the PAA PDI increases the amount of  $\text{PS}_{300}\text{-}b\text{-PAA}_{11}$  in the mixture also increases from 48% in the PAA PDI 1.64 sample to 57% in the PAA PDI 1.85 sample and finally to 73% in the PAA PDI 2.13 sample. This increase in the number of small chains possibly allows a more efficient segregation; therefore, the inner surface of the vesicle has a higher ratio of short to long chains. At PAA PDIs with low amounts of  $\text{PS}_{300}\text{-}b\text{-PAA}_{11}$ , there will have to be other chains present on the inner surface of the vesicle. The more  $\text{PS}_{300}\text{-}b\text{-PAA}_{11}$  in the mixture, the more likely it is that the inner wall will contain only (or

mostly) PS<sub>300</sub>-*b*-PAA<sub>11</sub>. As the relative amount of PS<sub>300</sub>-*b*-PAA<sub>11</sub> in the inner wall increases, a smaller radius of curvature becomes possible, and therefore the size of the vesicle decreases.

At the highest values of PAA PDI, for example 1.85 and 2.13, spherical micelles were observed along with vesicles. At these PAA PDIs there were large amounts of PS<sub>300</sub>-*b*-PAA<sub>11</sub>, which, for vesicles, would preferentially segregate to the inner surface, while the longer PS<sub>310</sub>-*b*-PAA<sub>45</sub> and PS<sub>300</sub>-*b*-PAA<sub>74</sub> make up the majority of the outer surface. As the number of PS<sub>300</sub>-*b*-PAA<sub>74</sub> chains increased in the mixture the repulsion among them would also increase, which would tend to decrease the outside radius due to increased corona repulsion. As the number of long chains increases, the free ends of the longer chains need to be progressively further apart due to corona repulsion, and the shorter chains could then be placed in between the longer chains as shown schematically in figure 2-7. Beyond some point, the vesicle would no longer be favored and spheres with both PS<sub>300</sub>-*b*-PAA<sub>74</sub> and PS<sub>300</sub>-*b*-PAA<sub>11</sub> would form. These are indeed observed in the PAA PDI 1.85 and 2.13 samples. The average sphere diameters (as shown in table 2-3) are similar at the different PAA PDIs. It is interesting that the sphere diameter stays the same for the two polydispersities. Part two of this series of papers will investigate effects of PAA PDI on spherical morphologies.

Also, an estimate of the mass fraction (m.f.) of the spheres was calculated using Equation 2.2.

$$m.f. = \frac{m_s}{m_s + m_v} \quad (2-2)$$

where  $m_s$  and  $m_v$  are the total masses of spheres or vesicles in a given area.



The mass of the spheres was calculated using Equation 2.3, while the mass of the vesicles was calculated using Equation 2.4.

$$m_s = n_s V_s \rho \quad (2-3)$$

where  $n_s$  is the number of spheres in a given area,  $V_s$  is the volume of the sphere ( $4/3\pi r^3$ )

and  $\rho$  is the density of the polymer (taken to be 1 g/ml), and

$$m_v = n_v V_v \rho \quad (2-4)$$

where  $n_v$  and  $\rho$  are the number of vesicles in a given area and the polymer density, while

$V_v$  is the volume of the vesicle wall, which is calculated by Equation 2.5.

$$V_v = \frac{4}{3}\pi(R^3 - r^3) \quad (2-5)$$

where  $R$  is the average outer vesicle radius and  $r$ , the inner radius, is obtained by subtracting the wall thickness from the average outer vesicle radius.

Both the PAA PDI 1.85 and the PAA PDI 2.13 samples had relatively high mass fractions of spheres, as shown in table 2-3. The mass fractions are not similar to the ratio of the component polymers in the mixture suggesting that segregation of the polymers into different aggregates is not occurring extensively. This is discussed in more detail in section 2.3.4 below. It is interesting to note that the PAA PDI 1.85 has a higher mass fraction of spheres than the PAA PDI 2.13 sample. It should be noted that the limited number of particles in the TEM pictures do not give a very accurate estimate of the actual mass fraction. However, the DLS data can also be used to calculate a mass fraction. Since the vesicles in the PAA PDI 1.85 are of similar size to those in the PAA PDI 2.13 sample, and the sphere sizes in both samples are also similar, the only factor that would

change the average size of all particles in the sample is the ratio of spheres to vesicles. The greater the ratio of spheres to vesicles in the sample, the smaller would be the average diameter of all the particles. The DLS data (which is a measure of the average diameter of all particles in the sample) shows a smaller diameter for the PAA PDI 2.13 sample, indicating a higher mass fraction of spheres.

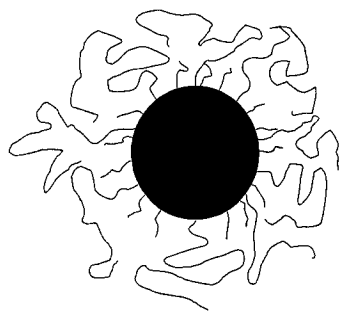


Figure 2-7: Spheres made from mixtures of  $\text{PS}_{300}\text{-b-PAA}_{74}$  and  $\text{PS}_{300}\text{-b-PAA}_{11}$ . The longer PAA chains are kept away from each other by regions containing only the short PAA chains, thereby reducing the repulsions among corona chains.

There is one experimental point that deviates from the general trend of decreasing vesicle size with increasing PAA PDI. This is the slight increase in vesicle size that accompanies the increase in PAA PDI from 1.10 to 1.37. This could conceivably be due to experimental error; however, since both methods of size measurement show this trend, it is most likely real. A possible reason for this increase is the ratio of the chain lengths that were mixed together. The “monodisperse” sample ( $\text{PDI} = 1.10$ ) contained mainly chains with a PAA degree of polymerization of 28. When the vesicles were formed, the chains were distributed on the inside and the outside of the vesicle with only some segregation because of the relatively small value of the PAA PDI. As the polydispersity was artificially broadened to 1.37 by mixing three different polymers (the  $\text{PS}_{300}\text{-b-PAA}_{11}$ ,  $\text{PS}_{310}\text{-b-PAA}_{36}$  and  $\text{PS}_{310}\text{-b-PAA}_{45}$ ), there were three populations of chains. In this case,

the short chains (PAA<sub>11</sub>) preferentially segregated to the inside of the vesicle bilayer while the longer chains (PAA<sub>36</sub> and PAA<sub>45</sub>) segregated to the outside of the vesicle bilayer. However, this mixture contained 10mol% of the PS<sub>310</sub>-*b*-PAA<sub>45</sub>, 56% of the PS<sub>310</sub>-*b*-PAA<sub>36</sub> and only 34% of the PS<sub>300</sub>-*b*-PAA<sub>11</sub> to give an average of PS<sub>300</sub>-*b*-PAA<sub>28</sub>. Because the mixture contained so many PS<sub>310</sub>-*b*-PAA<sub>36</sub> and PS<sub>310</sub>-*b*-PAA<sub>45</sub> chains, relative to the number of PS<sub>300</sub>-*b*-PAA<sub>11</sub> chains, the inner surface of the vesicle must have contained some chains that were larger than 28 units of PAA, along with the PAA<sub>11</sub>. The vesicles with PAA PDI 1.37 thus contain longer chains on the inner surface than the vesicles with PAA PDI of 1.10, which, most likely, is the reason why the average diameter is larger.

### 2.3.3 Dioxane System

The study described above focused on large vesicles. In order to determine the effect of corona chain polydispersity on smaller vesicles also, another solvent, dioxane, which is known to produce smaller vesicles, was used.<sup>36</sup> The copolymer (0.5% w/w) was dissolved in dioxane and water was added slowly until a final content of 15% w/w, at which point the solution was quenched by lowering the temperature of a drop of solution to near liquid nitrogen temperature followed by sublimation of the dioxane/water mixture. This “freeze-drying” technique was employed whenever possible (i.e. in water and dioxane); however, freeze drying can not be used for THF or DMF solutions, so the other, longer technique described above was used in those cases. When size was plotted as a function of polydispersity, generally the same trend was found as for the large vesicles, i.e. a decrease in vesicle diameter with increasing polydispersity, as shown in figure 2-8. Spheres were also found in the mixtures with polydispersities of 1.85 and 2.13, as was seen before in the THF/DMF system. There are two differences between the DMF/THF and the dioxane systems; 1) the vesicle sizes at each polydispersity in the dioxane system

are smaller than those for DMF/THF, which was expected, and 2) although the overall trend is the same as the THF/DMF system, the outliers are found at different PAA PDIs in each system. At present time we cannot explain the slight increase in vesicle diameter at a PAA PDI of 1.85 for the dioxane system.

One possibility for the difference between the two solvent systems could be the amount of solvent in the core or vesicle wall. Studies which shed light on the amount of solvent in the core have been made previously by studying the effect of water on homopolystyrene solutions.<sup>18</sup> The homopolymer was dissolved in either dioxane, DMF, or THF and water was added until phase separation occurred. The amount of solvent in the PS homopolymer solution phase was then determined. This data was used to try to estimate the amount of solvent in the wall of the vesicles in the present study. From the previous study, a dioxane system containing 15% water should contain  $\sim 0.40\text{v/v}$  dioxane in the polystyrene. For the THF/DMF system an extrapolation of the data from the previous study was needed. At 50 wt% water, for THF, we can estimate that there is approximately  $0.40\text{v/v}$  in the core and that for DMF the value will be less than  $0.20\text{v/v}$ . Therefore amount of solvent in the core should be similar in both the THF/DMF system and the dioxane system. However; changing from one solvent system to another induces many changes such as changes in coil dimensions, interfacial energies, etc. At this time the interrelation of all of these factors is not fully understood, so it is hard to estimate how the two solvent systems effect the size of the vesicles.

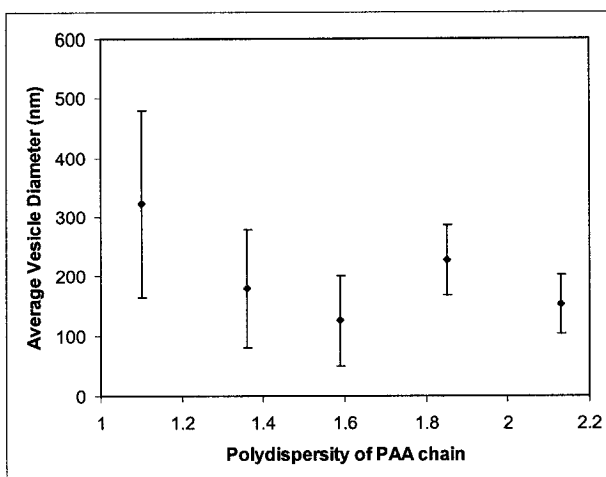


Figure 2-8: Size as a function of polydispersity for vesicles in the dioxane system. The first point is courtesy of Choucair et al.<sup>38</sup>

#### 2.3.4 Is There Segregation of Different Polymers into Different Aggregates?

One question of interest is whether there is a segregation of the individual components into different aggregates. The fact that the sizes of the vesicles change supports the hypothesis that there is mixing of the polymers before they self-assemble. Supplemental evidence for the mixing of the copolymers can be found by looking at the aggregates formed by the individual copolymers by themselves and comparing them with the aggregates formed from the mixtures under the same conditions.

The partial phase diagrams for each individual copolymer are shown in figure 2-9. Under the conditions at which the mixtures were made (15% water), only one (the PS<sub>310</sub>-*b*-PAA<sub>36</sub>) of the four copolymers used to prepare the mixtures (the PS<sub>310</sub>-*b*-PAA<sub>28</sub> was not used in any of the blends) formed vesicles by itself. The PS<sub>300</sub>-*b*-PAA<sub>11</sub> formed LCM's,

the PS<sub>300</sub>-*b*-PAA<sub>75</sub> only made spheres and the PS<sub>310</sub>-*b*-PAA<sub>45</sub> produced a mixture of rods and vesicles. When comparing the morphology of each individual copolymer with the resulting morphology of the mixtures that include it, the following is observed: The PS<sub>300</sub>-*b*-PAA<sub>11</sub> was used in all of the mixtures but there were no LCM's observed in the resulting aggregates. This clearly shows that, in the mixtures, none of the aggregates contain PS<sub>300</sub>-*b*-PAA<sub>11</sub> exclusively. The PS<sub>300</sub>-*b*-PAA<sub>11</sub> would be the most likely to form aggregates by itself since the hydrophilic block is the shortest. The average size of the vesicles formed by only the PS<sub>310</sub>-*b*-PAA<sub>36</sub> was 125±40 nm.<sup>39</sup> The mixtures that contain the PS<sub>310</sub>-*b*-PAA<sub>36</sub> form vesicles with different average sizes (i.e. the vesicles made from the PAA PDI 1.37 mixture have an average diameter of 180±100 nm), therefore, as mentioned above, the copolymers must be mixing in order for us to observe such a difference in size. In the mixtures containing the PS<sub>310</sub>-*b*-PAA<sub>45</sub> no rods were observed, showing that none of the aggregates in the mixtures contain only the PS<sub>310</sub>-*b*-PAA<sub>45</sub>. At a PAA PDI of 1.59 no spheres were observed, which implies that none of the aggregates in the mixture contain only PS<sub>300</sub>-*b*-PAA<sub>74</sub>. A further example for the evidence of mixing of the polymers is seen for PAA PDI of 2.13. Vesicles and spheres are observed; however, neither the PS<sub>300</sub>-*b*-PAA<sub>11</sub> nor the PS<sub>300</sub>-*b*-PAA<sub>74</sub> (the only two components in the mixture) made vesicles by themselves; therefore, the polymers must be mixing in order to form vesicles.

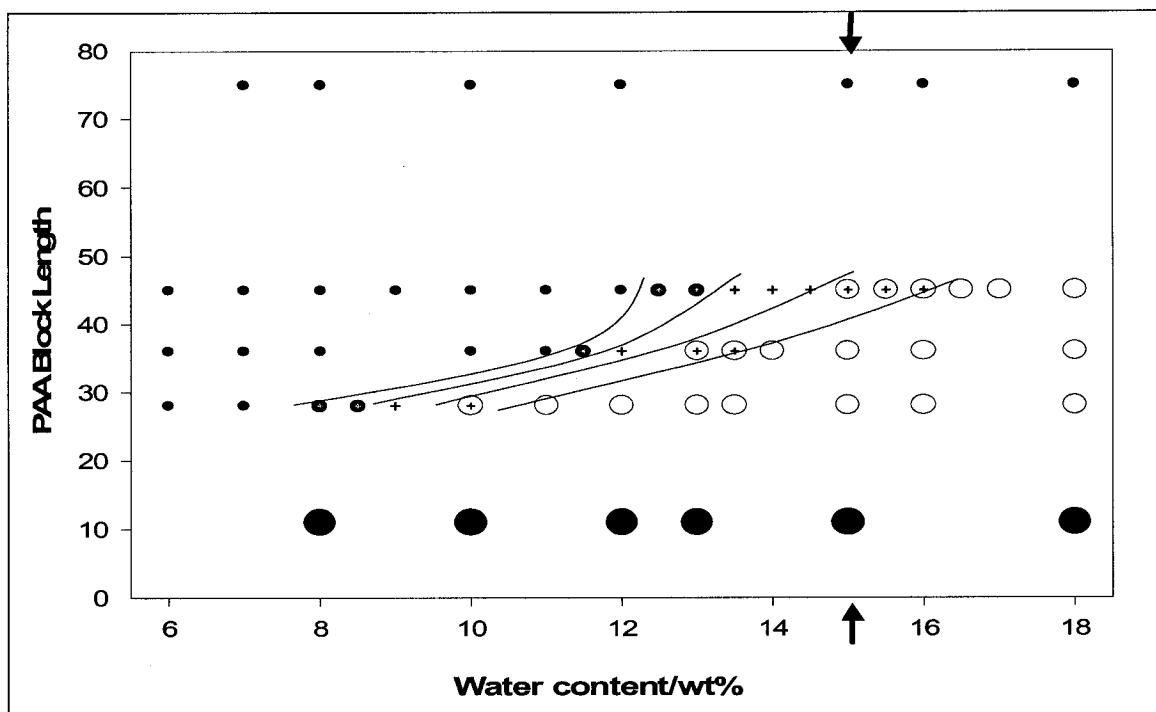


Figure 2-9: Partial phase diagram of individual copolymers. - ● Large compound micelles; • - Spheres; ● - Spheres and rods; + - Rods; ⊕ - Rods and vesicles; O - Vesicles. The arrows indicate the conditions at which the mixtures were made.

## 2.4 CONCLUSIONS

The effect of the corona block polydispersity was investigated on the morphology and size of PS-*b*-PAA vesicles by using samples with artificially broadened PAA block length distributions. The vesicle size was generally found to decrease with increasing PAA PDI, the magnitude of the change increasing with increasing PAA PDI. The decrease in vesicle size is attributed to the segregation of the smaller chains to the inside of the vesicle bilayer while the longer chains form the outer surface. The polymers used in the mixtures do not segregate into different aggregates, there is only segregation within the aggregate itself, as is evident from the fact that mixtures of polymers give different

morphologies than the individual component copolymers by themselves under identical conditions.

This is the first of a series of investigations of the effect of block length polydispersity on aggregation of PS-*b*-PAA copolymers in solution. Subsequent papers will report on the effect of PAA polydispersity on other regions of the phase diagram, on different mixtures of copolymers of different block lengths but similar polydispersity, and on the effect of broadening the core chain polydispersity.

## 2.5 LINKING TEXT

This chapter presented results on the effect of PAA PDI on the size of vesicles. In the next chapter, the effect of the PAA PDI on spheres, and rods are presented. During these studies spherical micelles were observed at high PAA PDI and water content. The appearance of spheres in a region where only vesicles are usually present prompted a study of PAA PDI on other morphologies. The phase boundaries will also be studied to see if they change with increased PAA PDI.

## 2.6 ACKNOWLEDGEMENTS

The authors thank Dr. Zhao-tie Liu for his help in the phase diagram study and Rhodia, NSERC and FCAR for financial support.

## 2.7 REFERENCES

1. Zhang L.; Eisenberg, A. *Science* **1995**, 268, 1728-1731.



2. Cameron, N. S.; Corbierre, M. K.; Eisenberg, A. *Can. J. Chem.* **1999**, *77*, 1311-1326.
3. Loppinet, B.; Sigel, R.; Larsen, A.; Fytas, G.; Vlassopoulos, D.; Liu, G. *Langmuir* **2000**, *16*, 6480-6484.
4. Schlaad, H; Kukula, H; Smarsly, B; Antonietti, M; Pakula, T. *Polymer* **2002**, *43*, 5321-5328.
5. Becker, M. L.; Remsen, E. E.; Wooley, K. L. *J. Polym. Sci., Part A: Polym. Chem.* **2001**, *39*, 4152-4166.
6. Bailey, T.S; Pham, H.D; Bates, F.S. *J. Phys Chem. B.* **2002**, *34*, 6994-7008.
7. Massey, J.; Power, K. N.; Manners, I.; Winnik, M. A. *J. Am. Chem. Soc.* **1998**, *120*, 9533-9540.
8. Wei, L.; Zhang, W.; Chen, Y.; Zhu, M.; Du, F.; Li, Z.; Li, F. *Gaofenzi Xuebao* **2002**, *4*, 548-551.
9. Zhang, L.; Eisenberg A. *Polymers for Advanced Technologies* **1998**, *9*, 677-699.
10. Halperin, A.; Tirrell, M.; Lodge, T.P. *Adv. Polym. Sci.* **1992**, *100*, 31-71.
11. Zhang L.; Eisenberg A. *J. Am. Chem. Soc.* **1996**, *118*, 3168-3181.
12. Shen, H.; Eisenberg, A. *J. Phys. Chem. B.* **1999**, *103*, 9473-9487.
13. Zhang L.; Eisenberg A. *Macromolecules* **1999**, *32*, 2239-2249.
14. Shen, H.; Zhang, L.; Eisenberg, A. *J. Am. Chem. Soc.* **1999**, *121*, 2728-2740.

15. Zhang, L.; Yu, K.; Eisenberg, A. *Science* **1996**, *272*, 1777-1779.
16. Zhang, L.; Eisenberg, A. *Macromolecules* **1996**, *29*, 8805-8815.
17. Zhang, L.; Eisenberg, A. *J.Poly Sci B: Poly. Phys.* **1999**, *37*, 1469-1484.
18. Yu, Y.; Zhang, L.; Eisenberg, A. *Macromolecules* **1998**, *31*, 1144-1154.
19. Desbaumes, L.; Eisenberg, A. *Langmuir* **1999**, *15*, 36-38.
20. Georges, M.K; Hamer, G.K; Listigovers, N.A. *Macromolecules* **1998**, *31*, 9087-9089.
21. Oiu, J.; Charleaux, B.; Matyjaszewski, K. *Progress in Polymer Science* **2001**, *26*, 2083-2134.
22. Linse, P. *Macromolecules* **1994** *27*, 6404-6417.
23. Sommerdijk, N, A, J, M.; Holder, S. J.; Hiron, R. C.; Jones, R. G.; Nolte, R. J. M. *Macromolecules* **2000**, *33*, 8289-8294.
24. Nardin, C.; Hirt, T.; Leukel, J.; Meier, W. *Langmuir*, **2000**, *16*, 1035-1041.
25. Hadziioannou, G.; Skoulios, A. *Macromolecules* **1982**, *15*, 267-271.
26. Zhulina, E.; Birshtein, T. M. *Polymer* **1991**, *32*, 1299-1308.
27. Lin, E. K.; Gast, A. P.; Shi, A.-C.; Noolandi, J.; Smith, S. D. *Macromolecules* **1996**, *29*, 5920-5925.
28. Kane, L.; Satkowski, M. M.; Smith, S. D.; Spontak, R. J. *Macromolecules* **1996**, *29*, 8862-8870.

29. Court, F.; Hashimoto, T. *Macromolecules* **2002**, *35*, 2566-2575.
30. Nguyen, D.; Zhong, X.F.; Williams C.E.; Eisenberg, A. *Macromolecules* **1994**, *27*, 5173-5181.
31. Discher, B. M.; Won, Y.-Y.; Ege, D.S.; Lee, J. C.; Bates, F.S.; Discher, D.E.; Hammer, D.A, *Science*, **1999**, *284*, 1143-1146.
32. Discher, D.E.; Eisenberg, A.; *Science*, **2002**, *297*, 967-973.
33. Kabanov, A.V.; Bronich, T.K.; Kabanov, V.A.; Yu K.; Eisenberg, A. *J. Am. Chem. Soc.* **1998**, *120* 9941-9942.
34. Cameron, N. S.; Eisenberg, A.; Brown, G. R.; *Biomacromolecules* **2002**, *3*, 116-123.
35. Wilczek-Vera, G.; Yu, Y.; Waddell, K.; Danis, P. O.; Eisenberg, A. *Macromolecules* **1999**, *32*, 2180-2187.
36. Luo, L.; Eisenberg, A. *Langmuir* **2001**, *17*, 6804-6811.
37. Stoenescu, R.; Meier, W. *Chem Commun.* **2002**, 3016-3017.
38. Choucair, A.; Eisenberg, A. *to be submitted*.
39. Choucair, A.; Eisenberg, A. *Langmuir* **2003**, *19*, 1001-1008.

## CHAPTER 3

---

### **EFFECT OF POLY(ACRYLIC ACID) BLOCK LENGTH DISTRIBUTION ON POLYSTYRENE-*b*-POLY(ACRYLIC ACID) BLOCK COPOLYMER AGGREGATES IN SOLUTION. 2. A PARTIAL PHASE DIAGRAM.**

---

#### ABSTRACT

The first paper of the series, which focused on the effect of polydispersity on the self-assembly of block copolymer vesicles, showed that an increase in the width of the poly(acrylic acid) (PAA) block length distribution resulted in a decrease in the size of the vesicles formed. In this paper, the rest of the phase diagram is explored. For the present study, a series of polystyrene-*b*-poly(acrylic acid) copolymers of an identical polystyrene length of 325 units but of varying degrees of polymerization of the PAA was synthesized. Mixtures of the copolymers were made to artificially broaden the molecular weight distribution of PAA at a constant number average of 48 in the polydispersity index (PDI) range of 1.1-3.3. The mixtures were dissolved in dioxane, and water was added slowly to predetermined amounts. Transmission electron microscopy was used to observe aggregate morphologies at different water contents and PAA PDIs. At low water contents, dynamic light scattering was also used to measure the sizes of the aggregates. A partial phase diagram as a function of the water content and PAA PDI was obtained. Large compound micelles and spherical micelles (average diameter of 40 nm) were found at low water contents; however, at a water content of 12% (w/w), a continuum of

morphologies from spheres to rods to vesicles was found with increasing PAA PDI. In addition, each copolymer was investigated by itself under identical conditions to those used for the mixtures to determine if there was any segregation of the individual polymers into separate aggregates. No evidence for such segregation was found.

### **3.1 INTRODUCTION**

In the first paper of this series, the effect of corona block length polydispersity on vesicle size was discussed. A general decrease in vesicle size was observed with increased poly(acrylic acid) (PAA) polydispersity index (PDI) as a result of the preferential segregation of short chains to the inner surfaces and long chains to the outer surfaces of the vesicles.<sup>1</sup> As the mixtures became more polydisperse, there were more long and more short chains, allowing for enhanced segregation. Electrostatic charges and steric interactions among the longer chains on the outside of the vesicle caused increased repulsion relative to the lower repulsive interactions among the shorter chains on the inside of the vesicle bilayer. Enhanced segregation allowed for the radius of the vesicle to decrease. Also, at high PAA PDIs ( $>1.85$ ), spherical micelles were found. This fact raised the question whether corona block polydispersity could be a general morphogenic factor, which, in turn, prompted a broader study of the phase diagram for samples with polydisperse coronae.

It had been found that the specific morphology of aggregates of block copolymers can be attributed to a balance of three contributions to the free energy of the system: chain stretching in the core, the interfacial energy, and repulsion among corona chains.<sup>2,3</sup> Any

factors that affect the balance of these three forces will affect the morphology of the resulting aggregates. To date, a number of such factors have been shown to affect the morphology. The most relevant to the present study are summarized in the following.

It is well-known that the relative block length of the corona and core forming blocks of the copolymer can influence the morphology of the resulting aggregates in solution.<sup>4-6</sup> Increasing the polystyrene (PS) block length results in an increased core volume and, therefore, a larger aggregate. By contrast, as the relative amount of PAA increases, the repulsion among corona chains increases; therefore, the increased repulsion of the corona chains will tend to decrease the radius of curvature of the aggregate; increasing the length of the PAA block will result in a transition from vesicles to rods to spheres.

The concentrations of the precipitant<sup>7</sup> (i.e. water) and of the copolymer<sup>8</sup> are morphogenic factors. Phase diagrams<sup>7</sup> have shown that, as the water content increases, the morphologies change from spheres to rods, followed by lamellae or vesicles. This occurs because, with increasing water content, the solvent becomes worse for the core block; therefore, there is an increase in the interfacial energy: the system will attempt to decrease the total interfacial area, and it does so by increasing the core size and decreasing the number of particles. This results in a higher degree of stretching in the core and higher repulsion among corona chains.

The aggregation number ( $N_{agg}$ ) has been found to be proportional to the concentration of the polymer<sup>9</sup>; therefore, as the concentration of the polymer increases,  $N_{agg}$  increases, causing higher repulsion in the corona and a higher degree of stretching in

the core. Thus, a transition from spheres to rods to bilayers is observed with increasing polymer concentration.

More recently, small-molecule surfactants have been shown to change morphologies.<sup>10</sup> The addition of sodium dodecyl sulfate to diblock copolymers in solution can induce changes in morphology from spheres to rods and from rods to vesicles. The nature of the changes is attributed to the screening of the corona block by the surfactant and the incorporation of the hydrophobic tail into the core of the micelle. This allows for a larger aggregation number, which yields a bigger core and, therefore, more stretching of the core chains, which eventually induces a morphological transition.

We have shown in the previous publication that increasing the PAA PDI decreases the vesicle size and eventually causes the appearance of spheres.<sup>1</sup> We now ask whether the PAA PDI is a more general morphogenic factor. This becomes especially relevant because new polymerization techniques<sup>11,12</sup> are giving rise to block copolymers with a range of polydispersities. To take advantage of these newer, cheaper polymers, the effect of polydispersity on self-assembly needs to be explored.

In the past, studies of aggregate morphology in its relation to polydispersity have been made on polystyrene-*b*-polyisoprene<sup>13-17</sup> mixtures in the bulk phase and polystyrene-*b*-poly(methyl methacrylate)<sup>18</sup> thin films. Shi and Noolandi<sup>19</sup> have theorized on the subject of the effect of mixtures of polymers on morphology, while Chun and Han<sup>20</sup> have explored the effect of blending of three different polymers and its effect on morphology. Chang et al.<sup>21</sup> reported seeing different morphologies in the bulk when fractionating a parent copolymer into many smaller fractions with smaller polydispersities. However, these fractions also differed in composition, and, therefore, different morphologies would

be expected because of the different relative block lengths. Studies of PS-*b*-PAA copolymers in the bulk have been reported by Bendejacq et al.<sup>22</sup> They describe the well-ordered microdomain structure obtained from symmetric diblock copolymers with polydispersities greater than 2. Nguyen et al. have explored the effect of polydispersity of the ionic block on the size of the cores of inverse micelles of polystyrene-*b*-poly-4-vinylpyridinium methyl iodide and of polystyrene-*b*-poly(cesium methacrylate). They showed that the sizes of ionic microdomains varied linearly with the polydispersity of the ionic chain; however, if the copolymers micellized far from equilibrium, the polydispersity of the ionic group showed no effect on the sizes of the domains.<sup>23</sup> A wide range of other studies, not necessarily related to polydispersity but relevant to morphologies of block copolymer aggregates in solution, have been reported.<sup>4,5,24-33</sup>

To carry out the present investigation, as before, a series of block copolymers of a narrow molecular weight distribution was synthesized by anionic techniques. The copolymers were then mixed to artificially broaden the molecular weight distribution of the corona-forming (PAA) block while keeping the number average molecular weight ( $M_n$ ) constant, as was done in the previous study. The copolymer mixtures were dissolved in dioxane, and water was added until a predetermined amount was reached. Direct observations of the morphologies were made by transmission electron microscopy (TEM), and the sizes were measured from the electron micrographs. Dynamic light scattering (DLS) was also used to measure the sizes of the aggregates in solution, and the results of the two methods were compared.



## 3.2 EXPERIMENTAL

### 3.2.1 Anionic Synthesis

The polystyrene-*b*-poly(*tert*-butyl acrylate) block copolymers were synthesized by sequential anionic polymerization of styrene followed by *tert*-butyl acrylate (*t*-BuA) using *sec*-butyllithium as the initiator (See Appendix A).<sup>34</sup> A series of diblock copolymers, with the same PS block but with varying degrees of polymerization of poly(*t*-BuA) was synthesized. The diblock copolymers were refluxed in toluene along with *p*-toluenesulfonic acid (catalyst) to convert the poly(*t*-BuA) into PAA.

The degree of polymerization of the homopolystyrene precursor and the polydispersity of the polymers were determined by gel permeation chromatography (GPC). The degree of polymerization of the poly(*t*-BuA) block was calculated from the polymer composition, which had been determined by NMR. The homopolymer and the copolymers had narrow and monomodal molecular weight distributions. (See Appendix C for more detail on the analysis of the polymer characterization) The molecular parameters of the polymers are listed in Table 3-1. The polymers are denoted as PS<sub>*x*</sub>-*b*-PAA<sub>*y*</sub> where *x* and *y* stand for the number average degrees of polymerization of the PS and PAA blocks, respectively. For example, PS<sub>325</sub>-*b*-PAA<sub>48</sub> represents a copolymer containing 325 styrene units and 48 acrylic acid units.

Table 3-1. Characteristics of the Individual Block Copolymers (<sup>a</sup> Assuming that the polydispersity of the second block of the diblock is equal to the polydispersity of a homopolymer of comparable length prepared under similar conditions.)

Polymer	PDI of PS block	PDI of copolymer	PDI of PAA block <sup>a</sup>
PS <sub>325</sub> - <i>b</i> -PAA <sub>10</sub>	1.08	1.10	1.16
PS <sub>325</sub> - <i>b</i> -PAA <sub>48</sub>	1.08	1.09	1.07
PS <sub>325</sub> - <i>b</i> -PAA <sub>58</sub>	1.08	1.08	1.07
PS <sub>325</sub> - <i>b</i> -PAA <sub>124</sub>	1.08	1.08	1.04
PS <sub>325</sub> - <i>b</i> -PAA <sub>210</sub>	1.08	1.12	1.03

### 3.2.2 Fractionation

To remove any homopolystyrene present in the copolymers, a previously developed technique<sup>35</sup> was used. The PS-*b*-PAA polymers were dissolved in tetrahydrofuran (THF; 5% w/w). NaOH (1 M) was added in a 1:1 ratio relative to the acrylic acid content. The solution acquired a bluish color as the inverse micelles with a sodium acrylate core and styrene corona formed. At this point, an aliquot was taken for GPC analysis, which showed two peaks: one for the inverse micelles and one for the homopolymer. The inverse micelle solution was stirred, and water was added dropwise until the solution remained turbid for several minutes after the addition of the last drop. At this point, the solution was left to stand overnight. Two layers were found: the top layer contained the homopolystyrene while the bottom layer contained the inverse micelles, which were heavier and settled to the bottom. The top layer was removed. The bottom layer was dissolved in THF, and GPC analysis was performed again. The process

was repeated until GPC showed only one peak (~4 times). It should be noted that the disappearance of the peak in the GPC chromatogram does not necessarily mean that all of the homopolymer had been removed; it could also mean that the limits of detection of the GPC had been reached. The least detectable amount of PS present in the samples was 1% (w/w); the disappearance of the peak does mean that, if there was any homopolymer present in the samples, there was less than 1% (w/w), which is less than the amount needed to induce any kind of morphological changes.<sup>6</sup> Once the homopolystyrene was removed, the polymer was converted back to acrylic acid by stirring the inverse micelles in a mixture of 15% acetic acid, 5% deionized water, and 80% THF overnight and then precipitated into a mixture of 95% methanol, 4% deionized water, and 1% HCl. This procedure was repeated until there were no micelles detected by DLS.

### 3.2.3 Molecular Weight Distributions

The polydispersity of the PAA block was determined as reported earlier (See Appendix D).<sup>1,23</sup> Figure 3-1 shows the molecular weight distributions of PAA in the family of PS-*b*-PAA copolymers.

Blends were then prepared, keeping  $M_n$  constant but varying  $M_w$  and, thus, the PDI. The detailed compositions are shown in Table 3-2. The molecular weight distribution curves for the blends were obtained by taking the summation of all the distributions of the components in proportion to their ratios in the mixtures. From these distributions,  $M_n$  and  $M_w$  of the blends could be calculated using standard formulas, and their ratio gave the PAA polydispersity of the blend. Appendix D contains the PAA molecular weight distributions of different blends of PS-*b*-PAA copolymers with a constant  $M_n$  of 48 acrylic acid units.

Table 3-2. Blends and Resulting PDIs of the PAA block (<sup>a</sup> Assuming PAA values from Table 3-1 for the individual components).

mol % of PS <sub>325</sub> - <i>b</i> -PAA <sub>10</sub>	mol % of PS <sub>325</sub> - <i>b</i> -PAA <sub>48</sub>	mol % of PS <sub>325</sub> - <i>b</i> -PAA <sub>58</sub>	mol % of PS <sub>325</sub> - <i>b</i> -PAA <sub>124</sub>	mol % of PS <sub>325</sub> - <i>b</i> -PAA <sub>210</sub>	resulting PAA PDI <sup>a</sup>
-----	100	-----	-----	-----	1.07
20	-----	80	-----	-----	1.25
32	-----	56	12	-----	1.58
47	-----	32	23	-----	1.89
56	-----	12	32	-----	2.17
46	-----	42	-----	12	2.46
65	-----	15	-----	20	3.28

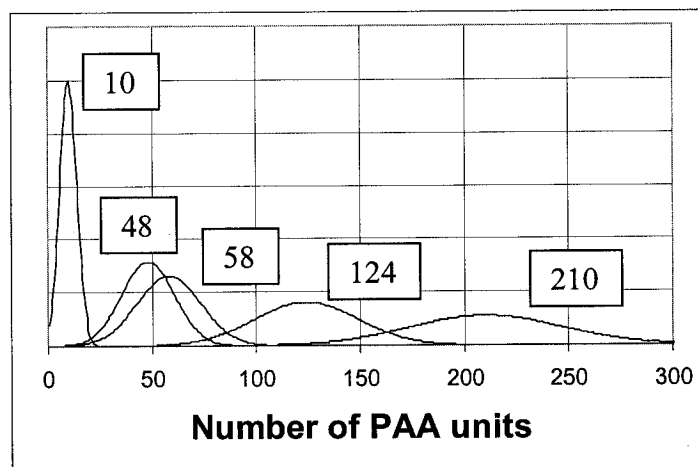


Figure 3-1: Molecular weight distributions of PAA block of individual copolymers assuming that the polydispersity of the block is the same as that of a homopolystyrene of similar length prepared under identical conditions.

### 3.2.4 Preparation of Aggregates

The PS-*b*-PAA copolymer mixtures (1% w/w) were dissolved in dioxane and stirred overnight to obtain single chains in solution. Water was then added slowly [dropwise: one drop/min, which corresponds to ~0.7% (w/w)/min] to a predetermined

final concentration. The aggregates were then stirred overnight to avoid the appearance of transient morphologies. Previous studies have shown that most morphological changes occur within minutes of the water addition;<sup>7</sup> nevertheless, the aggregates were stirred overnight, and this time scale also allowed the elimination of the effect of the rate of stirring. The morphology of the aggregates was then “frozen” by rapidly adding the aggregate solution to an excess of water (5 times the weight of the aggregate solution). Choucair et al.<sup>36</sup> have observed that the morphologies of PS-*b*-PAA aggregates are identical whether they are quenched in water or the dioxane solution is frozen on the TEM grid. The samples were then dialyzed against milli-Q water to remove any remaining dioxane. At this point, the PS was below its glass transition temperature and, therefore, glassy, and without addition of heat or a plasticizer (solvent that was good for the PS) the morphology would not change. This preparation allowed the samples to be in a dilute aqueous solution, which was advisable for two reasons: (1) the particles in the TEM pictures would be separated (concentrated samples make it hard to observe the individual particles) and (2) the dynamic light scattering data analysis is easier in one solvent (water) instead of a mixture (of dioxane and water).

### 3.2.5 Transmission Electron Microscopy

A JEOL 2000FX microscope was used for the TEM studies. The dilute dialyzed samples were deposited on electron microscopy grids that had been precoated with a thin film of Formvar [poly(vinylformaldehyde) plastic] and then coated with carbon. The water evaporated at room temperature overnight, leaving the solid aggregates on the grids. Because the PS was considerably below its glass transition temperature and the dioxane

had been removed by exhaustive dialysis, the morphologies should not have changed as the water evaporated.

### 3.2.6 Dynamic Light Scattering

DLS experiments were performed using a Brookhaven Instruments photon correlation spectrophotometer equipped with a BI-9000AT digital correlator and compass 315M-150 laser (532 nm) from Coherent Technologies. All measurements were made in water at 20 °C. The dilute aqueous aggregate solutions were added to dust-free vials. The Contin algorithm was first used to analyze the data at a detection angle of 90°. Subsequent measurements were made at five different concentrations, ranging from 0.014 to 0.153 g/L, and angles of 35, 60, 90, 105, and 135°. Because the TEM pictures showed mixtures of spherical micelles and large compound micelles (LCMs) for some samples, while other samples had predominately one of the morphologies, both the exponential and the double-exponential algorithms were used to analyze each correlation function obtained. For each concentration and angle, chi-squared was calculated for each algorithm and used as an indication as to which algorithm better represented the experimentally obtained correlation function. For all of the samples, there was no major change in the measured size of the aggregates with a decrease in concentration, indicating that concentration-related errors were absent.

## 3.3 RESULTS AND DISCUSSION

A partial phase diagram of aggregate morphology as a function of water content and PAA PDI, at a constant polymer concentration, was created and is shown in figure 3-2. At every water concentration, a change in the morphology is seen with increasing PAA PDI. Figure 2 shows that the higher the PAA PDI, the lower the water contents at which

morphological boundaries occur. The trend manifests itself in a downward slope of the morphological boundaries above a PAA PDI of about 1.2. There is also a discontinuity in the morphological boundary trend at the PAA PDI  $\sim 1.2$ . This discontinuity occurs between the monomodal sample of the narrowest molecular weight distribution (PAA PDI 1.10) and the first mixture (PAA PDI 1.25). The effect is thought to be due to the shape of the molecular weight distribution of the mixtures. Studies of this effect will be described in a separate paper.

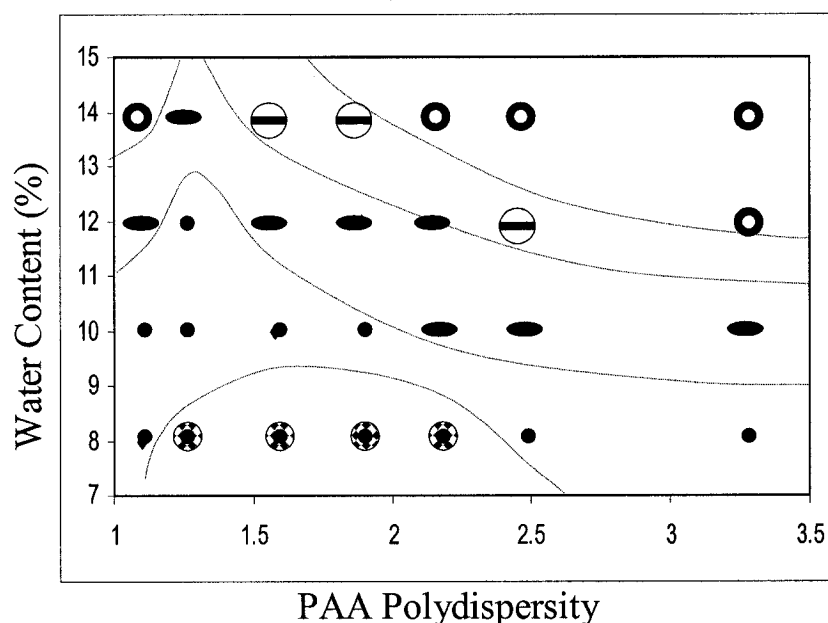


Figure 3-2. Partial phase diagram of PAA PDI and water content for mixtures with a number-average composition of  $\text{PS}_{325}\text{-}b\text{-PAA}_{48}$  at a constant concentration. •spheres,  $\bullet$  rods and spheres,  $\ominus$  rods and vesicles,  $\circ$  vesicles,  $\oplus$  spheres and LCMs. The dotted lines are meant as guides for the trend in the morphological boundaries.

Starting at the lowest water content in the partial phase diagram, the simplest and most common morphology of block copolymer aggregates in solution, the spherical

micelle, was found. At the lowest water contents at which aggregation takes place, spheres are usually observed, regardless of the common solvent or the block lengths of the copolymer; therefore, this study started with observing the effect of PAA PDI on spherical micelles at low precipitant (water) contents. The water content was then increased to observe PAA PDI effects on the rod morphology and the locations of the morphological boundaries between spheres, rods, and vesicles.

Before examining the phase diagram in detail, it is important to make sure that the observed differences in morphology are, in fact, due to mixing of the copolymers, especially because regions of coexistence of morphologies were found for some of the mixtures used in the study. Therefore, the individual copolymers were also explored. This is a similar study to the one performed in the previous paper; however, the copolymers used in this study had different relative block lengths than those used in the previous study, so it was necessary to investigate the polymers in the current study also. In the previous paper, the aggregates of each polymer were observed at a concentration of 1% (w/w) in dioxane, the same concentration as the total polymer in the mixture of copolymers. However, the pure components are present in the mixtures at lower individual concentrations than the total concentration of the copolymer; therefore, in the present study, the aggregates of the pure copolymers were studied under conditions similar to those in the mixture (i.e., at concentrations <1% w/w). For example, the mixture that gave a PAA PDI of 1.25 contained PS<sub>325</sub>-*b*-PAA<sub>10</sub> and PS<sub>325</sub>-*b*-PAA<sub>58</sub> at a total copolymer concentration of 1% w/w. The PS<sub>325</sub>-*b*-PAA<sub>10</sub> was therefore present at a concentration of only 0.2% w/w, so the aggregates formed from the unmixed PS<sub>325</sub>-*b*-PAA<sub>10</sub> were studied at an initial concentration of 0.2% w/w. This difference is important



because the copolymer concentration is important in determining the morphology of the aggregates that self-assemble.

Table 3-3 lists the morphologies of the aggregates found for the individual copolymers at the concentration in each mixture and the resulting morphology of the aggregates of the mixture of copolymers. For example, the PAA PDI 2.46 mixture was made from 46 mol % PS<sub>325</sub>-*b*-PAA<sub>10</sub>, 42 mol % PS<sub>325</sub>-*b*-PAA<sub>58</sub> and 12 mol % PS<sub>325</sub>-*b*-PAA<sub>210</sub>; therefore, the second column of the second to last row of Table 3-3 shows that the PS<sub>325</sub>-*b*-PAA<sub>10</sub>, by itself, formed LCMs and some spheres by itself at a starting concentration of 0.46 mol %. The third column states that the PS<sub>325</sub>-*b*-PAA<sub>58</sub>, by itself, formed spheres and some LCMs at 0.42 mol%, while the fifth column states the aggregates that were formed by the PS<sub>325</sub>-*b*-PAA<sub>210</sub>, by itself, were spheres and some LCMs at a starting concentration of 0.12 mol %. The last column states that the morphology of the aggregates from the self-assembly of the mixture of the copolymers was a mixture of spheres, rods, and vesicles. For low PAA PDI mixtures, there are very few changes in the morphology between the aggregates formed by each of the components of the mixture by themselves and the morphology of the aggregates formed by the mixture. All of the individual components and mixtures form spherical micelles; however, there are no LCMs found in the mixtures even though the individual copolymers formed them. At PAA PDIs above 2.17, larger effects start to be seen. At a PAA PDI of 2.46, rods and vesicles are formed even though the components by themselves make only spheres and LCMs. At PAA PDIs greater than 2.46, the mixtures form only vesicles, while the components still make only spheres and LCMs. The absence of pure component morphologies in the mixtures, along with the presence of morphologies that are not present in the pure components, clearly suggests that the strong segregation of

polymers into different aggregates is absent. This agrees with the observation in the previous paper.

### 3.3.1 Effect of Corona Polydispersity on Spheres at a Low Water Content (8% w/w)

Returning to the phase diagram, comparison micrographs of the spherical particles that were observed at 8% (w/w) water for the systems with different PDI values are shown in Figure 3-3. At the lowest PAA PDI of 1.10, the monomodal molecular weight sample, only primary spherical micelles were observed; however, LCMs were seen in all of the mixtures. This is not an uncommon occurrence at low water contents for crew-cut aggregates with low percentages of PAA (i.e. short PAA block lengths).<sup>37</sup> The very small PAA blocks are small enough to form small pockets of inverse micelles within a PS phase. PAA chains also extend from the polystyrene phase, which keeps the LCM soluble in solution, as described by Zhang et al.<sup>37</sup> It has been suggested that residual homopolystyrene from the synthesis of the copolymers may also contribute to the formation of the LCMs. While this is possible, we believe it is not very likely because the fractionation process has removed most of the homopolystyrene (less than 1% w/w remaining) and Zhang and Eisenberg<sup>6</sup> have shown that the size of spherical micelles did not change when as much as 5% homopolymer was added to micelles.

In the mixture with the lowest PAA PDI (which contained the PS<sub>325</sub>-*b*-PAA<sub>10</sub> and the PS<sub>325</sub>-*b*-PAA<sub>58</sub>), mainly polydisperse LCMs were observed along with a few primary spherical micelles. From the TEM pictures, it appeared, qualitatively, that increasing the PAA PDI from 1.25 to 1.58 resulted in fewer LCMs and more primary spherical micelles (attempts were made to separate the spheres and the LCMs in the data analysis by plotting a histogram of the sizes of all of the measured particles in the sample; however, there was an overlap of size distributions and two distinct populations could not be separated, and

Table 3-3. Morphologies of Each of the Individual Copolymers and the Resulting Morphology from the Mixtures at a Final Water concentration of 12% (w/w) Water in Dioxane.<sup>a</sup>

PAA PDI of the mixture	PS <sub>325</sub> - <i>b</i> -PAA <sub>10</sub> alone		PS <sub>325</sub> - <i>b</i> -PAA <sub>58</sub> alone		PS <sub>325</sub> - <i>b</i> -PAA <sub>124</sub> alone		PS <sub>325</sub> - <i>b</i> -PAA <sub>210</sub> alone		Morphology of mixture
	Morph	Conc (% w/w)	Morph	Conc (% w/w)	Morph	Conc (% w/w)	Morph	Conc (% w/w)	
1.25	LCM, spheres	0.19	spheres, LCM	0.81	N/A	0	N/A	0	spheres
1.58	LCM, spheres	0.32	spheres, LCM	0.57	Spheres	0.1 1	N/A	0	spheres
1.89	LCM, spheres	0.45	spheres, LCM	0.32	Spheres	0.2 3	N/A	0	spheres
2.17	LCM, spheres	0.56	spheres, LCM	0.12	Spheres	0.3 2	N/A	0	spheres
2.46	LCM, spheres	0.46	spheres, LCM	0.42	N/A	0	spheres, LCM	0.12	spheres, rods, vesicles
3.28	LCM, spheres	0.65	LCM, spheres	0.15	N/A	0	spheres, LCM	0.20	vesicles

<sup>a</sup>If two morphologies were present, the dominant morphology is placed first

therefore, quantitative numbers for the ratios of LCMs to spheres were not obtained). The mixtures with PAA PDIs of 1.58, 1.89, and 2.17 all contained the same polymers in the blend but in differing amounts. The sphere-to-LCM ratio seemed to increase with increasing PAA PDI in this series. This increase in PAA PDI was coupled to an increase in the amount of  $\text{PS}_{325}\text{-}b\text{-PAA}_{124}$  within the mixture. A second change in the composition of the mixtures occurred between the PAA PDI of 2.17 and the PAA PDI of 2.46. At this PDI,  $\text{PS}_{325}\text{-}b\text{-PAA}_{210}$  was included in the mixtures. Once again, the sphere-to-LCM ratio seemed to increase. Finally, at a PAA PDI of 3.28, mainly primary spherical micelles were observed. Figure 3-4 contains a plot of the sizes of the spherical particles as measured in the TEM micrographs. With the exception of the PAA PDI 1.25 sample, there is little change in the size of the spherical particles. The lowest PAA PDI sample contains no LCMs, and, therefore, the average particle size is smaller than the average particle size of any of the mixtures of copolymers, which contain mixtures of primary spherical micelles and LCMs. The LCMs in the mixtures had larger radii than the spherical micelles, and it is practically impossible to determine which particles are small LCMs and which are primary spherical micelles; therefore, the average radius of all spherical particles (LCMs and primary spherical micelles) was measured. Because there are actually two overlapping populations of particles of different sizes, the population standard deviation of the average diameter of all of the aggregates was large, which is reflected in the large bars in Figure 3-4. At PAA PDI 1.25 there were mainly LCMs and few spherical micelles observed in the TEM pictures, and that is the reason the average radius is so much larger for this sample than for any of the others.

The apparent change in the ratio of spheres to LCMs can be explained by looking at the compositions of the mixtures. As the PAA PDI increases, there are more long

chains; these longer chains could help to stabilize the spherical micelles and result in fewer LCMs. Aggregates that contain mainly short chains will have very short coronae, and the possibility of forming pockets of PAA in a PS-rich phase will be high. As the PAA PDI is increased, by adding longer chains, the coronae now become larger, as depicted schematically in Figure 3-5. There will be more repulsion between the slightly ionized PAA chains, and the possibility of forming PAA pockets in the PS-rich phase will be less; therefore, LCMs are not favored. Yu et al. have also found that blending of copolymers helped to stabilize polystyrene-*b*-poly(ethylene oxide) copolymers in solution.<sup>38</sup>

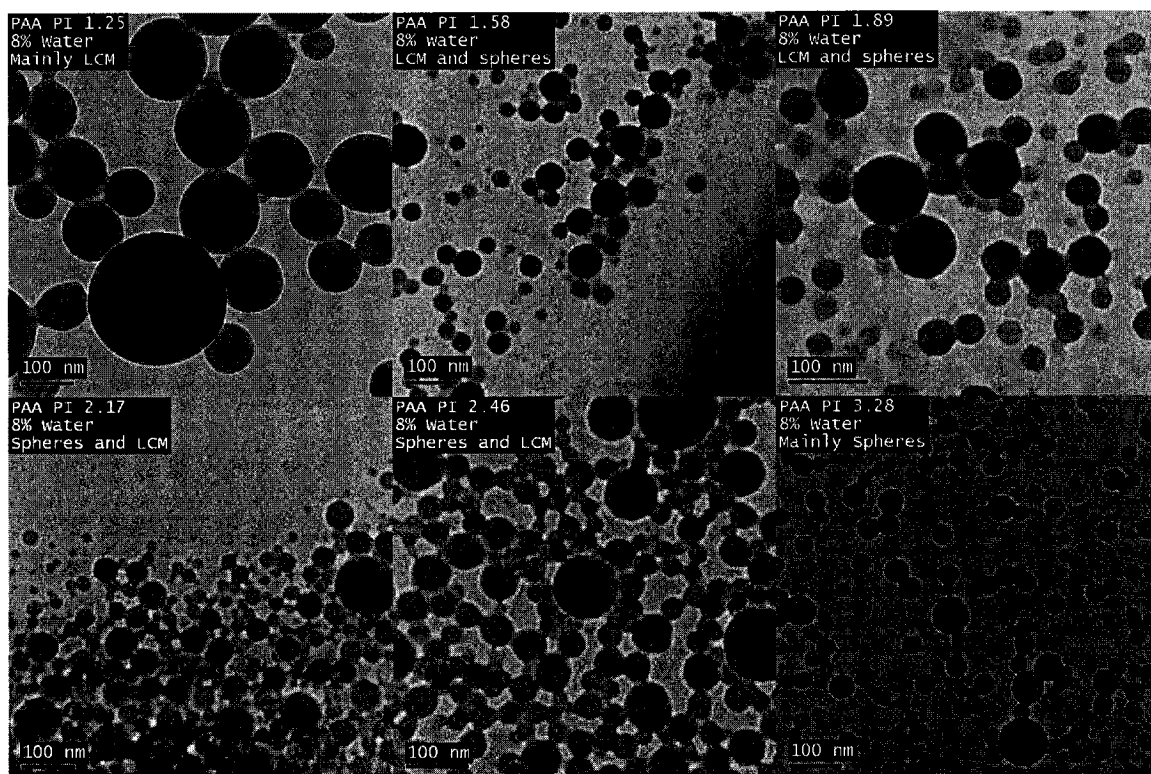


Figure 3-3. Comparison micrographs of spherical aggregates made from mixtures of block copolymers, with an artificially broadened PAA block polydispersity, at 8% water (w/w). The polydispersity of the PAA block increases from 1.25 (a) to 1.58 (b) to 1.89 (c) to 2.17 (d) to 2.46 (e) to 3.28 (f). In all cases, spherical aggregates were observed.

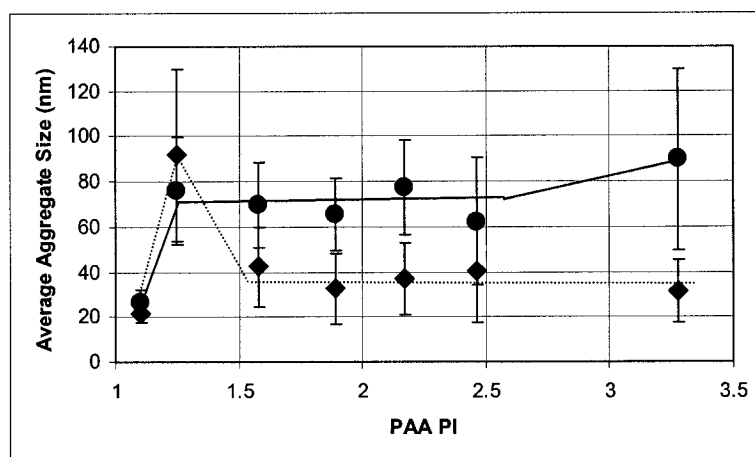


Figure 3-4. Average aggregate diameter (and population standard deviation) as a function of PAA polydispersity, as measured by TEM ( $\blacklozenge$ ) and DLS ( $\bullet$ ). The TEM measurements are an average of 250-300 particles. The DLS measurements are the result of the Contin program (number average) at a detection angle of  $90^\circ$ .

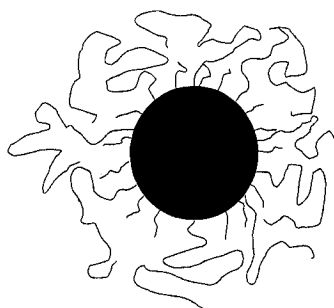


Figure 3-5. Spherical micelle with a polydisperse corona. The longer chains will stretch further away from the core and prevent secondary aggregation or LCM formation.

DLS was also used to determine the size of the spherical particles. When using the Contin algorithm, at a detection angle of  $90^\circ$ , all but one of the averages are higher than those from the corresponding TEM data; this observation is similar to what has been found previously.<sup>1</sup> There are two regions that show unusual differences between the TEM and the DLS data, i.e. at PAA PDIs of 1.25 and 3.28. At PAA PDI 1.25, the average

diameter, as measured by DLS, is smaller than that from the TEM measurement. At this time, we cannot explain this result; it may be due to the limited number of aggregates observed in the TEM Pictures.

The increase in aggregate diameter at high PAA PDI, as measured by DLS can be explained by looking at the mixtures of chains used. From Table 3-1, the mixtures from samples of PAA PDIs greater than three contain relatively high amounts of the PS<sub>325</sub>-*b*-PAA<sub>210</sub> polymer. In solution (as is the case when making DLS measurements), the PAA chains were stretched out to some extent, while a solid aggregate (i.e., as used for TEM) will have collapsed corona chains. As a first approximation to the difference in size, one can calculate the average length of chain in a fully stretched or planar zigzag conformation and compare it with the size of the collapsed corona. For a chain of 210 units, the difference is approximately 50 nm, while for a chain of 58 units, the difference is only 13 nm. Therefore, the aggregates that contain more of the longer chains will have a bigger difference in size between the value in solution and that as a solid aggregate. Because the samples with higher PAA PDI contain more of the longer chains, the difference between the size of the particle in solution and that as a solid will be larger. However, the corona chains are obviously not fully stretched in our case; there are other factors that contribute to the difference between the two measurement techniques.

To obtain more detailed information on the size distribution of the particles, the exponential and double-exponential algorithms were used to analyze the correlation functions for each sample at different angles and concentrations. For samples with only one size, the single exponential should fit better than the double exponential, while mixtures of the two morphologies should have correlation functions best described by the double-exponential algorithm. One drawback to this method is that the aggregates are

very polydisperse in size, as seen in Figure 3-3. Because there is an overlap of the two size distributions, there may or may not be a double-exponential algorithm to best describe a mixture of overlapping size distributions. From the coefficients before each exponential term in the double-exponential algorithm, it might have been possible to calculate the LCM-to-sphere ratio for each PAA PDI; however, due to the polydispersity of the aggregate sizes, a meaningful value would not be obtained. Nonetheless, the data were analyzed to see if there were any patterns that could be found.

The scattering for both the PAA PDI 1.10 and the PAA PDI 1.25 samples was described exclusively by single-exponential functions. For the PAA PDI 1.10 sample, the single-exponential best described the DLS data at all angles, each giving an average diameter of ~20 nm. This corresponds to the TEM pictures, which show mainly spherical aggregates of 20 nm, which was expected for aggregates of a narrow distribution of sizes. For the PAA PDI 1.25 sample, single-exponential algorithms of the correlation functions gave average diameters of ~60 nm. At higher angles, for some of the concentrations, a double-exponential term best described the correlation function. The resulting average diameters were ~50 and 450 nm. The double exponential could be due to the polydispersity of the sizes of the LCM, as observed in the TEM pictures, for this sample. The rest of the PAA PDI mixtures all had a mixture of single-exponential correlation functions and double-exponential correlation functions. The double-exponential correlation functions were observed mainly at high angles of detection, and all of them gave one radius of 30 nm and the other of ~200 nm. This is similar to the mixtures of the LCMs and the spheres as seen in the TEM pictures. The single-exponential correlation functions gave averages of ~70 nm. The single-exponential correlation functions occurred at low angles of detection where the detection of larger particles was more



sensitive. The fact that single-exponential correlation functions best describe the data at low angles is not surprising because the samples contained mixtures of highly polydisperse large particles. At higher angles, the detection of the large particles is not as sensitive and the influence of the spherical micelles predominates with only trace amounts of the LCMs contributing to the overall radius, which results in a single-exponential correlation function.

### 3.3.2 Effect of corona polydispersity on rods

After spherical micelles, the next aggregate in the continuum of morphologies as the water content is increased is the rod. In dioxane, using PS<sub>310</sub>-*b*-PAA<sub>52</sub> copolymers with a low PAA PDI, rods have been found at water contents around 14% (w/w).<sup>7</sup> This study, therefore, used a water content of 14%. In the partial phase diagram above (Figure 3-2) no pure rod region was found; however, at 14% (w/w) water many rods were found in mixtures of morphologies. At a PAA PDI of 1.25, a mixture consisting mainly of rods with a few spheres was observed, as shown in Figure 3-6. As the PAA PDI increased to 1.58 and 1.89, a mixture of vesicles and rods was observed. A further increase in the PAA PDI resulted in vesicles as the only observable morphology.

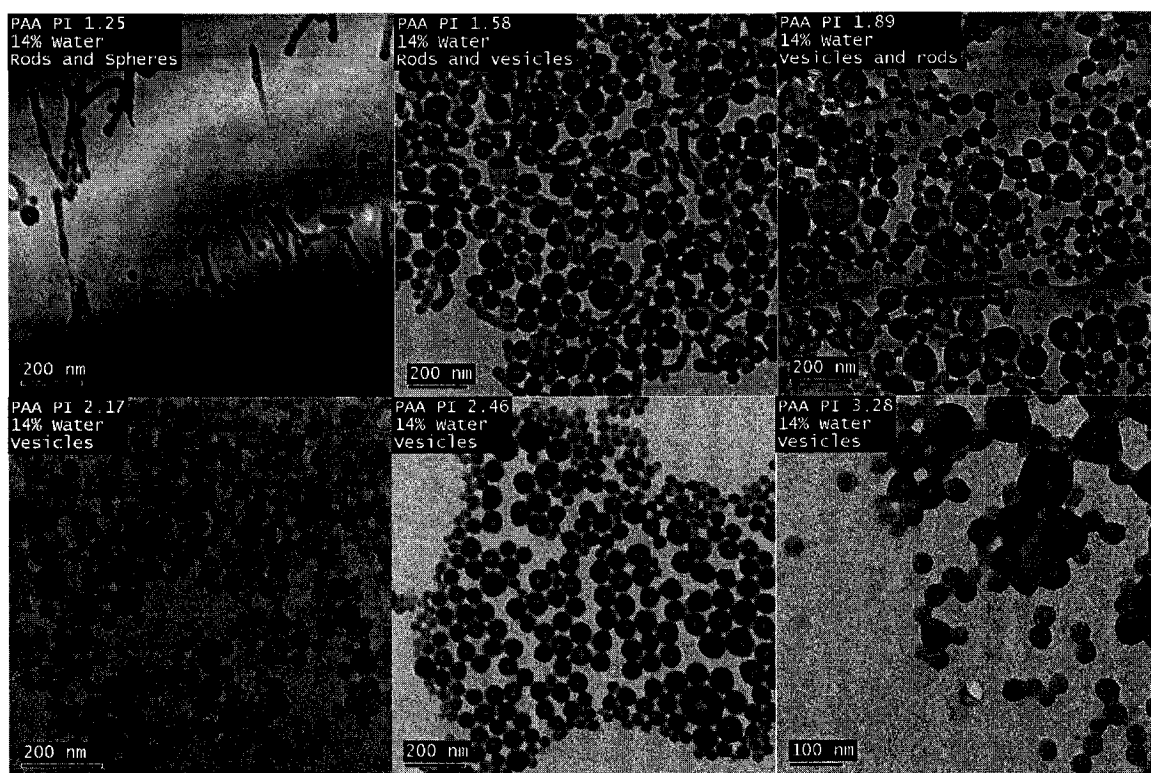


Figure 3-6. Effect of PAA PDI on rods. At 14% water (w/w), at a low PAA PDI of 1.25 rods are observed, and as the polydispersity of the PAA block is increased to 1.58 a mixture of rods and vesicles is observed. A further increase to a PAA PDI of 1.89 shows rods and spheres, while increasing the PAA PDI further to 2.17, 2.46, or 3.28 results in the formation of vesicles.

The change in morphology from rods to vesicles resulting from a change in the PAA PDI brings up another question: can spheres also undergo morphological transitions to rods or even vesicles by an increase in the PAA PDI? A water content of 12% (w/w) was used to obtain spherical micelles at a low PAA PDI. Under these conditions, an increase in PAA PDI from 1.25 to 1.58 resulted in morphological changes from spheres to elongated spheres and rods, and upon a further increase in the PAA PDI to 3.28, a

transition to vesicles took place, as shown in Figure 3-7. At 12% (w/w) water no pure rod region was found.

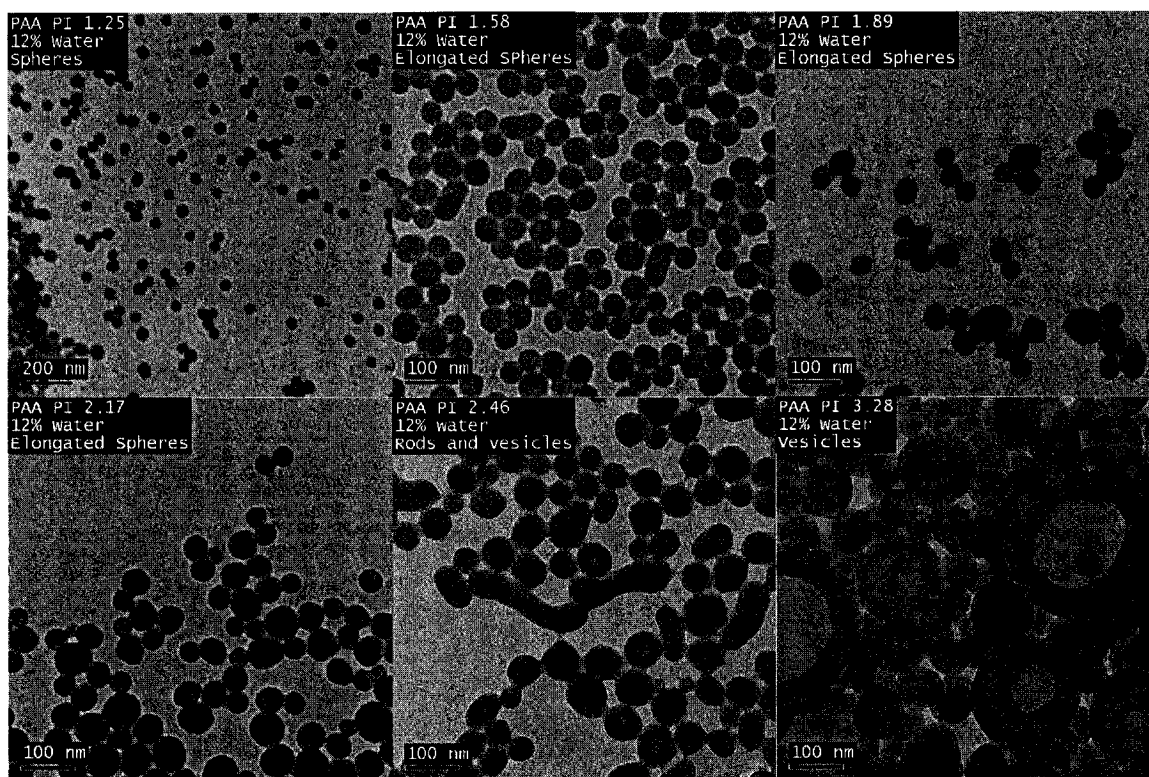


Figure 3-7. Effect of the PAA PDI at 12% water (w/w). The complete range of morphologies from spheres to rods to vesicles is observable. At a low PAA PDI of 1.25, spheres are seen. Increasing the PAA PDI to 1.58, 1.89, and 2.17 shows spheres that are elongated along one axis (i.e., starting to form rods). Vesicles are observed in a mixture of rods and spheres at a PAA PDI of 2.46, while only vesicles are observed at a PAA PDI of 3.28.

The following explanation is suggested for the observed change in morphology as the PAA PDI is increased. Figure 3-8 contains a schematic of the explanation. The short corona chains act as spacers between the long chains; therefore, the steric and electrostatic repulsion of the slightly ionized long PAA chains is diluted. This phenomenon is similar

to the small-molecule surfactant effect,<sup>10</sup> except that the hydrophilic headgroup does not cause shielding of the charge in the corona like the small-molecule surfactants do. As the polydispersity is increased artificially, the number of short chains ( $\text{PS}_{325}\text{-}b\text{-PAA}_{10}$ ) in the mixture increases, allowing a greater separation between the long chains. The long chains, meanwhile, stretch out further from the core-corona interface, and, therefore, the total corona volume is larger for a given number of chains. If the total corona volume is increased but the total average number of corona block units is the same, the overall repulsive interactions per unit volume will be smaller. This allows the aggregation of more copolymer chains. The aggregation of more corona chains causes an increase in the core size of the aggregate, which in turn causes an increase in the degree of stretching of the core chains, which is not entropically favored. The aggregate will elongate, decreasing the average radius, to allow the core chains to be less stretched. This leads to the formation of rods. As the number of chains keeps increasing further, the aggregation number increases, and eventually, a transition from rods to vesicles occurs. The PAA PDI 1.25 mixture contains  $\text{PS}_{325}\text{-}b\text{-PAA}_{10}$  and  $\text{PS}_{325}\text{-}b\text{-PAA}_{58}$  copolymers only. The PAA PDI 1.58 mixture contains the same polymers but also has  $\text{PS}_{325}\text{-}b\text{-PAA}_{124}$  within it. The longer chains are now longer than in the PAA PDI 1.25 mixture, creating a larger corona shell and, therefore, less total corona repulsion and more aggregation, as seen in the last column of Table 3-3 (Appendix E contains the details of how  $N_{\text{agg}}$  was calculated). Increasing the polydispersity to 1.89 and 2.17 results in a slightly higher aggregation number (and, therefore, size); however, the mixtures are made of the same three copolymers (just in different ratios) and, therefore, the corona size should not change drastically. At PAA PDI 2.46,  $\text{PS}_{325}\text{-}b\text{-PAA}_{210}$  is added to the mixture. Once again, the

longer chains are longer than those in the lower PAA PDI mixtures. The corona shell will become bigger, and once again, more aggregation occurs, as seen in Table 3-4.

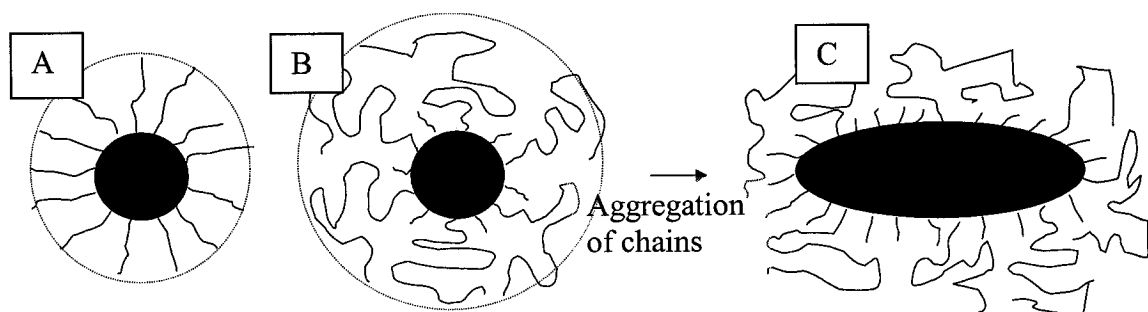


Figure 3-8. Aggregate made of the same number of chains with (A) a monodisperse corona and (B) a polydisperse corona. The dotted lines are guides to the radius of the corona. Chain repulsion in the corona causes curvature in part A. In part B the long chains cause an increase in the corona volume. Since the number of corona units is the same in parts A and B, because  $M_n$  of the corona block is the same, the repulsions per unit volume are smaller in part B; this allows more aggregation of chains. As more chains aggregate, the size of the micelle increases; this also increases stretching of the core chains, which is not entropically favored. Eventually, the micelle will elongate to reduce the stretching of the core chains resulting in an elongated sphere (C).

Table 3-4. Physical Characteristics of Aggregates in 12 % w/w Water<sup>a</sup>

PAA PDI	Morphology	Size (nm) (from TEM)	Volume of PS (nm <sup>3</sup> )	N <sub>agg</sub>
1.10	Sphere	35	21000	380
	Rod	l = 170, d = 35	160000	2800
1.25	Sphere	40	36000	650
1.58	Sphere	45	49000	870
1.89	Sphere	45	49000	870
2.17	Sphere	50	57000	1000
2.46	Sphere	60	130000	2300
	Rod	l = 200, d = 65	610000	11000
	Vesicle	d = 80, t = 25	240000	4200
3.28	Vesicle	D = 147, t = 30	1400000	24000

<sup>a</sup>For rods, l is the length, and d is the diameter of the rod, for vesicles, d is the outer diameter, and t is the wall thickness.

### 3.4 CONCLUSIONS

The effect of the corona block polydispersity on the morphology and size of PS-*b*-PAA aggregates was investigated by artificially broadening the PAA block length distribution. At low water contents, LCMs and primary spherical micelles were observed. An increase in the PAA PDI did not affect the sizes of the spherical micelles; however, the sphere-to-LCM ratio increased with an increase in the PAA PDI. It was found that an increase in the PAA PDI could cause morphological changes to occur at higher water contents. Increasing the PAA PDI (at 12% w/w water) from 1.25 to 2.17 changed the morphology from spheres to spheres and rods, and with even greater PAA PDI (to 3.28) to vesicles. Phase diagram studies of the copolymers used to make the artificially

broadened molecular weight distribution indicated that the aggregates of the pure copolymers, at comparable concentrations, had different morphologies than those in the mixture, suggesting that segregation of the chains into different aggregates was not important, as was also found for vesicles in the previous study. The morphology change with increased PAA PDI was explained by the fact that mixtures of chains of different sizes allow for more chains to aggregate and, thus, the core chain stretching becomes a more important component in the total free energy of the aggregate. To relieve this stress, a morphological change occurs.

### **3.5 LINKING TEXT**

This chapter shows how the PAA PDI can affect spherical micelles and rods. Coupled with chapter two, the effect of the PAA PDI on most of the phase diagram has been explored. One factor that has not been dealt with in these two studies is the fact that the molecular weight distributions are polymodal. While mixing copolymers can increase the PDI, the resulting molecular weight distributions are not one continuous, broad peak. In some cases there are very few, if any, chains of the average degree of polymerization of the PAA block. The following chapter will present studies that involved changing the shape of the molecular weight distribution.

### **3.6 ACKNOWLEDGEMENTS**

The authors thank Rhodia, NSERC and FQRNT for financial support.

### 3.7 REFERENCES

1. Terreau, O.; Luo, L.; Eisenberg, A. *Langmuir* **2003**, *19*, 5601-5607.
2. Zhang, L.; Eisenberg A. *Polymers for Advanced Technologies* **1998**, *9*, 677-699.
3. Halperin, A.; Tirrell, M.; Lodge, T. P. *Adv. Polym. Sci.* **1992**, *100*, 31-71.
4. Antonietti, M.; Heinz, S.; Schmidt, M.; Rosenauer, C. *Macromolecules* **1994**, *27*, 3276-3281.
5. Svensson, B.; Olsson, U.; Alexandridis, P. *Langmuir* **2000**, *16*, 6839-6846.
6. Zhang, L.; Eisenberg A. *J. Am. Chem. Soc.* **1996**, *118*, 3168-3181.
7. Shen, H.; Eisenberg, A. *J. Phys. Chem. B.* **1999**, *103*, 9473-9487.
8. Zhang, L.; Eisenberg, A. *Macromolecules* **1999**, *32*, 2239-2249.
9. Zhang, L.; Eisenberg, A. *Polym. Adv. Technol.* **1998**, *9*, 677-699.
10. Burke, S. E.; Eisenberg, A. *Langmuir* **2001**, *17*, 8341-8347.
11. Georges, M. K.; Hamer, G. K.; Listigovers, N. A. *Macromolecules* **1998**, *31*, 9087-9089.
12. Oiu, J.; Charleaux, B.; Matyjaszewski, K. *Progress in Polymer Science* **2001**, *26*, 2083-2134.
13. Hadziioannou, G.; Skoulios, A. *Macromolecules* **1982**, *15*, 267-271.
14. Zhulina, E.; Birshtein, T. M. *Polymer* **1992**, *33*, 2750-2756.



15. Lin, E. K.; Gast, A. P.; Shi, A.-C.; Noolandi, J.; Smith, S. D. *Macromolecules* **1996**, *29*, 5920-5925.
16. Kane, L.; Satkowski, M. M.; Smith, S. D.; Spontak, R. J. *Macromolecules* **1996**, *29*, 8862-8870.
17. Court, F.; Hashimoto, T. *Macromolecules* **2002**, *35*, 2566-2575.
18. Mayes, A. M.; Russell, T. P.; Deline, V. R.; Satija, S. K.; Majkrzak, C. F. *Macromolecules* **1994**, *27*, 7447-7453.
19. Shi, A.-C.; Noolandi, J. *Macromolecules* **1995**, *28*, 3103-3109.
20. Chun, S. B.; Han, C. D. *Macromolecules* **2000**, *33*, 3409-3424.
21. Park, S.; Cho, D.; Ryu, J.; Kwon, K.; Lee, W.; Chang, T. *Macromolecules* **2002**, *35*, 5974-5979.
22. Bendejacq, D.; Ponsinet, V.; Joanicot, M.; Loo, Y.-L.; Register, R. A. *Macromolecules* **2002**, *35*, 6645-6649.
23. Nguyen, D.; Zhong, X. F.; Williams C. E.; Eisenberg, A. *Macromolecules* **1994**, *27*, 5173-5181.
24. Baines, F. L.; Armes, S. P.; Billingham, N. C.; Tuzar, Z. T. *Macromolecules* **1996**, *29*, 8151-8159.
25. Liu, F.; Liu, G. *Macromolecules* **2001**, *34*, 1302-1307.
26. Raez, J.; Manners, I.; Winnik, M. *J. Am. Chem. Soc.* **2002**, *124*, 10381-10395.

27. Kalinina, O.; Kumacheva, E. *Macromolecules* **1999**, *32*, 4122-4129.
28. Booth, C.; Attwood, D. *Macromol. Rapid Commun.* **2000**, *21*, 501-527.
29. Talingting, M. R.; Munk, P.; Webber, S. E.; Tuzar, Z. *Macromolecules* **1999**, *32*, 1593-1601.
30. Nardin, C.; Hirt, T.; Leukel, J.; Meier, W. *Langmuir* **2000**, *16*, 1035-1041.
31. Stepanek, M.; Podhajecka, K.; Tesarova, E.; Prochazka, K.; Tuzar, Z.; Brown, W. *Langmuir* **2001**, *17*, 4240-4244.
32. Gohy, J.-F.; Antoun, S.; Jerome, R. *Macromolecules* **2001**, *34*, 7435-7440.
33. Choucair, A.; Eisenberg, A. *Eur. Phys. J. E.* **2003**, *10*, 37-44.
34. Cameron, N. S.; Eisenberg, A.; Brown, G. R. *Biomacromolecules* **2002**, *3*, 116-123.
35. Shen, H.; Zhang, L.; Eisenberg, A. *J. Phys. Chem. B.* **1997**, *101*, 4697-4708.
36. Choucair, A.; Kycia, A.; Eisenberg, A. *Langmuir*, **2003**, *19*, 1001-1008.
37. Zhang, L.; Eisenberg, A. *Science* **1995**, *268*, 1728-1731.
38. Yu, K.; Bartels, C.; Eisenberg, A. *Langmuir* **1999**, *15*, 7157-7167.

## CHAPTER 4

---

### **EFFECT OF POLY(ACRLIC ACID) BLOCK LENGTH DISTRIBUTION ON POLYSTYRENE-*b*-POLY(ACRYLIC ACID) BLOCK COPOLYMER AGGREGATES IN SOLUTION. 3. THE SHAPE OF THE MOLECULAR WEIGHT DISTRIBUTION CURVE**

---

#### ABSTRACT

Two factors were studied in their relation to the effect of the corona block polydispersity on the aggregation of polystyrene-*b*-poly(acrylic acid) diblock copolymers in solution. The modality of the molecular weight distribution was found to have a significant effect on the morphology of the aggregates. The extent of the changes in morphology, which had been reported previously<sup>1</sup>, was diminished when using a molecular weight distribution that more closely mimicked a unimodal distribution of similar polydispersity. In order to mimic the unimodal distribution, the molecular weight distributions were altered by the addition of the diblock copolymer PS<sub>325</sub>-*b*-PAA<sub>48</sub>, which had the same average corona block length as that of the mixtures. It was found that the addition of large amounts of the PS<sub>325</sub>-*b*-PAA<sub>48</sub> copolymer resulted in the morphologies of the aggregates looking similar to those obtained with the narrow distribution, monomodal samples. While the molecular weight distribution was found to influence morphologies, a separate study indicated that the relative molecular weight of the blocks still had a greater effect. Attempts to form rods and vesicles from mixtures which had bimodal molecular weight distributions but, in which the average poly(acrylic acid) block

lengths were higher than 15% acrylic acid as compared to the styrene block, were unsuccessful. The molecular weight distribution affected the morphology only when the relative average molecular weight of the poly(acrylic acid) block was small enough to allow multiple morphologies for samples of monomodal, narrow molecular weight distribution polymers.

#### **4.1 INTRODUCTION**

Block copolymer aggregates in solution have been receiving considerable attention recently, both academically<sup>2-6</sup>, and because of the potential applications in areas such as drug delivery<sup>7-9</sup>, separations<sup>10</sup>, and catalysis<sup>11</sup>. The different morphologies afforded by aggregation of block copolymers in selective solvents can potentially be tailored for specific uses. For example, primary spherical micelles could be used for the delivery of hydrophobic drugs, while a vesicular aggregate could be used to deliver a hydrophilic drug or as a dual delivery system with a hydrophobic drug solubilized in the vesicle wall while a hydrophilic drug is encapsulated in the center of the vesicle. In order to fully utilize such aggregates, we must be able to understand and control the self-assembly process.

Many factors have been found to influence the aggregation of block copolymers, as reported earlier<sup>12</sup>. Some of these (such as polymer concentration, amount of precipitant added to the solution, and the presence of additives) are relatively easy to control. Other factors depend more on the physical properties of the copolymer itself, and, thus, require greater effort for effective control. Molecular weight is one such factor; while the

molecular weight is controllable, it is not as easy to vary as solution parameters such as water content or polymer concentration. The block length polydispersity index (PDI) is a variable that normally changes from polymer to polymer depending on many factors, such as the synthetic method and the specific conditions of the synthesis. Newer polymerization techniques are being used to produce block copolymers. While these techniques are more versatile and potentially afford cheaper production of block copolymers than older techniques, such as anionic polymerization, the newer materials often have increased molecular weight distributions.<sup>13</sup> Block length polydispersity has been shown to affect polymer behaviour such as the steady shear response,<sup>14</sup> the self-assembly of polypeptide molecules on charged surfaces,<sup>15</sup> and in some cases the absorption of copolymers onto surfaces.<sup>16,17</sup> More recently, Matsushita et al. have shown that the microdomain spacing of PS-*b*-poly(2-vinylpyridine) increases with an increase in the polydispersity of either block.<sup>18</sup> Understanding the effect of block length polydispersity on the self-assembly of aggregates will allow a wider range of copolymers to be potentially available for the various applications.

In the first study of this series, the effect of corona block length PDI on vesicle size was investigated. A general decrease in vesicle size was observed with increased poly(acrylic acid) (PAA) PDI. The increase in the PDI was coupled to an increase in both the number of short chains (i.e. chains shorter than the number average block length) and the number of chains longer than the average block length. Since the long chains preferentially segregate to the outside surface of the vesicle, there is more repulsion between the chains on the outer surface than the inner surface. The smaller chains that segregate to the inside of the vesicle wall will not take up as much space as the chains on

the outside and the combination of these two factors causes a decrease in the vesicle radius.<sup>19</sup> The second study showed that morphologies could be changed from spheres to rods and eventually to vesicles with an increase in the PAA PDI.<sup>1</sup> In both studies, mixtures of polymers with identical polystyrene (PS) blocks, but varying PAA block lengths were used to broaden artificially the polydispersity of the PAA block. This created bimodal, or in some cases, even trimodal distributions of PAA block lengths in the mixtures. Jain and Bates<sup>20</sup> used bimodal distributions to artificially increase the polydispersity of the corona forming block and have found morphologies that were not prevalent in systems composed of the nearly monodisperse copolymers. The presence of multiple peaks in the molecular weight distribution raises the question of the effect of multiple peaks in the molecular weight distribution on self-assembly properties of the copolymer. This is particularly relevant to the polymers produced by techniques that give one, broad, monomodal peak and comparing the aggregates they make with those made by mixtures of copolymers. To understand better the nature of the underlying factors that create the effects of the polydispersity of the corona block on self-assembly, a study of the shape of the molecular weight distribution is necessary.

The effect of mixtures of two monodisperse block copolymers on morphologies in the melt has been treated theoretically by Dan and Safran.<sup>21</sup> Three self-adjusting quantities were found to determine the structure of a bilayer with a given curvature: the surface density of the inner monolayer, the surface density of the outer bilayer and the compositional difference between the two monolayers. This was calculated using mixtures of two diblocks in which the core-forming block was identical. In this study they also show that when demixing of the chains occurs, vesicles are preferred over

bilayers. Since Luo et al.<sup>22</sup> have shown that there is segregation of the chains within vesicles in solution, a mixture of two copolymers should result in stable vesicular morphologies. The previous report<sup>1</sup> showed a movement of the rod – vesicle boundary to lower water contents with increased PAA PDI. This is consistent with the results of Dan and Safran. We now try to distinguish whether the effect is due to the polydispersity or the detailed shape of the distribution of the corona blocks in the mixture.

In order to investigate the effect of a multimodal PAA block length distribution, mixtures of copolymers were used that gave identical number and weight average molecular weights (and thus identical polydispersity indices) but differing z-average molecular weights. The mixtures were then dissolved in dioxane and water was added slowly until predetermined levels had been reached. The resulting morphologies were then compared.

During the study, it became clear that the modality (the number of peaks) of the molecular weight distribution was affecting the morphology of the self-assembled aggregates. This dependence raised the question as to which factor was more important in determining the morphology of the aggregate: the molecular weight, or the molecular weight distribution of the corona block. A second study was performed in order to determine which factor was more effective in controlling the morphology. Using two of the family of copolymers mixtures were made of differing amounts of the two copolymers. Each mixture; therefore, had a different average molecular weight of the corona block, while the PDI of the mixtures was large, and bimodal. The mixtures were self-assembled over a range of water contents to create partial phase diagrams for the two-

copolymer systems. It was found that the relative molecular weight was more important than the PDI of the corona block in determining the morphology of the aggregate.

## 4.2 EXPERIMENTAL

### 4.2.1 Anionic Synthesis

The polystyrene-*b*-poly(*tert*-butyl acrylate) block copolymers that were used in the present study were the same ones as those used in the previous study (See Appendix A for the synthesis)<sup>1</sup>. They were synthesized by sequential anionic polymerization of styrene followed by *tert*-butyl acrylate (*t*-BuA) using *sec*-butyllithium as the initiator.<sup>23</sup> A series of diblock copolymers was prepared, all with the same polystyrene block but of varying degree of polymerization of poly(*t*-BuA) block. The diblock copolymers were refluxed in toluene along with *p*-toluenesulfonic acid (catalyst) to convert the poly(*t*-BuA) into poly(acrylic acid).

The degree of polymerization of the homopolystyrene and the polydispersity of the polymers were determined by GPC. The degree of polymerization of the poly(*t*-BuA) block was calculated from the polymer composition, which had been determined by NMR (Appendix C contains more detailed information on the characterization of the copolymers). The homopolymer and the copolymers had narrow and monomodal molecular weight distributions. The molecular parameters of the polymers are listed in table 4-1. The polymers are denoted as PS<sub>*x*</sub>-*b*-PAA<sub>*y*</sub> where *x* and *y* stand for the number average degrees of polymerization of the PS and PAA blocks, respectively. For example, PS<sub>325</sub>-*b*-PAA<sub>48</sub> represents a copolymer containing 325 styrene units and 48 acrylic acid units.



Table 4-1: Characteristics of the individual block copolymers (\* assuming that the polydispersity of the second block of the diblock is equal to the polydispersity of a homopolymer of comparable length prepared under similar conditions.)

Polymer	PDI of Styrene block	PDI of copolymer	PDI of Acrylic Acid block*
PS <sub>325</sub> -b-PAA <sub>10</sub>	1.08	1.10	1.16
PS <sub>325</sub> -b-PAA <sub>48</sub>	1.08	1.09	1.07
PS <sub>325</sub> -b-PAA <sub>58</sub>	1.08	1.08	1.07
PS <sub>325</sub> -b-PAA <sub>124</sub>	1.08	1.08	1.04
PS <sub>325</sub> -b-PAA <sub>210</sub>	1.08	1.12	1.03

#### 4.2.2 Fractionation

To remove any homopolystyrene present in the copolymers, following the anionic synthesis a previously developed technique<sup>24</sup> was used.

#### 4.2.3 Molecular Weight Distributions

The polydispersity of the PAA block was estimated as reported earlier.<sup>1,25</sup> The molecular weight distributions of the PAA blocks in the family of PS-*b*-PAA copolymers is available in Appendix D.

Blends were then mixed keeping  $M_n$  and  $M_w$  constant and thus the polydispersity index. Using the estimated polydispersity indexes of PAA in table 4-1, the compositions of the mixtures were calculated. The molecular weight distribution curve for the PAA block in the blends was obtained by taking the summation of all the distributions of the components in proportion to their ratio in the mixture. From these distributions,  $M_n$ ,  $M_w$ ,

and  $M_z$  of the blends could be calculated using standard formulas. Mixtures were made to give identical  $M_n$ , and  $M_w$  but differing in  $M_z$ . The molecular weight distributions of these mixtures are shown in figure 4-1. Since the amounts of the very long diblock copolymers in the mixtures were very small, the log of the proportion of the chains with a given block length is plotted vs. the chain block length. This kind of plot allows the amount of the longer chains in the mixture to be more clearly seen in the molecular weight distributions.

Table 4-2: Blends and resulting PDIs of the PAA block

Mol % of PS <sub>325</sub> - b- PAA <sub>10</sub>	Mol % of PS <sub>325</sub> - b- PAA <sub>48</sub>	Mol % of PS <sub>325</sub> -b- PAA <sub>58</sub>	Mol % of PS <sub>325</sub> - b- PAA <sub>124</sub>	Mol % of PS <sub>325</sub> - b- PAA <sub>210</sub>	$M_n$	$M_w$	PAA PDI <sup>a</sup>	$M_z$	PZ
-----	100	-----	-----	-----	48	52	1.1	55	1.1
35	-----	55	35	-----	48	77	1.6	96	2.0
16	80	-----	-----	4	48	77	1.6	130	2.7
48	-----	32	20	-----	48	91	1.9	110	2.3
45	33	-----	22	-----	48	91	1.9	115	2.4
50	-----	41	-----	9	48	115	2.4	178	3.7
40	50	-----	-----	10	48	115	2.4	182	3.8

a assuming PAA values from table 1 for the individual components.

b  $PZ = M_z/M_n$

#### 4.2.4 Preparation of aggregates

The aggregates were prepared by a similar method to those used in the last study.<sup>1</sup> In brief, the dry copolymers were weighed out and mixed in the calculated proportions. The dry mixtures were then dissolved in dioxane (1% w/w). Water was added slowly until a predetermined concentration was reached. At this point the solutions were stirred overnight. The following day, the solutions were quenched by rapid addition into an excess of water. Dialysis was used to remove any remaining dioxane.

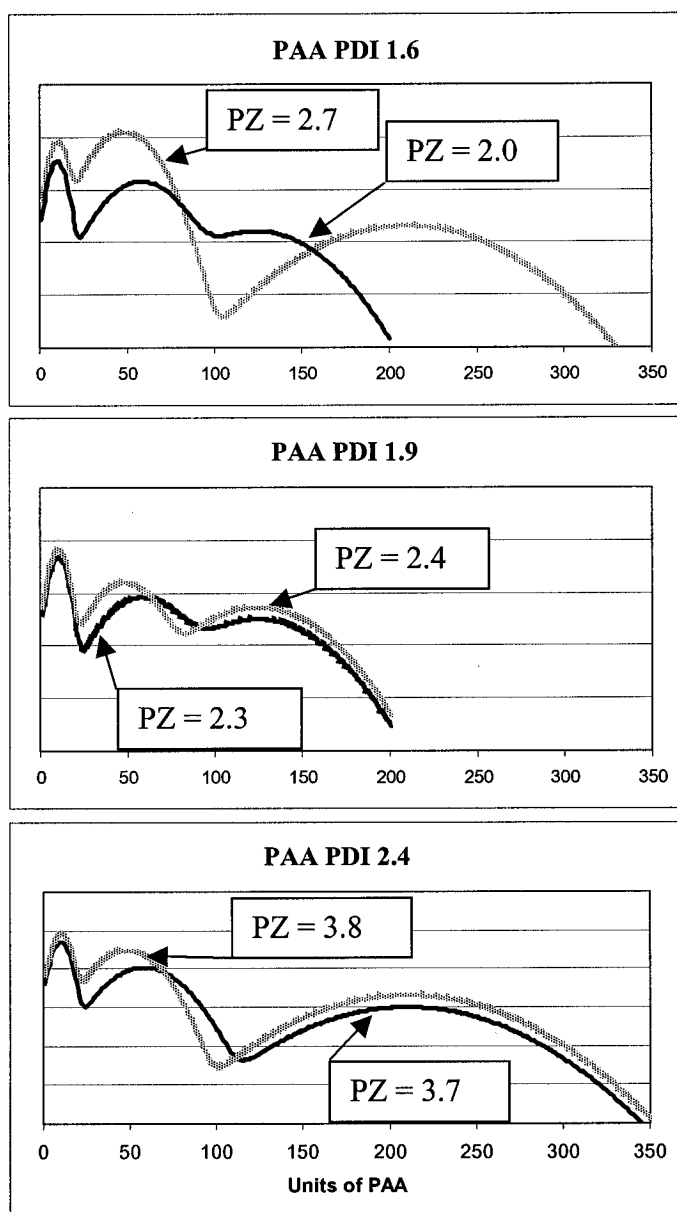


Figure 4-1: Molecular Weight Distributions of PAA block in Mixtures.

#### 4.2.5 Transmission Electron Microscopy

A JEOL 2000FX microscope was used for the transmission electron microscopy (TEM) studies. The dilute dialyzed samples were deposited on EM grids that had been precoated with a thin film of Formvar (poly(vinylformaldehyde) plastic) and then coated

with carbon. The water evaporated at room temperature overnight leaving the solid aggregates on the grids.

## 4.3 RESULTS AND DISCUSSION

### 4.3.1 Molecular Weight Distribution Effects

During the first two studies in this series one question has remained unanswered; how does the shape of the molecular weight distribution of the copolymers affect self-assembly in solution (i.e. does a broad unimodal distribution share the same self-assembly properties as a bimodal mixture of the same PDI)? In order to determine this, mixtures were prepared that had similar number and weight averages but differing z-average molecular weights. The PDI of the two samples were, thus, equivalent.

Since this study contains mixtures of copolymers, which results in polydisperse molecular weight distributions, some care in the use of various terms for describing the molecular weight distributions is needed. The number average molecular weight,  $M_n$ , weight average molecular weight,  $M_w$ , and z-average molecular weights,  $M_z$ , are, respectively, the first, the ratio of the second to the first, and the ratio of the third to the second moments of the molecular weight distribution and are calculated in the same manner as described in any standard polymer textbook. The standard definition of the polydispersity index (PDI) is also used (i.e.  $PDI = M_w/M_n$ ). Since there are mixtures with identical PDIs but made of combinations of different copolymers, thus resulting in different molecular weight distributions, another parameter was needed to distinguish between two different mixtures with identical PDIs. To distinguish the mixtures, the ratio of the z-average molecular weight to the number average molecular weight was calculated and given as PZ.

$$PZ = M_z/M_n \quad (4-1)$$

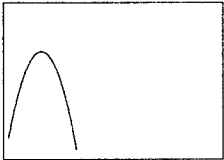
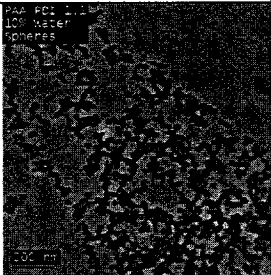
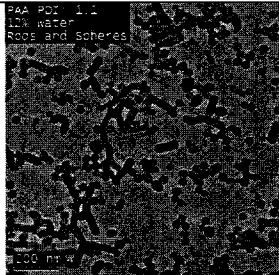
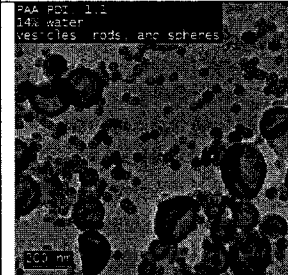
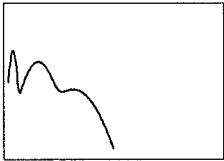
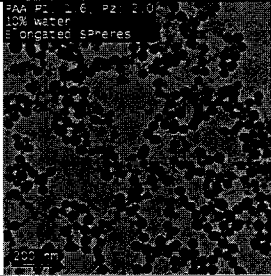
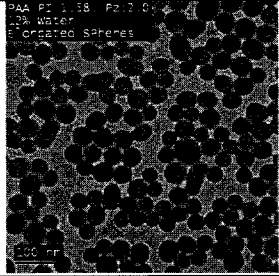
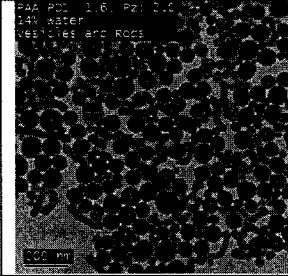
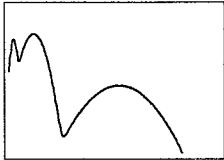
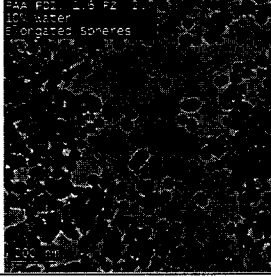
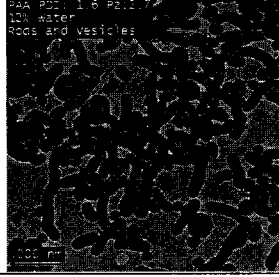
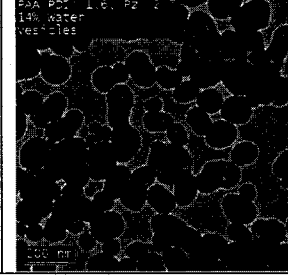
The addition of some of the PS<sub>325</sub>-*b*-PAA<sub>48</sub> copolymer to the binary mixtures that were averaged to 48 units of PAA was an easy way to decrease the polydispersity of the mixture while keeping the number average the same. This also decreased the z-average molecular weight of the mixture. This addition allowed the mixtures to have more components similar to the average and thus was closer to mimicking a unimodal distribution; however, the sample was now a ternary mixture. By adding enough PS<sub>325</sub>-*b*-PAA<sub>48</sub> to the binary mixtures, it was possible to have a resulting PDI that was the same as the ternary mixtures containing combinations of the PS<sub>325</sub>-*b*-PAA<sub>10</sub>, PS<sub>325</sub>-*b*-PAA<sub>58</sub>, PS<sub>325</sub>-*b*-PAA<sub>125</sub>, and PS<sub>325</sub>-*b*-PAA<sub>210</sub> copolymers. This gave samples with identical PDIs but made up of different components, and therefore, different molecular weight distributions. Three different polydisperse samples were studied, with PAA PDI values of 1.6, 1.9, and 2.4. For each PDI two different compositions were used, one that had none of the PS<sub>325</sub>-*b*-PAA<sub>48</sub> and one that did. In all three cases the mixture that contained the PS<sub>325</sub>-*b*-PAA<sub>48</sub> had a larger z-average molecular weight. Table 4-2 contains the compositions of the mixtures, and the resulting number, weight and z-average molecular weights of the samples. The biggest difference between two samples with the same PDI is between the PAA PDI 1.6 samples, while the smallest difference is between the PAA PDI 1.9 samples. Since it was found previously<sup>1</sup> that most morphological boundaries changed around water contents of 10-14%, the same region of water concentration was explored in the current study.

Table 4-3 contains TEM Pictures of the monomodal, narrow distribution sample of PS<sub>325</sub>-*b*-PAA<sub>48</sub> at water contents of 10, 12, and 14 % w/w. Also, pictures of the

aggregates for the polydisperse samples PAA PDI 1.6: PZ 2.0 and 2.7, PAA PDI 1.9: PZ 2.3 and 2.4, PAA PDI: 2.4 PZ 3.7 and 3.8 are presented. The PAA PDI 1.6 PZ 2.0 (where PAA PDI 1.6 PZ 2.0 represents the mixture with a resulting PAA PDI of 1.6 and PAA PZ of 2.0) sample contains none of the  $\text{PS}_{325}\text{-}b\text{-PAA}_{48}$  while the PAA PDI 1.6 PZ 2.7 contains mainly  $\text{PS}_{325}\text{-}b\text{-PAA}_{48}$ . These two samples are very different in composition (as shown in the second column) yet they give the same PAA PDI. The PZ of 2.7 has a higher concentration of components that are closer to the average of 48 units. When looking at the two PAA PDI 1.6 samples, it is seen that the morphology of the aggregates with a higher PZ is similar to the morphology of the aggregates made from the narrow, monomodal distribution (PAA PDI 1.1). The lower PZ sample (of the two PAA PDI 1.6 samples), however, had aggregates of a different morphology. At 12% w/w water there were elongated spheres but no rods. The higher PZ sample and the PAA PDI 1.1 sample both contain rods. At 14% w/w water, a mixture of rods and vesicles was observed for the PZ 2.0 sample, while mainly vesicles were present in the PZ 2.7 sample. Once again, the aggregates formed from the polydisperse sample that was more centered around 48 units of acrylic acid were similar to those in the PAA PDI 1.1 sample.

Two mixtures were made with slightly different compositions for the PAA PDI 1.9 and 2.4 samples. For the PAA PDI 1.9 samples, there were minor differences in the amounts of  $\text{PS}_{325}\text{-}b\text{-PAA}_{10}$  and  $\text{PS}_{325}\text{-}b\text{-PAA}_{124}$  in the mixtures. The major difference is

Table 4-3: TEM Pictures of different molecular weight distributions at different water contents

PAA PDI	PZ	10 % H <sub>2</sub> O (w/w)	12 % H <sub>2</sub> O (w/w)	14 % H <sub>2</sub> O (w/w)
1.1	1.1 			
1.6	2.0 			
	2.7 			

1.9	2.3				
2.4	2.4				
2.4	3.7				
2.4	3.8				



that the PZ 2.3 sample contains PS<sub>325</sub>-*b*-PAA<sub>58</sub> while the PZ 2.4 sample contains PS<sub>325</sub>-*b*-PAA<sub>48</sub> instead. The PZ 2.4 sample has a slightly more symmetrical molecular weight distribution. This slight variation in the composition had no effect on the aggregates formed by each mixture as the TEM pictures in rows 4 and 5 of Table 4-3 illustrate.

In the PAA PDI 2.4 samples, the amounts of PS<sub>325</sub>-*b*-PAA<sub>10</sub> and PS<sub>325</sub>-*b*-PAA<sub>210</sub> are slightly different. As was the case in the PAA PDI 1.9 samples, the main difference between the two PAA PDI 2.4 samples was that one contained PS<sub>325</sub>-*b*-PAA<sub>48</sub> and the other contained PS<sub>325</sub>-*b*-PAA<sub>58</sub>. While the difference in the compositions between the PAA PDI 2.4 samples is bigger than that in the PAA PDI 1.9 samples, the difference is still not big enough to create any changes in morphology in the aggregates, as shown in rows 6 and 7 of Table 4-3. This is not surprising when looking at the overall shape of each mixture in the second column of table 4-3, the PAA PDI 2.4 samples, like the PAA PDI 1.9 samples, are very trimodal and similar to each other.

In order to explain the difference for the PAA PDI 1.6 samples, we must start with the explanation given for the change in morphology with increased polydispersity that was given in the previous report<sup>1</sup>. In the mixtures, the presence of long chains increased the corona thickness, but since the average corona block length was still the same as that for the monomodal sample, the total number of charges was the same. An increase in corona thickness, while keeping the number of charges equivalent, created a decrease in the corona repulsion. This decrease in corona repulsion would allow more chains to aggregate. As more chains are incorporated into the core, its size would increase, and so would the degree of stretching of the core chains. Since, entropically, stretching of polymer chains is not favored, at some critical point the morphology of the aggregate changes to allow the core chains to relax. It should be recalled that the primary cause of

the morphology change is the increase in the corona thickness (i.e. the distance from the core to the outer edge of the corona chains). The compositions of the mixtures in the current study were ternary mixtures with asymmetric, not monomodal molecular weight distributions even if they did contain PS<sub>325</sub>-*b*-PAA<sub>48</sub>. Only one mixture was close to mimicking a monomodal distribution, the PAA PDI 1.6 PZ 2.7 sample. The aggregates made of this sample looked like those found for the narrow, monomodal distribution sample. In the PAA PDI 1.6 PZ 2.0 sample, most of the chains were 48 units long and, therefore, the corona thickness was not increased (compared to the PAA PDI 1.1 sample). This is shown schematically in figure 4-2. Since there are very few long chains in the monomodal yet high PDI sample, the corona thickness is not increased and, therefore, the overall corona repulsion stays the same, and no morphological change occurs. It seems that the polydispersity effect that was reported in the previous study is mainly due to the bimodal (or trimodal) nature of the mixtures. If polymers with increased polydispersity but of a monomodal distribution were to be used in a similar study, it is likely that there would not be a difference in the morphology as compared to narrow distribution samples of the same molecular weight. This would suggest that the newer polymerization techniques that give rise to polymers with broader, yet still monomodal molecular weight distributions should afford aggregates of similar morphology when undergoing self-assembly. Benedejacq et al. have shown that, indeed, PS-*b*-PAA copolymers with PDIs close to 2 will aggregate to form well-ordered microdomain structures in the melt.<sup>26</sup> Our study also shows that mixing copolymers of different corona lengths can be used as a morphological control.

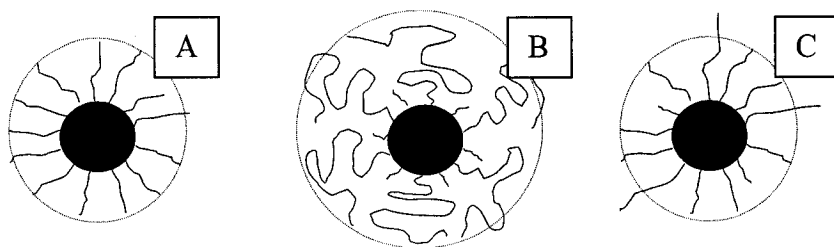


Figure 4-2: Schematic of aggregates made from copolymers with A) a monodisperse corona PDI, B) a polydisperse, bimodal corona PDI, and C) a polydisperse, monomodal PDI. In B the corona volume is larger than either A or C.

#### 4.3.2 Phase Diagrams For Mixtures of Two Polymers

A second question that, until now, had not been dealt with in the previous studies was how universal was the polydispersity effect? It is well known that the relative molecular weight of the diblock copolymer controls the morphology of the aggregates, and above a certain ratio only spherical micelles are formed when the polymer undergoes self-assembly. The previous studies had used mixtures that were averaged to specific PAA block lengths, with length ratios that were small enough to allow multiple morphologies. Could blending of polymers allow multiple morphologies to form from mixtures of copolymers that had a resulting average block length, which, as a monomodal distribution, would not lead to the formation of multiple morphologies? In order to answer these questions, a study was performed using two members of the family of copolymers, those with the shortest and the longest corona block lengths. In the first paper of this series, it was shown that blends of the diblock copolymers with the shortest and longest PAA blocks resulted in the formation of vesicles, even though by themselves, both the shortest and longest diblocks made only primary spherical micelles. In the present study, a partial phase diagram was obtained for blends of the two copolymers, as shown in Figure 4-3. Four mixtures of the two copolymers, dissolved in dioxane, were

made keeping the total polymer concentration the same, but varying the relative amounts of each copolymer. This resulted in four different average lengths of the PAA block, which were calculated and are plotted along the top axis in Figure 4-3. Each mixture also had a bimodal molecular weight distribution. Water was added to each mixture until predetermined levels had been reached, and the morphologies were compared for each mixture.

Starting from the left side of Figure 4-3, the pure  $\text{PS}_{325}\text{-}b\text{-PAA}_{210}$  makes only primary spherical micelles. As the amount of  $\text{PS}_{325}\text{-}b\text{-PAA}_{10}$  increases from 0% to 60% the only observable morphology is still only primary spherical micelles. It is only at a composition of 80% of the  $\text{PS}_{325}\text{-}b\text{-PAA}_{10}$  in the mixture that any kind of morphological change occurs, at which point vesicles are observed. The average copolymer composition is  $\text{PS}_{325}\text{-}b\text{-PAA}_{50}$  at this point. This is an average composition with a short enough corona-forming block to be in the crew cut region. At 100%  $\text{PS}_{325}\text{-}b\text{-PAA}_{10}$  large compound micelles (LCMs) are observed; LCMS have generally been seen for copolymers with very short corona blocks. The fact that morphological transitions occur only when the average PAA block length is  $< 60$  repeat units, which corresponds to a relative PAA molecular weight of  $\sim 15$  mol %, indicates that the polydispersity effect can only cause changes in morphology in areas where the relative average block length is small enough.

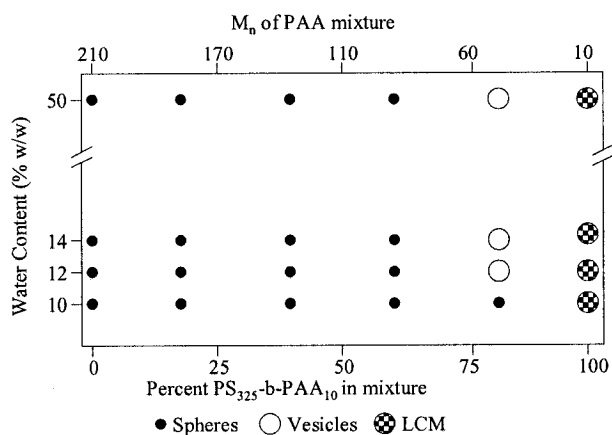


Figure 4-3: A two-polymer phase diagram for mixtures of PS<sub>325</sub>-b-PAA<sub>10</sub> and PS<sub>325</sub>-b-PAA<sub>210</sub>.

Two component phase diagrams for mixtures of the PS<sub>325</sub>-b-PAA<sub>10</sub> / PS<sub>325</sub>-b-PAA<sub>124</sub> system and the PS<sub>325</sub>-b-PAA<sub>124</sub> / PS<sub>325</sub>-b-PAA<sub>210</sub> were also explored, and shown in figure 4-4. The phase diagram of the PS<sub>325</sub>-b-PAA<sub>10</sub> / PS<sub>325</sub>-b-PAA<sub>124</sub> system was similar to the PS<sub>325</sub>-b-PAA<sub>10</sub> / PS<sub>325</sub>-b-PAA<sub>210</sub> phase diagram, in that morphology changes were only seen when the average relative PAA block length was again short enough to place the block in the crew cut region. The PS<sub>325</sub>-b-PAA<sub>124</sub> / PS<sub>325</sub>-b-PAA<sub>210</sub> system showed no changes in morphology, spherical micelles were found throughout the phase diagram. These two partial phase diagrams confirm that while mixing block copolymers with different PAA chain lengths can cause changes in morphology, the average block length of the mixture must still be small enough to be able to form crew cut micelles.

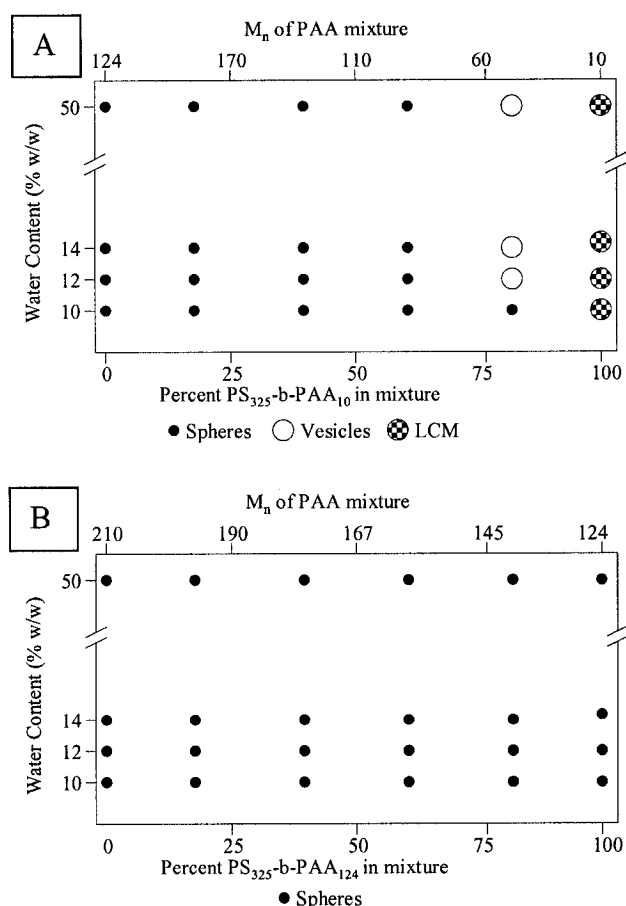


Figure 4-4: Two-polymer phase diagrams of the: A)  $PS_{325}$ -b- $PAA_{10}$  /  $PS_{325}$ -b- $PAA_{124}$  system, and B)  $PS_{325}$ -b- $PAA_{124}$  /  $PS_{325}$ -b- $PAA_{210}$  system.

#### 4.4 CONCLUSIONS

The effect of the shape of the molecular weight distribution of the corona block on the resulting morphologies of self-assembled diblock copolymers was explored. It was found that multimodal molecular weight distributions of the corona block (made from mixtures of diblock copolymers) can change the morphology of the aggregates obtained. It is predicted that a sample with an increased PAA PDI, but with a monomodal molecular weight, will not show the same changes in morphology as mixtures of copolymers with PAA PDI identical to that of the monomodal sample. Attempts were made to use the

bimodality of mixtures of copolymers to obtain more complex architectures, which were not obtainable with monomodal samples of similar number average molecular weight. These studies showed that the average molecular weight of the sample is still the dominant factor in the resulting morphology of the aggregates. The molecular weight distribution of the corona block is only a morphogenic factor when the relative average block length is small enough.

#### 4.5 LINKING TEXT

This chapter completes the presentation of the research on the effect of the PAA molecular weight distribution on the morphology and size of PS-*b*-PAA copolymer aggregates. The next step in the project was to investigate the effect of the molecular weight distribution of PS block on the morphology and size of PS-*b*-PAA aggregates in solution. Chapter 5 presents the results of this research.

#### 4.6 ACKNOWLEDGEMENTS

The authors thank Rhodia, NSERC and FQRNT for financial support.

#### 4.7 REFERENCES

1. Terreau, O.; Bartels, C.; Eisenberg, A. *Langmuir* **2004**, *20*, 637-645.
2. Weaver, J. V. M.; Armes, S. P.; Liu, S. *Macromolecules* **2003**, *36*, 9994-9998.
3. Kelarakis, A.; Havredaki, V.; Yuan, X.-F.; Yang, Y.-W.; Booth, C. *Journal of Materials Chemistry* **2003**, *13*, 2779-2784.

4. Jelinek, K.; Uhlik, F.; Limpouchova, Z.; Matejicek, P.; Humpolickova, J.; Prochazka, K.; Tuzar, Z.; Spirkova, M.; Hof, M. *Molecular Simulation* **2003**, *29*, 655-660.
5. Huang, Y.-Y.; Chen, H.-L.; Hashimoto, T. *Macromolecules* **2003**, *36*, 764-770.
6. Yang, L.; Alexandridis, P.; Steytler, D.C.; Kositza, M.J.; Holzwarth, J.F. *Langmuir* **2000**, *16*, 8555-8561.
7. Lim Soo, P.; Luo, L.; Maysinger, D.; Eisenberg, A. *Langmuir* **2002**, *18*, 9996-10004.
8. Gebhart, C. L.; Kabanov, A. V. *Journal of Controlled Release* **2001**, *73*, 401-416.
9. Harada-Shiba, M.; Yamauchi, K.; Harada, A.; Takamisawa, I.; Shimokado, K.; Kataoka, K. *Gene Therapy* **2002**, *9*, 407-414.
10. Wang, G.; Henselwood, F.; Liu, G. *Langmuir* **1998**, *14*, 1554-1559.
11. Bronstein, L. M.; Chernyshov, D.M.; Karlinsey, R.; Zwanziger, J.W.; Matveeva, V.G.; Sulman, E.M.; Demidenko, G.N.; Hentze, H.-P.; Antonietti, M. *Chemistry of Materials* **2003**, *15*, 2623-2631.
12. Cameron, N. S.; Corbierre, M. K.; Eisenberg, A. *Can. J. Chem.* **1999**, *77*, 1311-1326.
13. Matyjaszewski, K.; Xia, J. *Chem Rev.* **2001**, *101*, 2921-2990.
14. Ma, S., X.; Cooper, S.L. *Macromolecules* **2002**, *35*, 2024-2029.
15. Kitaev, V.; Kumacheva, E. *Langmuir* **1998**, *14*, 5568-5572.



16. Jeong, J.-B.; Kim, J.-Y.; Cha, J.-H.; Kim, J.-D. *Colloids and Surfaces A: Physiochem. Eng. Aspects* **2002**, 207, 161-167
17. Pattanayek, S. K.; Juvekar, V. A. *Macromolecules* **2003**, 36, 956-960.
18. Matsushita, Y.; Inuma, A. N.; Suzuki, J.; Ohtani, H.; Takano, A. *Macromolecules* **2003**, 36, 8074-8077.
19. Terreau, O.; Luo, L.; Eisenberg, A. *Langmuir* **2003**, 19, 5601-5607.
20. Jain, S.; Bates, F.S.; *Macromolecules* **2004**, 37, 1511-1523.
21. Dan, N; Safran, S. A. *Macromolecules* **1994**, 27, 5766-5772.
22. Luo, L.; Eisenberg, A. *Langmuir* **2001**, 17, 6804-6811.
23. Hautekeer, J. P.; Varshney, S. K., Fayt, R.; Jacobs, C.; Jerome, R.; Teyssie, P. *Macromolecules* **1990**, 23, 3893-3898.
24. Shen, H.; Zhang, L.; Eisenberg, A. *J. Phys. Chem. B.* **1997**, 101, 4697-4708.
25. Nguyen, D.; Zhong, X.F.; Williams C.E.; Eisenberg, A. *Macromolecules* **1994**, 27, 5173-5181.
26. Bendejacq, D.; Ponsinet, V.; Joanicot, M.; Loo, Y.-L.; Register, R.A. *Macromolecules* **2002**, 35, 6645-6649.

## CHAPTER 5

---

### **EFFECT OF POLYSTYRENE BLOCK LENGTH DISTRIBUTION ON POLYSTYRENE-*b*-POLY(ACRYLIC ACID) BLOCK COPOLYMER AGGREGATES IN SOLUTION**

---

#### ABSTRACT

The effect of the molecular weight distribution of the core-forming (polystyrene) block on the morphologies resulting from the self-assembly of polystyrene-*b*-poly(acrylic acid) block copolymers in solution was studied. Binary mixtures of block copolymers with similar poly(acrylic acid) blocks, but differing polystyrene (PS) block lengths, were prepared in order to artificially broaden the molecular weight distribution of the PS block while keeping the number average molecular weight constant. This created bimodal molecular weight distributions of the polystyrene block with polydispersities (PDIs) ranging from 1.04 to 2.8. The mixtures of copolymers were dissolved in dioxane, and water was added until a predetermined amount had been reached. The morphologies of the aggregates were then frozen, by quenching into water, and transmission electron microscopy was performed. In contrast to the effect of increasing the poly(acrylic acid) molecular weight distribution, it was observed that the morphology of the aggregates changed from vesicles to spheres with increased polystyrene molecular weight distribution. The change in morphology is attributed to the bimodality of the distributions. Normally, morphological changes from spheres to rods and to vesicles are attributed, in part, to the progressively increasing degree of stretching of the core chains.

In the present case, because of the high polydispersity, a sufficient number of long chains is present to span the distance from the outer interface to the inner core regions to avoid the need for high degrees of stretching. This absence of high degrees of stretching allows the maintenance of the spherical shape.

## 5.1 INTRODUCTION

It is well known that highly asymmetric, amphiphilic block copolymers self-assemble when placed into a selective solvent or when the solvent is made selective by addition of a bad solvent for one block.<sup>1-5</sup> Multiple morphologies of diblock copolymers in solution have been of interest in both academia<sup>6-7</sup> and industry. Possible applications include drug delivery<sup>8-10</sup>, and removal of organic compounds from contaminated water<sup>11</sup>, among others. To utilize such aggregates fully, we must be able to understand and control the self-assembly process.

Many factors have been found to influence the aggregation of block copolymers, as reported earlier<sup>7</sup>. While some factors are relatively easy to control by the addition of chemical species (i.e. acids, bases, solvents, etc), other factors depend more on the physical properties of the copolymer itself. Molecular weight and block length polydispersity (PDI) are variables that vary from polymer to polymer. While the molecular weight is controllable directly, the PDI of the copolymer depends on many factors, such as the synthetic method and the specific conditions of the synthesis. Newer polymerization techniques are more versatile and potentially afford cheaper production of block copolymers than older techniques, such as anionic polymerization; however, the newer techniques often result in an increased molecular weight distribution of the

copolymers.<sup>12-13</sup> Understanding the effect of block length PDI on the self-assembly process will allow a wider range of copolymers to be potentially available for various applications.

Recently, studies of the effect of the corona block PDI on morphology and sizes of block copolymer aggregates in solution have been reported.<sup>14-17</sup> Mixtures of PS-*b*-PAA block copolymers were used to artificially broaden the molecular weight distribution of the corona block, while keeping the number average molecular weight constant. A partial phase diagram of aggregate morphologies as a function of water content and poly(acrylic acid) (PAA) PDI was constructed and showed that increasing the PAA PDI leads to a progressive change in morphology from spheres to rods, and from rods to vesicles.<sup>15</sup> Under conditions where vesicle formation was favored for the copolymers with the smallest PAA PDI, the size of the vesicles formed was found to decrease with increasing PAA PDI.<sup>14</sup> While the PAA PDI was found to influence the morphology of the aggregates, a subsequent study provided evidence that the polydispersity effect was partly due to the shape of the molecular weight distribution.<sup>16</sup> The same study also showed that the polydispersity effect was most evident in samples with an average molecular weight that would allow the formation of so called “crew-cut” aggregates. We now continue to study the effect of block length PDI on self-assembly by investigating mixtures with identical corona blocks but varying core forming blocks.

The effect of the ionic block polydispersity on the size of the resulting microdomains of PS-*b*-poly(methacrylic acid) and PS-*b*-poly-4-vinyl pyridine diblock copolymers in the bulk was studied by Ngyuen et al.<sup>18</sup> They found that the method of preparation affected the degree to which the polydispersity of the ionic core blocks

affected the size of the microdomains. If the microdomains were formed under non-equilibrium conditions (for example by the rapid addition of a non solvent to the single chain diblock solution) then the polydispersity of the ionic block did not affect the size of the microdomains. However, if the microdomain is formed under conditions close to thermodynamic equilibrium, the size of the microdomains was found to increase with increasing ionic block polydispersity. They attribute the increase in the radius to the presence of long chains. The long chains are thought to stretch from the center to the surface of the microdomain, while the smaller chains occupy the regions close to the surface.

Binary mixtures of diblock copolymers have been studied in the bulk.<sup>19-22</sup> Birshstein et al have shown theoretically that the thermodynamic advantage of a mixture of polymers of different lengths grafted onto a planar surface ensures that a single lamellar structure, made from two lamellae-forming diblock copolymers, is thermodynamically stable.<sup>19</sup> They later studied the effect of mixtures of chain lengths grafted to the surfaces of cylindrical domains. They found that the effects of mixing were more pronounced for concave surfaces than for the planar surface.<sup>20</sup> The concave surface means the chains were bidisperse in the domain-forming block. The system described in this chapter is similar, in that only the core-forming blocks of the PS-*b*-PAA diblock copolymers are bidisperse. Birshstein et al also predicted the possibility of forming cylindrical morphologies from mixtures of two lamellae-forming diblock copolymers under suitable conditions.<sup>21</sup> More recently, Court and Hashimoto have provided experimental results on PS-*b*-Poly(isoprene) systems that agree with the theory of Birshstein.<sup>22</sup>

To investigate the effect of a polydisperse PS block length distribution, binary mixtures of copolymers were used that gave identical number average molecular weights but differing weight average molecular weights, and therefore, differing PDIs of the PS block. The PAA block length was kept within narrow limits by selecting polymers with very similar PAA block lengths. The mixtures were then dissolved in dioxane, and water was added slowly until predetermined amounts had been added. The resulting morphologies were then compared by transmission electron microscopy.

## 5.2 EXPERIMENTAL

### 5.2.1 Anionic Synthesis

The polystyrene-*b*-poly(*tert*-butyl acrylate) block copolymers were synthesized by sequential anionic polymerization<sup>23</sup> of styrene followed by *tert*-butyl acrylate (*t*-BuA) using *sec*-butyllithium as the initiator. Tetrahydrofuran (THF) was used as the solvent. The diblock copolymers were refluxed in toluene along with *p*-toluenesulfonic acid (catalyst) to convert the poly(*t*-BuA) into poly(acrylic acid). (See Appendix A for a more detailed description of the polymer synthesis)

The degree of polymerization of the precursor homopolystyrene and the polydispersity of the polymers were determined by GPC. The degree of polymerization of the poly(*t*-BuA) block was calculated from the polymer composition, which had been determined by NMR. (Appendix C contains a more detailed description of the polymer characterization procedures) The homopolymer and the copolymers had narrow and monomodal molecular weight distributions. The molecular parameters of the polymers

are listed in table 5-1. The polymers are denoted as  $PS_x-b-PAA_y$  where  $x$  and  $y$  stand for the number average degrees of polymerization of the PS and PAA blocks, respectively. For example,  $PS_{200}-b-PAA_{20}$  represents a copolymer containing 200 styrene units and 20 acrylic acid units.

Table 5-1: Characteristics of the individual block copolymers.  $D_{ee}$ : End-to-end distance of PS block  $(=(6.76n)^{0.5}l)$ , where  $n$  is the number of styrene repeat units and  $l$  is taken to be 0.25 nm).  $D_s$ : End to end distance of PS block in a fully stretched planar zigzag form  $(=nl)$ .

Polymer	PDI of Styrene block	PDI of copolymer	$D_{ee}$ (nm)	$D_s$ (nm)
$PS_{52}-b-PAA_{20}$	1.06	1.06	4.6	13
$PS_{156}-b-PAA_{20}$	1.06	1.06	8.0	38
$PS_{200}-b-PAA_{20}$	1.04	1.04	9.2	50
$PS_{409}-b-PAA_{20}$	1.04	1.04	13	102
$PS_{660}-b-PAA_{18}$	1.03	1.03	17	165

### 5.2.2 Fractionation

A previously developed technique<sup>24</sup> was used to remove any homopolystyrene present in the copolymers following the anionic synthesis. In brief, in the first step, sodium hydroxide was added to a diblock solution in THF. The resulting sodium acrylate block was not soluble in THF, causing the formation of inverse micelles with poly (sodium acrylate) cores and polystyrene corona chains. The homopolystyrene was not incorporated in the micelles. A small amount of water was added to the solutions and they were left overnight to equilibrate. Two phases were formed, one containing the

inverse micelles and one containing the homopolymer. The homopolymer phase was removed, and an HCl / acetic acid mixture was used to convert the poly (sodium acrylate) back to acrylic acid.

### 5.2.3 Molecular Weight Distributions

The PDI of the precursor PS block was measured by GPC, which had been calibrated using polystyrene standards. In theory the molecular weight distributions of polymers made by anionic polymerization should be of Poisson distribution; however, usually the distribution is somewhat broader than the Poisson, due to the impurities inherently present during the synthetic procedure. A broader form of the Poisson distribution is the Gaussian distribution. The molecular weight distribution of the PS blocks of the copolymers used in this study were assumed to follow Gaussian statistics<sup>18</sup>:

$$f(x) = \frac{1}{(\sigma_n) * (2\pi)^{0.5}} \exp \left[ -\frac{(x - x_n)^2}{2\sigma_n^2} \right] \quad (5-1)$$

where

$$\sigma_n = x_n (PDI - 1)^{0.5}$$

$x_n$  is the average number of units in the PS block, and PDI is the measured polydispersity of the PS block. Figure 5-1 shows the calculated molecular weight distributions of the PS block in the individual copolymers.

Binary blends were then prepared keeping  $M_n$  constant but varying  $M_w$  and thus the PS PDI. The molecular weight distribution curve for the blends was obtained by taking the summation of all the distributions of the components in proportion to their ratio in the mixture.<sup>18</sup> From these distributions,  $M_n$  and  $M_w$  of the blends could be calculated



using standard formulas, and their ratio gave the PS polydispersity of the blend. Figure 5-2 shows PS molecular weight distributions of different blends of PS-*b*-PAA copolymers with a constant  $M_n$  of 200 styrene units, while table 5-2 contains the amount of each copolymer in the mixtures.

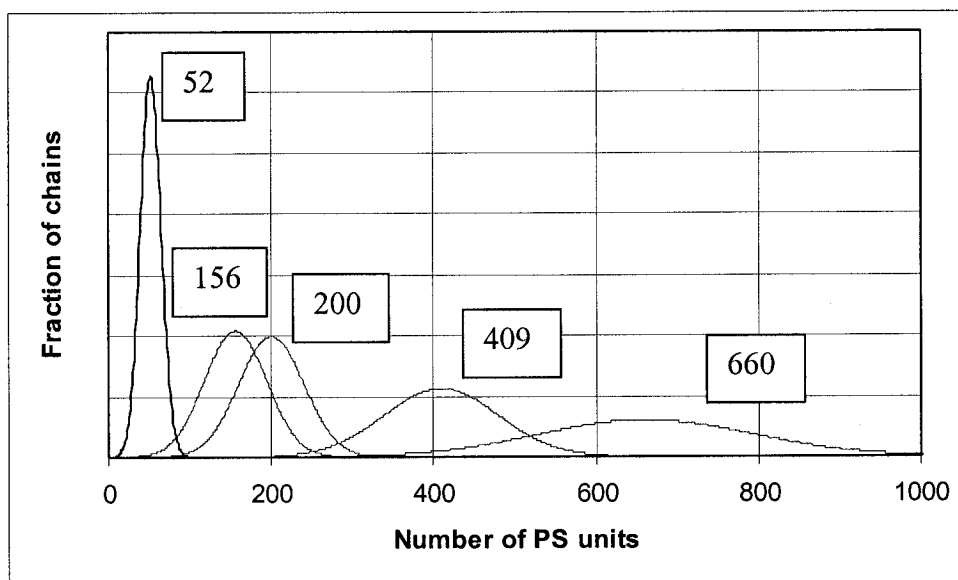


Figure 5-1: Molecular Weight Distributions of PS Block of Individual Copolymers

Table 5-2: Blends and resulting PDIs of the PS block

Mol % of PS <sub>52</sub> - <i>b</i> - PAA <sub>20</sub>	Mol % of PS <sub>156</sub> - <i>b</i> - PAA <sub>20</sub>	Mol % of PS <sub>200</sub> - <i>b</i> - PAA <sub>20</sub>	Mol % of PS <sub>409</sub> - <i>b</i> - PAA <sub>20</sub>	Mol % of PS <sub>660</sub> - <i>b</i> - PAA <sub>18</sub>	Resulting PS PDI
-----	-----	100	-----	-----	1.04
-----	83	-----	17	-----	1.3
59	-----	-----	41	-----	1.8
76	-----	-----	-----	24	2.8

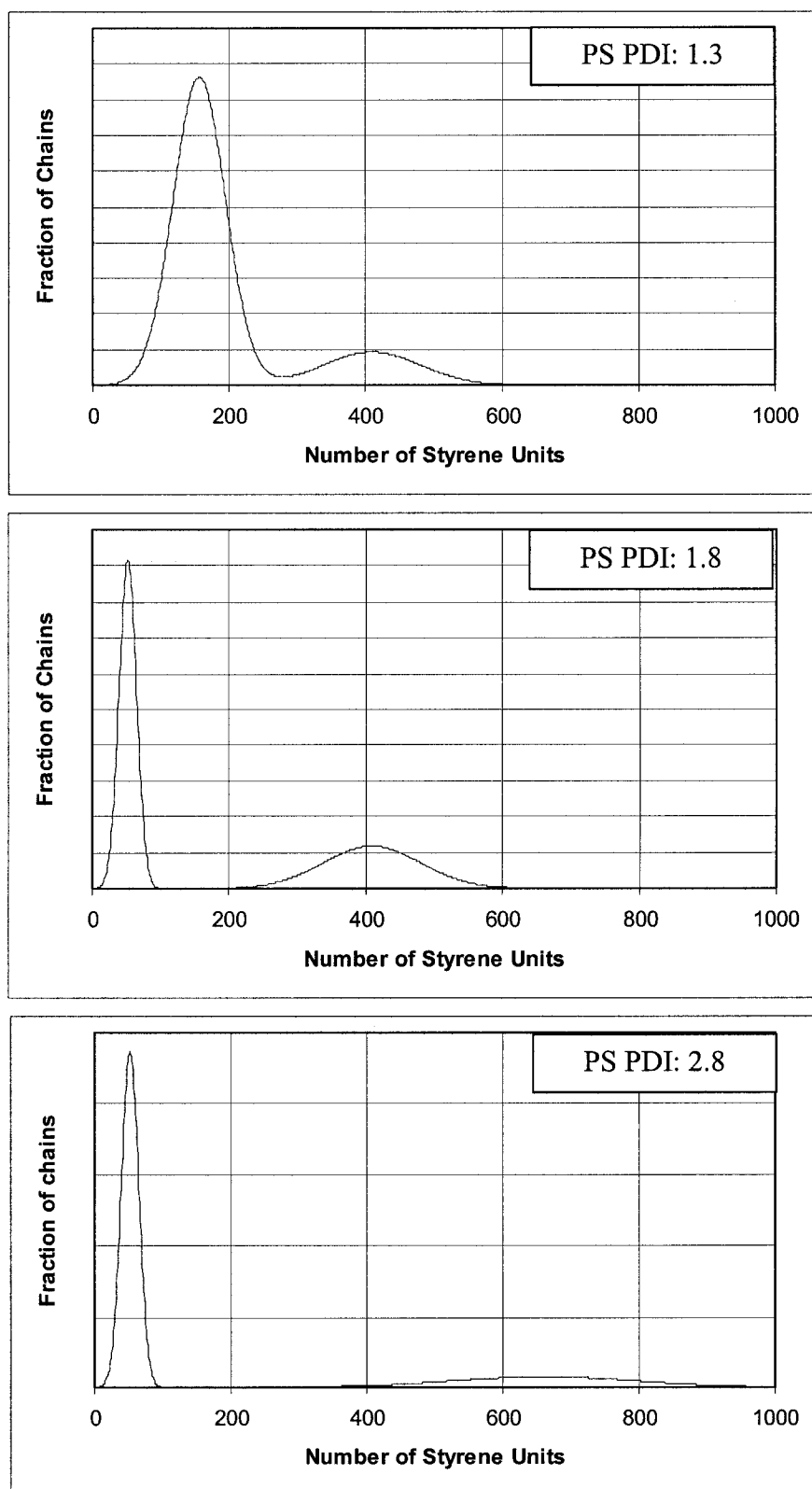


Figure 5-2: Molecular Weight Distributions of PS block in Mixtures.

#### 5.2.4 Preparation of aggregates

The PS-*b*-PAA copolymer mixtures (1% w/w) were dissolved in dioxane and stirred overnight. Water was then added slowly ( $\sim 0.7\%$  (w/w)/min) to a predetermined final concentration and the solutions were left stirring for 24 hours. The morphology of the aggregates was then “frozen” by adding them into an excess of water. The samples were then dialyzed against milli-Q water.

#### 5.2.5 Transmission Electron Microscopy

A JEOL 2000FX microscope was used for the transmission electron microscopy (TEM) studies. The dilute dialyzed samples were deposited on EM grids that had been precoated with a thin film of Formvar (poly(vinylformaldehyde) plastic) and then coated with carbon. The water evaporated at room temperature overnight leaving the solid aggregates on the grids.

### 5.3 RESULTS AND DISCUSSION

For each PS PDI, the morphology of the aggregates was observed at solvent contents of 10, 12, 14 and 50 percent water. These solvent compositions were picked because for samples with narrow molecular weight distributions, the sphere to rod transition occurs around 10-12 % (w/w) water, and the rod to vesicle transition occurs close to 14 % (w/w) water. At 50 % (w/w) water, the narrow distribution samples usually yield vesicles so the 50 % (w/w) region was used to study the effect of PS PDI on vesicles. Table 5-3 contains the observations of the morphology of the aggregates for each of the samples. At 10 percent water, all aggregates for all the samples were spherical micelles. At 12 percent water, the aggregates formed from the narrowest molecular weight

distribution sample consisted of a mixture of rods and primary spherical micelles, while the other molecular weight distributions yielded only primary spherical micelles. At 14 percent water, a mixture of morphologies (spherical micelles and vesicles) was observed for the PS PDI 1.1 and 1.3 samples, while the aggregates of the PS PDI 1.8 and 2.8 samples were spherical. Figure 5-3 contains TEM pictures of the aggregates formed at 50 % water for all of the samples. The sample with the smallest PS PDI (1.1) forms large polydisperse vesicles. The PS PDI 1.3 sample contained only elongated spherical micelles, no vesicles were observed. This seems to be close to a sphere to rod transition boundary in the phase diagram. The PS PDI 1.8, and 2.8 samples formed only spherical micelles at a concentration of 50 % (w/w) water.

Table 5-3 Morphologies and sizes of aggregates formed from mixtures of copolymers with different polystyrene molecular weight distributions. The numbers in brackets are the average diameter and population standard deviation of the diameter of the spherical particles (in nm) as measured from the TEM micrographs (n = 150-200 particles).

PS PDI	10% Water	12% Water	14% Water	50% Water
1.1	Spheres (22 ± 5)	Rods and spheres (22 ± 5)	Large polydisperse vesicles and spheres	Large, polydisperse vesicles
1.3	Spheres (20 ± 5)	Spheres (19 ± 4)	Spheres and small vesicles (26 ± 8)	Elongated Spheres (31 ± 10)
1.8	Spheres (16 ± 4)	Spheres (14 ± 3)	Spheres (16 ± 4)	Spheres (22 ± 7)
2.8	Spheres (32 ± 10)	Spheres (32 ± 9)	Spheres (38 ± 11)	Spheres (45 ± 11)

The change in morphology can be attributed to an effect similar to that of adding homopolymer to the micelle solution. The added homopolymer, which is usually of a

lower degree of polymerization than that of the core-forming block to avoid kinetic effects, can fill up the center of the micelle core.<sup>25</sup> This filling of the center allows the core to increase in size without an accompanying increase in the entropically unfavored stretching of the core chains of the diblock copolymer. A relatively small percentage of long chains in the mixtures fulfills the same role.

If the PS PDI is made to increase by mixing of two copolymers, then the sample obviously consists of a mixture, one component of which is longer than the average chain length, while the other is shorter than the average chain length. While both populations do have narrow polydispersities by themselves, the range of chains of different molecular weight is not the same. The population of larger chains has a larger range of chain sizes than the population of the smaller chains, even though the polydispersity of the larger chains is lower, as shown in Figures 5-2 and 1-3.

As water is added slowly to the mixture of chains in dioxane, the longer diblocks start to aggregate. As more water is added, the short chains will join the preformed aggregates of long chains and occupy the volume close to the surface of the micelle, as shown schematically in Figure 5-4. The middle of the core of the micelle will be mainly filled with the long chains, which because of their length are not very highly stretched. As the aggregation number increases further (by slow addition of water) and more chains are added to the micelle, the size of the micelle core increases, as is the case of the aggregate formed from a diblock with a narrow distribution of polystyrene chains. However, in the mixture, the core radius can increase without an undue entropic penalty because the long chains in the mixture have a longer end-to-end distance and, therefore, will be able to span greater distances. The high degree of stretching of the PS chains in the narrow distribution

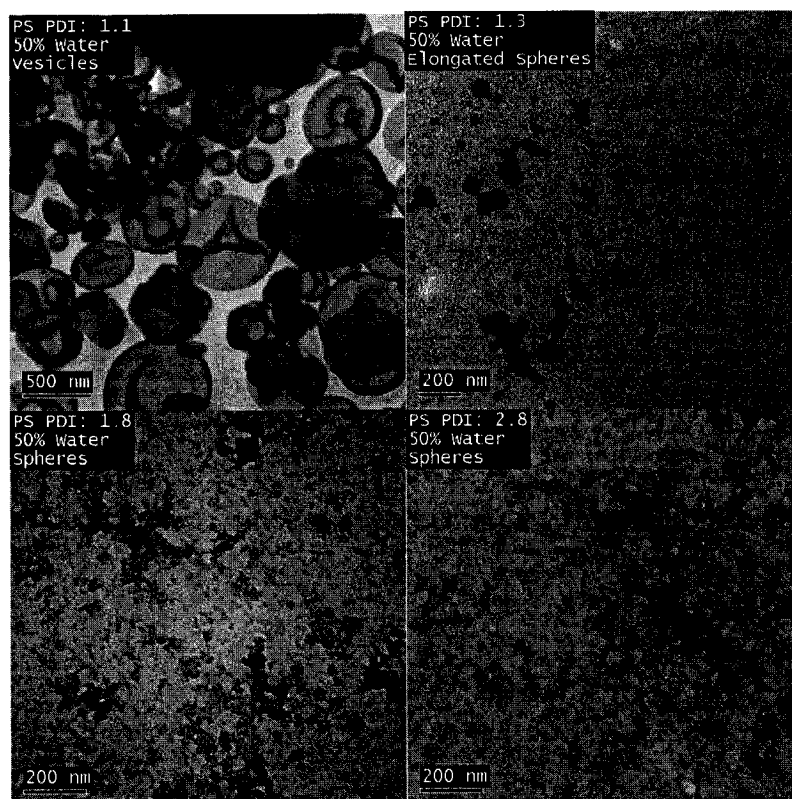


Figure 5-3: TEM micrographs of the PS PDI samples at 50 % water. A change in morphology from vesicles to spheres is observed with an increase in the PS PDI.

sample leads to the change in morphology from spheres to rods and, eventually, to vesicles. In the mixture, the radius of the spherical micelle increases without the high degree of stretching of any of the chains, and therefore there is no change in morphology of the aggregate.

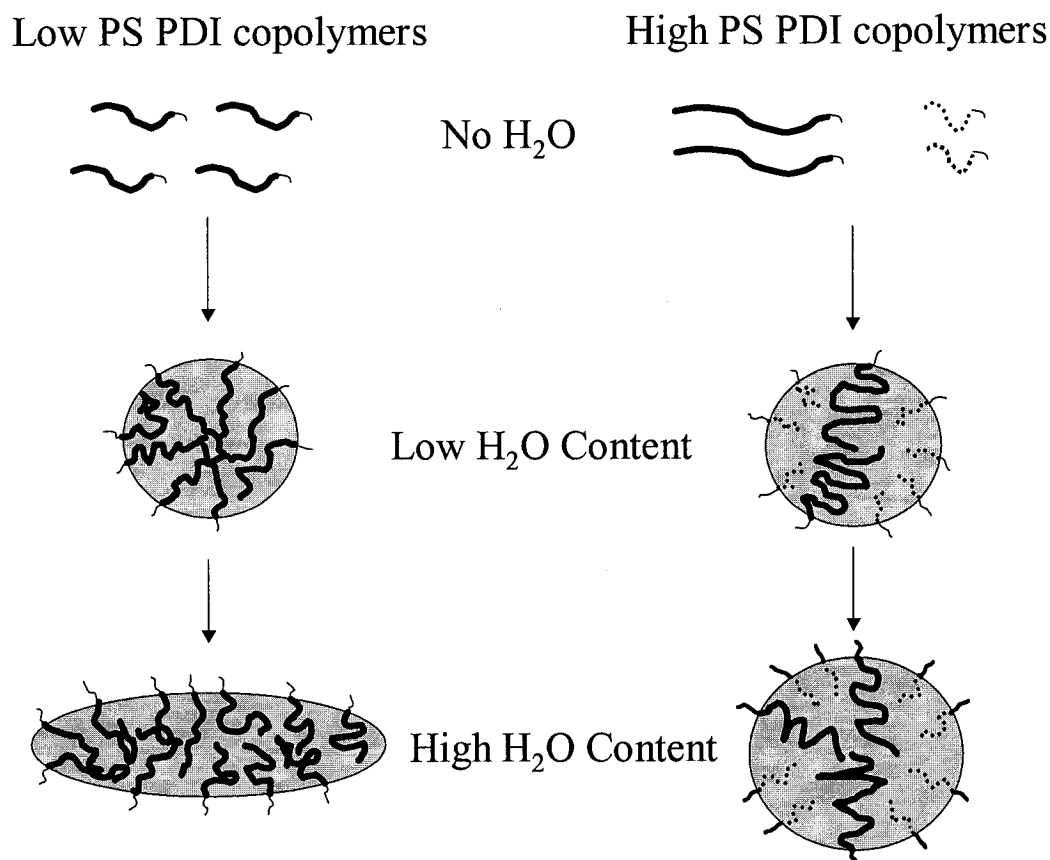


Figure 5-4: Schematic of aggregates formed from a diblock with a narrow distribution (low PS PDI), and a polydisperse (high PS PDI) distribution of the size of the core block. In both cases the single chains are dissolved in a good solvent. As water is added the chains start to aggregate. At low water contents spherical micelles are formed for both cases; however, the degree of stretching of the chains, which span from the surface to the middle of the micelle core, is higher for the sample made of copolymers with a narrow core block length distribution. A further increase in water content results in a change in morphology for the narrow molecular weight distribution sample in order to relax the high degree of stretching of the core chains. The average degree of stretching of the polydisperse sample is not very high; therefore, at high water concentrations, large spherical micelles are obtained.

To determine the degree of stretching in the core, the sizes of the aggregates were measured from the TEM pictures. For each styrene block of each of the copolymers used, the average end-to-end chain length,  $D_{ee}$ , and the theoretical limit of the fully stretched polystyrene chain,  $D_s$ , were calculated using Equations 5-2 and 5-3 respectively.

$$D_{ee} = l \times \sqrt{n \times 6.76} \quad (5-2)$$

$$D_s = l \times n \quad (5-3)$$

where  $l$  is the length of a PS segment ( $\sim 0.25$  nm) and  $n$  is the number of repeat units of PS. The factor 6.76 has been experimentally determined and takes into account the both long range and short-range interactions<sup>26</sup> (i.e. excluded volume, and the restricted bond angle of 109.5 for each carbon in the backbone of the polymer chain)

Table 5-1 contains the resulting average lengths. For the aggregates formed from each mixture, an estimate of the degree of stretching,  $S_c$ , was made by taking the radius of the spherical aggregate and dividing by the end-to-end distance of the polymer chain. For each mixture, the estimated degree of stretching of one long chain that stretched from the middle of the core to the surface of the micelle,  $S_{c,l}$ , was calculated. For the narrowest distribution there was only one population of chains and, therefore, there were no “long” chains in the mixture. The degree of stretching of the average chain length,  $S_{c,a}$ , was also calculated for each sample by dividing the radius of the sphere by the  $D_{ee}$  of the average chain length (PS<sub>200</sub>). Since the average chain length is the same for all samples, comparing  $S_{c,l}$  to  $S_{c,a}$  for each sample gives an idea of the reduction in the degree of stretching of a core chain when a bimodal distribution of core chain lengths is present. Table 5-4 contains the results of these calculations. These degrees of stretching are meant as qualitative guides. The real degree of stretching may be slightly different than what is



calculated. The more important factor is the estimated degree of stretching of one sample relative to that of another sample.

Table 5-4 Degree of stretching of a core chain stretching from the center of the core to the surface of the micelle.  $S_{c,l}$ : Degree of stretching of the long chain.  $S_{c,a}$ : Degree of stretching of a chain of average block length. \* There were also some rods present in the mixture but only the data from the spherical micelles was used.

PS PDI	10 % (w/w) water		12 % (w/w) water		14 % (w/w) water		50 % (w/w) water	
	$S_{c,l}$	$S_{c,a}$	$S_{c,l}$	$S_{c,a}$	$S_{c,l}$	$S_{c,a}$	$S_{c,l}$	$S_{c,a}$
1.1	N/A	1.29	N/A	1.29*	N/A	N/A	N/A	N/A
1.3	0.76	1.12	0.72	1.06	0.98	1.46	1.17	1.74
1.8	0.60	0.98	0.49	0.80	0.60	0.98	0.83	1.34
2.8	0.95	2.11	0.95	2.11	1.13	2.5	1.28	2.8

For each PS PDI sample the degree of stretching generally increases as the water content increases. This is in agreement to previous results.<sup>25</sup> The degree of stretching at 12 % (w/w) water is slightly less than that of the 10 % (w/w) samples. However, the decrease is very small and is most likely due to experimental error. For the narrow distribution sample, there are some rods present in the solution; however, only the data from the spherical micelles was used for the degree of stretching calculations. The observation of rods in the solution indicates that when the radius of the micelle of 1.3 times farther than the end-to-end distance of the polymer chain, the high degree of stretching of the core chains leads to morphological transitions. From table 5-4, the long chains in the mixtures all have end-to-end distances that are less than or close to the

radius of the spherical micelle. This suggests that the degree of stretching of the long chains in these micelles is not very high. Since the degree of stretching of the long chains in the mixture is less, no morphology change is expected. For larger PS PDI samples and high water contents of the medium PS PDI samples, the degree of stretching for chains of the average block length is higher than for those of the longest chains in the mixture. For example, in the PS PDI 2.8 sample at a water content of 14 % (w/w) the degree of stretching of the large chains is 1.1 while the degree of stretching of chains of 200 repeat units would be 2.5. For this sample the chains of smaller length will not stretch from the center of the micelle to the corona, only the long chains will.

The sample with PS PDI 2.8 at 50 % (w/w) water has a calculated degree of stretching of the long chains of 1.28. This degree of stretching is similar to the degree of stretching in the narrow molecular weight sample as it changes morphology. While the PS PDI 2.8 sample at 50 % (w/w) water may be close to the morphological boundary, the calculated degree of stretching may be higher than the real degree of stretching in this case. As mentioned above the population of the long chains has an average of 660 units of styrene but, there will be many chains that are longer than 660 units and these will not be stretched as much.

While increasing the PS PDI lowers the degree of stretching, the total distribution of the PS chains must also be important. Bimodal distributions of the corona block chains have been found to increase the effects of the PAA PDI on morphology.<sup>16</sup> The bimodal nature of the distribution of the core-forming block used in the current study almost certainly causes an increase in the observed effects in morphology. For a broad, unimodal system (i.e. one continuous peak in the distribution), the number of chains longer than the average chain length would be much smaller and, therefore, the decrease

in the degree of stretching of in the polydisperse sample would be less than that for a bimodal sample.

### 5.3.1 Are these Equilibrium Morphologies?

It has been reported before<sup>18</sup> that the effect of core block polydispersity in the bulk is found only when the aggregates are formed under conditions that are close to equilibrium conditions and that the method of preparation can determine whether or not the core polydispersity affects the size of the core of the aggregates. In the current study it appears that we are close to thermodynamic equilibrium, since water is added at slow rates and the aggregates are stirred overnight before they are quenched. In this time frame, it has been shown that near-equilibrium morphologies are reached for aggregates made from narrow distribution diblocks.<sup>27-29</sup> The fact that PDI effects are observed suggests, by itself, that we may be close to equilibrium. Nevertheless, a sample was tested to see if preparative techniques affected the results. Using the PS PDI 1.8 sample, aggregates were prepared using different rates of water addition, and the time each mixture was stirred before quenching was varied. Three different rates of water addition were used, a fast rate (all of the water was added in a stream), a medium rate (the water was added drop wise at one drop per minute, the same rate as for the samples prepared in the above PS PDI study), and a slow rate (the water was added at one drop per ten minutes). In every case the final water concentration was 10 % (w/w). For each rate of water addition, two samples were made; one that was quenched immediately after the water had been added, and one that was left stirring for a period of at least one day before being quenched. One sample was quenched immediately, while the other was left stirring overnight except in the case of the slow water addition samples; one was quenched

immediately, and one was left stirring for three weeks. Since the water content was fairly low, the kinetics of chain exchange (between different aggregates) would have been rapid.

A lot of precipitated polymer was visible in both of the samples that were made using the fast water addition. The medium water addition sample, that was quenched immediately, had some precipitate but not as much as the fast water addition method. The slow water addition samples had no visible precipitate. The morphologies of the resulting aggregates were observed by TEM. Surprisingly, some spherical micelles and LCM's were observed in the fast and medium water addition samples that had precipitate. The slow water addition samples contained aggregates of similar morphology to those prepared in the earlier study. The low rate of water addition sample that was stirred for three weeks should have been at or very near equilibrium since the kinetics of chain exchange were rapid at such low water contents, and an excess of time was allowed. The fact that the samples prepared for the first study (i.e. medium rate of water addition and stirring overnight) had aggregates of identical morphology to the near-equilibrium structure further suggests that the method of preparation used in the PS PDI studies afforded near-equilibrium morphologies.

## 5.4 CONCLUSIONS

The effect of the core block polydispersity was investigated on the morphology and size of PS-*b*-PAA aggregates by artificially broadening the polydispersity of the PS block. Samples with high PS PDI were found to form only spherical micelles. Only the two smallest PS PDIs were found to form vesicular aggregates. Even at water contents as high as 50 % (w/w), which usually produces vesicles, the mixtures of high PS PDI only produced spherical micelles. The absence of the vesicle morphology at high PS PDI was

explained by the presence of long polystyrene chains in the mixture. As the size of the spherical aggregates formed at low water increased with the addition of water, the degree of stretching of the core chains did not increase as much for cores made of longer chains. The lack of stretched chains allows the growth of the spherical aggregate without the entropic penalty to the free energy. The aggregates were also found to be close to equilibrium structures.

## 5.5 ACKNOWLEDGEMENTS

The authors thank Rhodia, NSERC and FCAR for financial support. Dr. Yisong Yu, Dr. Lifeng Zhang, and Dr. Hongwei Shen are thanked for the use of the synthesis of the polymers used in these studies.

## 5.6 REFERENCES

1. Zhang, L.; Eisenberg, A. *Science* **1995**, *268*, 1728-1731.
2. Lodge, T.P.; Bang, J.; Hanley, K.J.; Krocak, J.; Dahlquist, S.; Sujan, B.; Ott, J. *Langmuir* **2003**, *19*, 2103-2109.
3. Liu, F.; Liu, G. *Macromolecules* **2001**, *34*, 1302-1307.
4. Castelletto, V.; Hamley, I.W.; Ma, Y.; Bories-Azeau, X.; Armes, S.P.; Lewis, A.L. *Langmuir* **2004**, *20*, 4306-4309.
5. Jungmann, N.; Schmidt, M.; Maskos, M.; Weis, J.; Ebenhoch, J. *Macromolecules* **2002**, *35*, 6851-6857.

6. Dean, J. M.; Grubbs, R. B.; Saad, W.; Cook, R. F.; Bates, F. S. *J. Polym. Sci. B: Polym. Phys.* **2003**, *41*, 2444-2456.
7. Lim Soo, P.; Eisenberg, A. *J. Polym. Sci. PartB: Polym. Phys.* **2004**, *42*, 923-938.
8. Gebhart, C. L.; Kabanov, A. V. *Journal of Controlled Release* **2001**, *73*, 401-416.
9. Harada-Shiba, M.; Yamauchi, K.; Harada, A.; Takamisawa, I.; Shimokado, K.; Kataoka, K. *Gene Therapy* **2002**, *9*, 407-414. *Drug Delivery*
10. Lim Soo, P.; Luo, L.; Maysinger, D.; Eisenberg, A. *Langmuir* **2002**, *18*, 9996-10004.
11. Wang, G.; Henselwood, F.; Liu, G. *Langmuir* **1998**, *14*, 1554-1559.
12. Matyjaszewski, K.; Xia, J. *Chem Rev.* **2001**, *101*, 2921-2990.
13. Georges, M.K.; Hamer, G.K.; Listigovers, N.A. *Macromolecules* **1998**, *31*, 9087-9089.
14. Terreau, O.; Luo, L.; Eisenberg, A. *Langmuir*, **2003**, *19*, 5601-5607.
15. Terreau, O.; Bartels, C.; Eisenberg, A. *Langmuir*, **2004**, *20*, 637-645.
16. Terreau, O.; Eisenberg, A. *to be submitted*.
17. Jain, S.; Bates, F.S.; *Macromolecules* **2004**, *37*, 1511-1523.
18. Nguyen, D.; Zhong, X.F.; Williams C.E.; Eisenberg, A. *Macromolecules* **1994**, *27*, 5173-5181.
19. Zhulina, E.B.; Birshtein, T.M. *Polymer*, **1991**, *32*, 1299-1308.

20. Zhulina, E.B.; Lyatskaya, Y.V.; Birshstein, T.M. *Polymer*, **1992**, 33, 332-342.
21. Lyatskaya, Y.V.; Zhulina, E.B.; Birshstein, T.M. *Polymer*, **1992**, 33, 343-351.
22. Court, F.; Hashimoto, T. *Macromolecules*, **2002**, 35, 2566-2575.
23. Hautekeer, J.P.; Varshney, S.K.; Fayt, R.; Jacobs, C.; Jerome, R.; Teyssie, P. *Macromolecules* **1990**, 23, 3893-3898.
24. Shen, H.; Zhang, L.; Eisenberg, A. *J. Phys. Chem. B.* **1997**, 101, 4697-4708.
25. Zhang, L.; Eisenberg, A. *J. Am. Chem Soc.* **1996**, 118, 3168-3181.
26. de Gennes, P.-G. *Scaling Concepts in Polymer Physics* Cornell University Press **1979**.
27. Chen L.; Shen, H.; Eisenberg, A. *J. Phys. Chem B.* **1999**, 103, 9488-9497.
28. Burke, S.E.; Eisenberg, A. *Polymer* **2001**, 42, 9111-9120.
29. Choucair, A.; Kycia, A.; Eisenberg, A. *Langmuir* **2003**, 19, 1001-1008.

## CHAPTER 6

---

### CONCLUSIONS, CONTRIBUTIONS TO ORIGINAL KNOWLEDGE AND FUTURE WORK

---

The studies presented in this thesis were performed with the goal of elucidating the effect of the block length polydispersity on the sizes and morphology of block copolymer aggregates. Since diblock copolymers were used, there were two possible blocks to vary the polydispersity; therefore, a systematic investigation was performed. First the corona block polydispersity was varied, keeping the core block polydispersity constant, and then the corona block polydispersity was kept constant while the core block polydispersity was varied. In the studies of the corona block polydispersity, the effect on vesicles (Chapter 2) was first investigated, and then the effect of the PAA PDI on spheres and rods was also investigated, resulting in the creation of a partial phase diagram (Chapter 3). During these first two sets of studies, the question of the effect of the shape of the molecular weight distribution for samples of identical PAA PDI arose. Carefully selected mixtures were made with identical PAA PDI but varying shape of the molecular weight distribution (Chapter 4). Finally, to complete the study, the effects of the core block on the resulting morphologies were investigated (Chapter 5).

#### 6.1 Effects of Poly(Acrylic Acid) Polydispersity

##### 6.1.1 Vesicles

Samples with artificially broadened PAA block length distributions were used to study the effect of the corona block polydispersity on the morphology and size of PS-*b*-PAA vesicles. The vesicle size was generally found to decrease with increasing PAA



PDI, the magnitude of the change increasing with increasing PAA PDI. The decrease in vesicle size is attributed to the segregation of the smaller chains to the inside of the vesicle bilayer while the longer chains form the outer surface. These results may also help to explain the fact that vesicles have been found to decrease in size with an increase in PAA block length (for a given PS block length). For example, it has been found that the vesicle size for a polymer of PS<sub>310</sub>-*b*-PAA<sub>28</sub> is  $440 \pm 160$  nm at 20 % (w/w) water and a polymer concentration of 0.5 % (w/w) in dioxane.<sup>1</sup> Under the same conditions, the copolymer PS<sub>310</sub>-*b*-PAA<sub>45</sub> forms vesicles with an average diameter of  $110 \pm 20$  nm.<sup>1</sup> The PAA PDI is similar for both copolymers, but the molecular weight distribution of the PAA block of the PS<sub>310</sub>-*b*-PAA<sub>45</sub> is much broader (as can be seen in Appendix D) than that of the PS<sub>310</sub>-*b*-PAA<sub>28</sub>. Since it is broader there will be more chains longer than the average chain length and more chains shorter than the average chain length. This will allow for more segregation of chains between the outer and inner surfaces of the vesicle wall. The increased segregation could result in smaller vesicles, similar to the effect of having a bimodal distribution of chains.

### 6.1.2 Spheres and Rods

Chapter 3 investigated other regions of the phase diagram of PS<sub>325</sub>-*b*-PAA<sub>48</sub> copolymers of different PAA PDI and different water contents. At low water contents, LCMs and primary spherical micelles were observed. An increase in the PAA PDI did not affect the sizes of the spherical micelles; however, the sphere-to-LCM ratio seemed to increase with an increase in the PAA PDI. It was found that an increase in the PAA PDI could cause morphological changes to occur at higher water contents. Increasing the PAA PDI (at 12% w/w water) from 1.25 to 2.17 changed the morphology from spheres to a mixture of spheres and rods, and with even greater PAA PDI (to 3.28) to vesicles. The

morphology change with increased PAA PDI was explained by the fact that mixtures of chains of different sizes allow for more chains to aggregate and, thus, the core chain stretching becomes a more important component in the total free energy of the aggregate. To relieve this stress, a morphological change occurs. This research gives another method to control the morphology of PS-*b*-PAA aggregates.

### 6.1.3 The Shape of the Molecular Weight Distribution

The effect of the shape of the molecular weight distribution of the corona block on the resulting morphologies of self-assembled diblock copolymers was explored. It was found that multimodal molecular weight distributions of the corona block (made from mixtures of diblock copolymers) can change the morphology of the aggregates obtained. It is hypothesized that a sample with an increased PAA PDI, but with a monomodal molecular weight, will not show the same changes in morphology as mixtures of copolymers with PAA PDI identical to that of the monomodal sample. Attempts were made to use the bimodality of mixtures of copolymers to obtain more complex architectures, which were not obtainable with monomodal samples of similar number average molecular weight. These studies showed that the average molecular weight of the sample is still the dominant factor in the resulting morphology of the aggregates. The molecular weight distribution of the corona block is only a morphogenic factor when the relative average block length is small enough. The results presented in Chapter 4 are instrumental in understanding the effect of the PAA PDI on the self-assembly properties of the PS-*b*-PAA copolymers. Through the research presented in this chapter it becomes clear that mixing of two copolymers will possibly result in a change in morphology of the aggregates. Chapter 4 also allows us to know at what areas in the phase diagram the molecular weight effect will be possible.

## 6.2 Effects of Polystyrene Polydispersity

Chapter 5 reports results from studies of the effect of the core block polydispersity on the morphology and size of PS-*b*-PAA aggregates. Samples with high PS PDI were found to form only spherical micelles. Only the two smallest PS PDIs were found to form vesicular aggregates. Even at water contents as high as 50 % (w/w), which usually produces vesicles, the mixtures of high PS PDI only produced spherical micelles. The lack of the vesicle morphology at high PS PDI was explained by the presence of long polystyrene chains in the mixture. As the size of the spherical aggregates formed at low water content increased with the addition of water, the degree of stretching of the core chains did not increase as much for cores made of longer chains. The lack of stretched chains allows the growth of the spherical aggregate without the entropic penalty to the free energy. The aggregates were also found to be close to equilibrium structures.

## 6.3 Future Work

Since increasing the PS molecular weight distribution has the opposite effect than increasing the PAA molecular weight distribution, one might be interested in samples with an increase in the molecular weight distribution of both blocks. It would be interesting to see if one effect will be greater or if neither effect is seen (i.e. the two effects balance each other).

The results presented in Chapter 4 can also be used for a future, small project. The polymerization of the copolymers was done in a manner to keep the PS block identical for all of the copolymers. In the process of the synthesis, a sample of the homopolystyrene is removed from the reaction flask for analysis. This process may lead to the termination of some of the “living” polystyrene chains. The fact that there is

homopolymer present in the copolymer suggests that some termination has occurred. In a similar manner, when the first diblock of the series is removed, there may be some termination of the living diblocks that will be used to extend the PAA block. If some is terminated, that will mean that the molecular weight of the PAA block of the next sample is not one peak, but rather two populations of chains. From chapter 4, we now know that the shape of the molecular weight may cause changes in morphology. A simple study to test whether the method of polymer synthesis affects the molecular weight distribution could be interesting. In order to carry out such an experiment, a copolymer could be made of a given PS and PAA block length. A second synthesis could be carried out. In the second synthesis, many different PAA block lengths could be synthesized, making sure that the second or third copolymer in the series has the same degree of polymerization as that of the separate synthesis (The PS block should be similar to that of the first copolymer made). The two polymers with identical molecular weight could then be compared to see if any differences are found.

#### **6.4 Contributions to Original Knowledge**

At the time that this research was started, there had been no work on the effect of the block molecular weight distribution on the morphology and size of self-assembled aggregates in solution. There had been theoretical<sup>2-5</sup> and experimental<sup>6-13</sup> studies on the effect of mixtures of block copolymers on bulk morphologies. After our preliminary studies, Jain and Bates<sup>14</sup> published a similar study to ours, and their results were similar. The research presented in this thesis is fundamental research in the understanding of the self-assembly of amphiphilic block copolymers in solution. By mixing copolymers the morphology of the aggregates can be controlled. Through this research it has been shown

that the polymers that are blended will mix and do not segregate into different aggregates. This research is significant because newer, cheaper synthetic techniques are giving rise to copolymers with increased polydispersities. Through the research presented in this thesis the way in which the broader molecular weight distribution will affect the aggregation of high PDI copolymers can be predicted.

## 6.5 REFERENCES

1. Choucair, A.; Kycia, A.; Eisenberg, A. *Langmuir*, **2003**, *19*, 1001-1008.
2. Birshtein, T.M.; Lyatskaya, Y.V.; Zhulina, E.B. *Polymer* **1992**, *33*, 2750-2756.
3. Dan, N.; Safran, S.A. *Macromolecules* **1994**, *27*, 5766-5772.
4. Wickham, R.A.; Shi, A.-C. *Macromolecules* **2001**, *34*, 6487-6494.
5. Matsen, M.W. *Macromolecules* **2003**, *36*, 9647-9657.
6. Hadziioannou, G.; Skoulios, A. *Macromolecules* **1982**, *15*, 267-271.
7. Nguyen, D.; Zhong, X.-F.; Williams, C.; Eisenberg, A. *Macromolecules* **1994**, *27*, 5173-5181.
8. Mayes, A.M.; Russell, T.P.; Deline, V.R.; Satija, S.K.; Majkrzak, C.F. *Macromolecules* **1994**, *27*, 7447-7453.
9. Lin, E.K.; Gast, A.P.; Shi, A.-C.; Noolandi, J.; Smith, S. *Macromolecules* **1996**, *29*, 5920-5925.
10. Laurer, J.H.; Smith, S.D.; Sanseth, J.; Mortensen, K.; Spontak, R.J. *Macromolecules* **1998**, *31*, 4975-4985.
11. Koneripalli, N.; Levicky, R.; Bates, F.S.; Matsen, M.W.; Satija, S.K.; Akner, J.; Kaiser, H. *Macromolecules* **1998**, *31*, 3498-3508.
12. Court, F.; Hashimoto, T. *Macromolecules*, **2001**, *34*, 2536-2545.

13. Park, S.; Cho, D.; Ryu, J.; Kwon, K.; Lee, W.; Chang, T. *Macromolecules* **2002**, *35*, 5974-5979.
14. Jain, S.; Bates, F.S. *Macromolecules* **2004**, *37*, 1511-1523.

## APPENDIX A

---

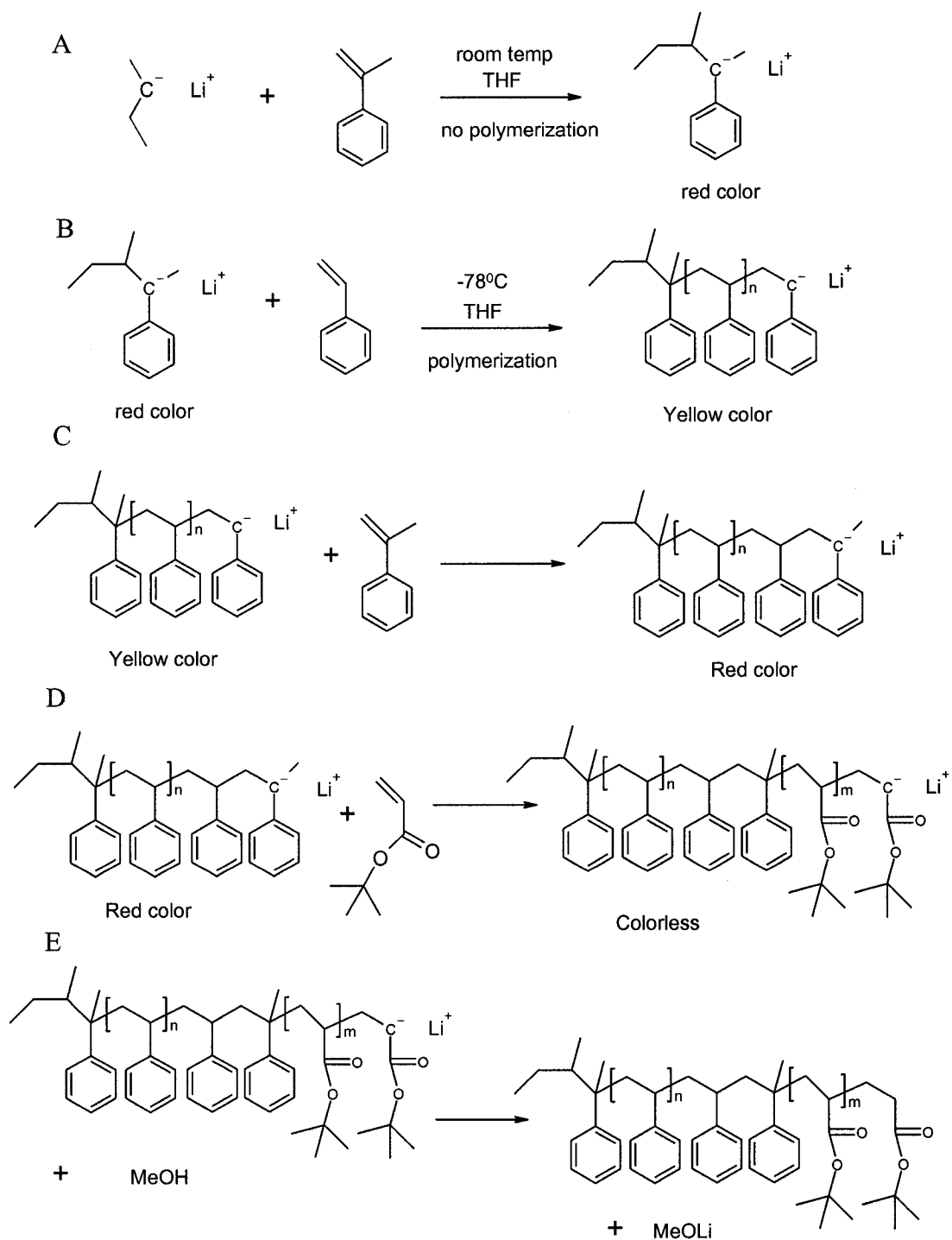
### POLYMER SYNTHESIS

---

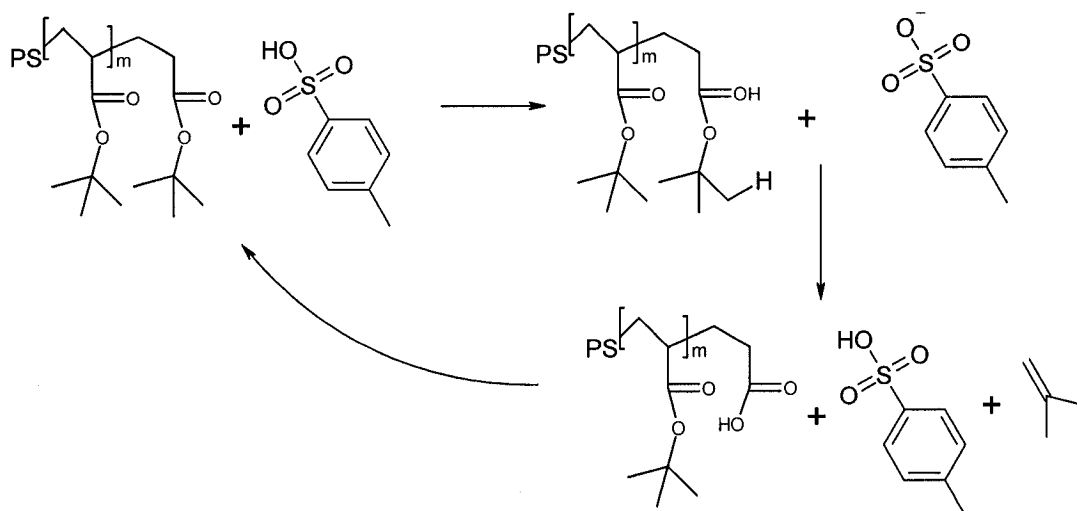
The synthesis of the PS-*b*-PAA block copolymers was performed using the technique of sequential anionic polymerization.<sup>1-4</sup> The following steps were performed. A very small amount (< 0.5 mL) of  $\alpha$ -methyl styrene was added to the reaction vessel, which already contained lithium chloride (excess gegen ion) dissolved in distilled THF. The initiator (*sec*-butyl lithium) was added drop wise at room temperature until a deep red color persisted. The deep red color derived from the  $\alpha$ -methyl styryl anion as shown in scheme A. Because the temperature was above the ceiling temperature of  $\alpha$ -methyl styrene, there was no polymerization, each initiator should have reacted with one  $\alpha$ -methyl styrene producing the  $\alpha$ -methyl styryl anion. If the  $\alpha$ -methyl styryl anion had reacted with any impurities (i.e. O<sub>2</sub>, H<sub>2</sub>O, CO<sub>2</sub>, or any other proton source) the anion would have been “killed” and the red color would not have persisted. The initiation was thus titrated to make sure the system was clear of any impurities. Once the red color was persistent, the calculated amount of initiator was added. The temperature of the reaction vessel was then slowly dropped to -78°C (acetone, dry ice bath). This temperature is below the ceiling temperature of  $\alpha$ -methyl styrene and, therefore, some  $\alpha$ -methyl styrene would have polymerized, however, the rate of propagation was slow. Next, styrene was added to the reaction vessel. The  $\alpha$ -methyl styryl anion was strong enough to polymerize the styrene monomer, evidence of the crossover came from the color change of the solution to a yellow/orange color, produced by the styryl anion as shown in scheme B. Styrene propagation is much faster than  $\alpha$ -methyl styrene propagation and, therefore, the

styrene monomer was consumed within minutes. When all of the styrene monomer had been consumed, the chains were capped with remaining  $\alpha$ -methyl styrene and the red color returned to the solution as shown in scheme C. At this point an aliquot was removed from the reaction vessel and terminated with methanol. This aliquot was used for the analysis of the polystyrene block. The second monomer (*tert*-butyl acrylate, *t*-BuA) was then added to the reaction vessel. The  $\alpha$ -methyl styryl anion could initiate the polymerization of the *t*-BuA, and the crossover was evident in the loss of color in the solution, as shown in scheme D. Of course, the loss of color could have also been due to termination of the polymerization, however, further characterization (appendix B) reveals the diblock copolymer was produced. To complete the diblock copolymerization, acidified methanol was added to the reaction vessel as shown in scheme E.





To produce the PS-*b*-PAA copolymers the *tert*-butyl groups had to be removed. This was done by refluxing the PS-*b*-Pt-BuA copolymer in toluene, using *para*-toluene sulfonic acid (5 mol % relative to the *t*-BuA content) as the catalyst.



The reaction is an elimination reaction resulting in the formation of 2-methylpropene as shown in scheme F. The 2-methylpropene has a boiling point of  $-6.9^{\circ}\text{C}$ , which is below the reflux temperature of toluene (and the temperature of the condenser), therefore the 2-methylpropene will be removed from the reaction flask.

*Para*-toluene sulfonic acid is hygroscopic and is present as a monohydrate. Because it is left on the shelf in the lab, there is a good chance that even more water is present in the system. The water may allow for the acid catalyzed hydrolysis of the ester resulting in PAA and 2,2-dimethyl ethanol. In either case the resulting polymer is the same. The completion of the reaction was confirmed by FT-IR of the polymer, see Appendix C.

## References

1. Hautekeer, J.P.; Varshney, S.K.; Fayt, R.; Jacobs, C.; Jerome, R.; Teyssie, P. *Macromolecules* **1990**, *23*, 3893-3898.
2. Zhong, X.F.; Varshney, S.K.; Eisenberg, A. *Macromolecules* **1992**, *25*, 7160-7167.
3. Cameron, N. S.; Eisenberg, A.; Brown, G. R.; *Biomacromolecules* **2002**, *3*, 116-123.
4. Terreau, O.; Luo, L., Eisenberg, A. *Langmuir* **2003**, *19*, 5601-5607.

## APPENDIX B

---

### MEASUREMENT OF $M_N$ AND $M_W$

---

#### Measuring $M_n$ : Osmometry

The classical method of measuring  $M_n$ , osmometry, is based on the osmotic pressure associated with bringing a polymer solution into thermodynamic equilibrium with the pure solvent through a semi permeable membrane (i.e. only permeable to the solvent).<sup>1-3</sup> The osmotic pressure is the pressure that would need to be exerted to raise the chemical potential of the solvent in the polymer solution ( $\mu_1$ ) to that of the pure solvent  $\mu_1^0$  at a standard pressure  $P$ .

$$\mu_1^0 = \mu_1 + \int_P^{P+\pi} \left( \frac{\partial \mu_1}{\partial P} \right)_T dP \quad (\text{B-1})$$

The compressibility of the solvent,  $(\partial \mu_1 / \partial P)_T$ , is equal to the molar volume of the solution,  $V_1$ , and is constant over small ranges of pressure and therefore does not need to be considered in the integral of Equation B-1. Solving the integral and rearranging the equation gives

$$\mu_1 - \mu_1^0 = -V_1 \pi \quad (\text{B-2})$$

The chemical potential difference can also be derived using thermodynamics of polymers in solution. The enthalpy and entropy can be derived and used to evaluate the Gibbs free energy of mixing the polymer and solvent. Taking the differential of the Gibbs free energy of the system with respect to the number of solvent molecules is equal to the difference in chemical potentials<sup>2</sup>

$$\Delta H^M = kT \chi_1 N_1 \phi_2 \quad (\text{B-3})$$

$$\Delta S^M = -k(N_1 \ln \phi_1 + N_2 \ln \phi_2) \quad (\text{B-4})$$

$$\Delta G^M = \Delta H^M - T\Delta S^M = kT[N_1 \ln \phi_1 + N_2 \ln \phi_2 + N_1 \phi_2 \chi_1] \quad (\text{B-5})$$

$$\frac{\partial \Delta G^M}{\partial N_1} = (\mu_1 - \mu_1^0) = RT \left[ \ln(1 - \phi_2) + \left(1 - \frac{1}{r}\right) \phi_2 + \chi_1 \phi_2^2 \right] \quad (\text{B-6})$$

where  $r = V_2/V_1$ . While this is not strictly valid for the dilute solution regime, it can be used to show non-ideality of solution behaviour when making measurements of the molecular weight by osmotic pressure measurements. The logarithmic term can be expanded<sup>1</sup>

$$\ln(1 - \phi_2) = -\phi_2 - \frac{\phi_2^2}{2} - \frac{\phi_2^3}{3} \dots \quad (\text{B-7})$$

Assuming  $\phi_2$  is small (dilute solution) the expansion is truncated after the squared term. The truncated expansion can be substituted into Equation B-6 to obtain<sup>1</sup>

$$\mu_1 - \mu_1^0 = -RT \left[ \frac{\phi_2}{r} + \left( \frac{1}{2} - \chi_1 \right) \phi_2^2 \right] \quad (\text{B-8})$$

but  $r = V_2/V_1$  and  $\phi_2 = c_2 \bar{u}_2$  ( $\bar{u}_2$  is the partial specific volume of the polymer) and  $\bar{u}_2 = V_2/M_2$ , therefore,

$$\mu_1 - \mu_1^0 = -RT \left[ \frac{c_2 V_1}{M_2} + \bar{u}_2^2 \left( \frac{1}{2} - \chi_1 \right) c_2^2 \right] \quad (\text{B-9})$$

which can be equated to Equation B-2 and after rearrangement gives

$$\frac{\pi}{c_2} = RT \left[ \frac{1}{M_2} + \frac{\bar{u}_2^2}{V_1} \left( \frac{1}{2} - \chi_1 \right) c_2 \right]. \quad (\text{B-10})$$

It can be seen from Equation B-10 that if  $\chi_1$  is equal to 0.5 (i.e. a theta solvent is used) then the higher order term drops out and  $\pi/c$  is independent of concentration.

Equation B-10 can be rewritten using a more general form with the inclusion of virial coefficients;

$$\frac{\pi}{c} = RT \left( \frac{1}{M_n} + A_2 c + A_3 c^2 + \dots \right) \quad (\text{B-11})$$

where  $A_2$  and  $A_3$  are the second and third virial coefficients.

For dilute solutions the terms after the second virial coefficient are negligible and a plot of  $\pi/c$  as a function of polymer concentration is linear giving a slope of  $RTA_2$  and a y-intercept of  $RT/M_n$ . For higher molecular weight samples the third virial coefficient is important and the equation must be manipulated. Introducing a polymer-solvent interaction parameter,  $g$ , ( $g = 0.25$  experimentally for a good solvent) in front of the third term in the bracket of equation 1-30 results in a plot of  $(\pi/c)^{0.5}$  being linear with respect to concentration.<sup>1</sup>

The osmotic pressure depends on the number of solute molecules present and therefore the number average molecular weight is determined using this method. Care has to be taken when using this method because polymers with molecular weights less than 10 000 may pass through the membrane and those with molecular weights above 300 000 will give osmotic pressures that are way too small.

### Measuring $M_w$ : SLS

Lord Rayleigh observed that when gaseous small molecules were placed in a beam of light that each small particle acted as a scattering centre and re-emitted the light in all directions.<sup>2</sup> The reduced intensity,  $R_\theta$ , (also known as the Rayleigh ratio) was

shown to be proportional to the molecular weight of the gas (M), the wavelength of the incident light ( $\lambda$ ) and the change in the refractive index ( $dn/dc$ );<sup>1,3</sup>

$$R_{\theta} = \left( \frac{2\pi^2}{N_A \lambda^4} \right) \left( \frac{dn}{dc} \right)^2 (1 + \cos^2 \theta) M \quad (\text{B-12})$$

In gases, as the number of particles increases, the number of scattering centres increases; therefore,  $dn/dc$  increases, however, in solution  $dn/dc$  should not change and should be zero. For a solution of dissolved polymer there are liquid inhomogeneities, which allow for scattering of a volume element to occur. There is also a fluctuation in polymer concentration that contributes to the scattering. In order to measure these effects due to the fluctuations the work of Debye is needed. He showed that  $R_{\theta} = R_{\theta(\text{solution})} - R_{\theta(\text{solvent})}$  and that this is related to the change in the Gibbs free energy with concentration of the solvent. Since the Gibbs free energy is related to the osmotic pressure;<sup>1</sup>

$$R_{\theta} = \left( \frac{2\pi^2 n_0^2}{\lambda^4} \right) (1 + \cos^2 \theta) \left( \frac{dn}{dc} \right)^2 \left( \frac{NM}{N_A} \right) \left( \frac{RT}{\left( \frac{d\pi}{dc} \right)_T} \right) \quad (\text{B-13})$$

where  $n_0$  and  $n$  are the refractive indices of the pure solvent and the solution respectively. Equation 1-32 can be expanded and rearranged to give;<sup>1</sup>

$$K'(1 + \cos^2 \theta) / R_{\theta} = 1 / M_w + 2A_2 c \quad (\text{B-14})$$

where

$$K' = \frac{2\pi^2 n_0^2 \left( \frac{dn}{dc} \right)^2}{\lambda^4 N_A} \quad (\text{B-15})$$

For particles with sizes that are smaller than  $\lambda'/20$  (where  $\lambda' = \lambda/n_0$ ),  $k'c/R_{90}$  plotted as a function of concentration will give a y-intercept of  $M_w^{-1}$ . For larger particles a more complex analysis is needed.

The origin of the problem with large particles stems from the fact that there are multiple scattering centres within the same particle. Therefore the scattering envelope is dependent on molecular shape. The scattering is zero in the direction incident to the beam but increases as the angle of detection increases. The difference can be measured by the dissymmetry coefficient,  $Z$ , which equals unity for small particles.<sup>1</sup>

$$Z = R_{\theta} / R_{\pi-\theta} \quad (B-16)$$

The ratio of the scattering intensity to the intensity in the absence of scattering (measured at the same angle) is called the particle scattering factor,  $P(\theta)$ . The shape scattering factor is shape dependent, however, the radius of gyration,  $\langle S^2 \rangle^{0.5}$ , is shape independent. The radius of gyration is defined as the average distance from the centre of gravity of a polymer coil to the chain end. For monodisperse randomly coiling polymers the relationship between  $P(\theta)$  and  $\langle S^2 \rangle^{0.5}$  is<sup>1</sup>

$$P(\theta) = \frac{2}{u^2} (e^{-u} - (1-u)) \quad (B-17)$$

where

$$u = \left( \frac{4\pi}{\lambda} \sin \frac{\theta}{2} \right)^2 \langle S^2 \rangle^{0.5} . \quad (B-18)$$

In the limit of small  $\theta$

$$P(\theta)^{-1} = 1 + u/3 - \dots \quad (B-19)$$

can be used and the coil size can be estimated from  $P(\theta)$  without assuming a particular model.

To calculate the weight average molecular weight, the Zimm method is most commonly used. This method uses a double extrapolation. Scattering data are collected at different angles and concentrations and an extrapolation to zero angle and zero concentration is performed to obtain  $M_w$ .<sup>1</sup>

This is based on the fact that  $P(\theta) = 1$  at  $\theta = 0$ , however this is experimentally difficult to measure. A modified version of equation B-14 is used, the ratio of scattering intensity is inserted to account for the angular dependence of the scattering of the large particles.<sup>1</sup>

$$\frac{Kc}{R_\theta} = \frac{1}{M_w} + \left( \frac{1}{M_w} \right) \left( \frac{16\pi^2}{3\lambda^2} \right) \sin^2 \left( \frac{\theta}{2} \right) < \bar{S} >_z^2 + 2A_2c + \dots \quad (\text{B-20})$$

A plot of  $Kc/R_\theta$  vs.  $\sin^2(\theta/2) + k'c$  (where  $k'$  is an arbitrary constant picked in order to give a desirable spread of the data) can be used for the double extrapolation. All the points of equal concentration are joined and extrapolated to zero angle. All of the points with identical angles are then joined and extrapolated to zero concentration. All of the points of zero angle are joined in a line and extrapolated to the axis. The same is done for the points of zero concentration. The two lines should intersect at the axis, which represents  $M_w^{-1}$ . The slope of the  $\theta = 0$  line yields the second virial coefficient and the radius of gyration can be found from the initial slope of the  $c = 0$  line.

While the above method works very well when dealing with homopolymers care has to be taken when dealing with multiblock copolymers.<sup>2</sup> The same method as described above can be used, however, the resulting molecular weight should be denoted as  $M_{w, \text{apparent}}$  because for the diblocks the index of refraction is different for each block.



To determine the real molecular weight, the  $(dn/dc)$  of the copolymer can be determined by taking a weighted average of  $dn/dc$  of the copolymers present in each block;<sup>2</sup>

$$\left(\frac{dn}{dc}\right)_{\text{copolymer}} = w_A \left(\frac{dn}{dc}\right)_A + (1 - w_A) \left(\frac{dn}{dc}\right)_B \quad (\text{B-21})$$

and the  $M_{w, \text{apparent}}$  will than be equal to;

$$M_{w, \text{app}} = \frac{1}{V_c^2} \left[ w_A M_w^A v_A^2 + (1 - w_A) M_w^B v_B^2 + 2v_A v_B M_w^{AB} \right] \quad (\text{B-22})$$

where  $M_w^A$  is the molecular weight of block A,  $v_a$ ,  $v_b$ , and  $v_c$  are the specific refractive indicies of block a, b and the copolymer respectively.  $M_w^{AB}$  has no true physical meaning but;

$$M_w^{AB} = \frac{1}{2} \left[ M_w^C - w_A M_w^A + (1 - w_A) M_w^B \right] \quad (\text{B-23})$$

where  $M_w^C$  is the true molecular weight of the copolymer, therefore;

$$M_{w, \text{app}} = M_w^C + 2[(v_A - v_B)/v_c]P + [(v_A - v_B)/v_c]^2 Q \quad (\text{B-24})$$

where

$$P = w_B (1 - w_B) [(M_w^A - M_n^A) - (M_w^B - M_n^B)] \quad (\text{B-25})$$

and

$$Q = w_B (1 - w_B) [(1 - w_B)(M_w^A - M_n^A) - w_B (M_w^B - M_n^B)] \quad (\text{B-26})$$

It can be seen that the more polydisperse a block is the larger P and Q will be. As the polydispersities become closer to one P and Q become negligible and  $M_{w, \text{app}}$  is close to the real  $M_w$  of the copolymer. For living polymerizations (with low PDI) the true  $M_w$  of the copolymer can be obtained if I) the absolute values of the refractive indicies of the two blocks are large and the sign of the refractive indicies of the two blocks is the same.<sup>2</sup>

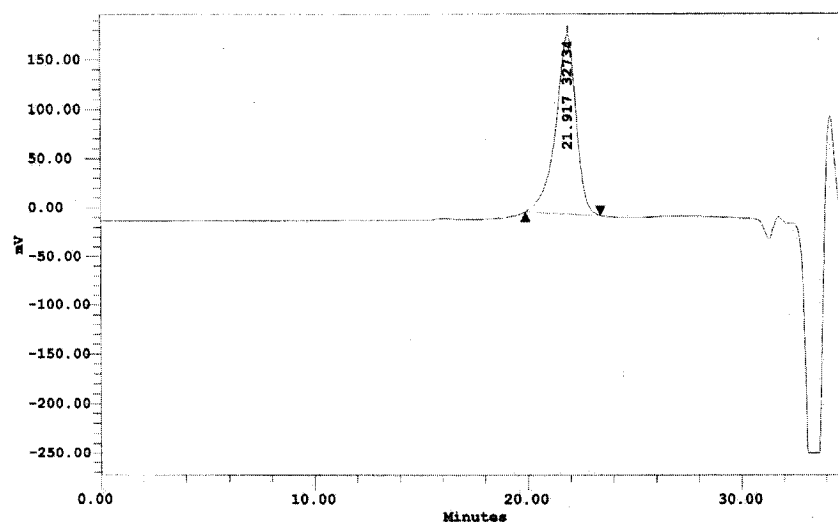
## **References**

1. Cowie, J.M.G. *Polymers: Chemistry & Physics of Modern Materials* 2<sup>nd</sup> ed.; Blackie Academic & Professional, New York, **1996**.
2. Hadjichristidis, N.; Pispas, S.; Floudas, G.A. *Block Copolymers: Synthetic Strategies, Physical Properties and Applications*. Wiley-Interscience, Hoboken, New Jersey, **2003**.
3. Allcock, H.R.; Lampe, F.W. *Contemporary Polymer Chemistry* 2<sup>nd</sup> ed.; Prentice Hall Inc, Toronto, **1990**.

## APPENDIX C

### POLYMER CHARACTERIZATION

All of the polymers used in this thesis were characterized in the same manner. As an example the spectra for the PS<sub>325</sub>-*b*-PAA<sub>48</sub> polymer are presented. During the polymer synthesis a sample of the styrene block was withdrawn from the reaction vessel. A small sample of this aliquot was analyzed by size exclusion chromatography (SEC). A waters model 410 pump was used to deliver solvent through the SEC system, which comprised of an injection port, a guard column (WATERS Styragel), two columns (WATERS Styragel HR4 and HR1) and a Varian RI-4 refractive index detector all connected in series. Polystyrene samples (of know molecular weight and narrow distribution) were used to calibrate the SEC instrument. The chromatogram of the polystyrene block is shown in figure C-1.



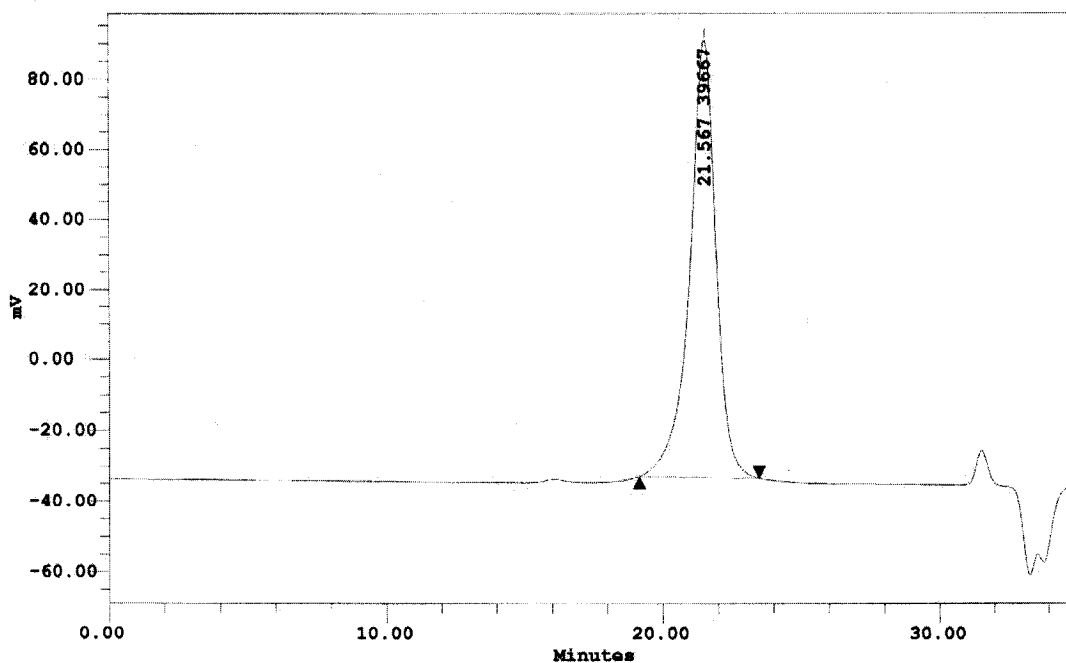
Summary

#	Name	Ret Time (min)	% Area	Mn (Daltons)	Mw (Daltons)	Mz (Daltons)	Polydispersity
1		21.917	100.00	33826	36497	39813	1.078954

Figure C-1: GPC chromatogram of polystyrene precursor.

The sample gives one single, narrow peak indicating a successful synthesis. The negative peaks at high retention time are due to impurities in the sample or solvent used in the SEC sample preparation. Water is one such impurity, which was present in the THF that would result in a negative peak due to its smaller index of refraction than that of THF. The positive peaks at high retention time are present in the chromatogram due to the presence of small molecules such as unreacted monomer or salts left over from the polymerization. These peaks are found in all of the SEC traces for all of the samples.

Figure C-2 presents the SEC chromatogram of the PS-*b*-*Pt*-BuA diblock copolymer. The shape is one narrow, single peak suggesting that there was no termination of any of the living PS block during the crossover to *t*-butyl acrylate. Once again, small molecule impurities are found at high retention time.



Summary

#	Name	Ret Time (min)	% Area	Mn (Daltons)	Mw (Daltons)	Mz (Daltons)	Polydispersity
1		21.567	100.00	40755	44434	49245	1.090276

Figure C-2: GPC chromatogram of diblock copolymer.

The molecular weight obtained by SEC gives a rough indication of the actual molecular weight. SEC cannot give an accurate determination of molecular weight for diblock copolymers. Nuclear magnetic resonance (NMR) was used to determine the composition of the copolymer. Figure C-3 shows the  $^1\text{H}$  NMR spectrum of the  $\text{PS}_{325}\text{-}b\text{-PtBA}_{48}$  sample.

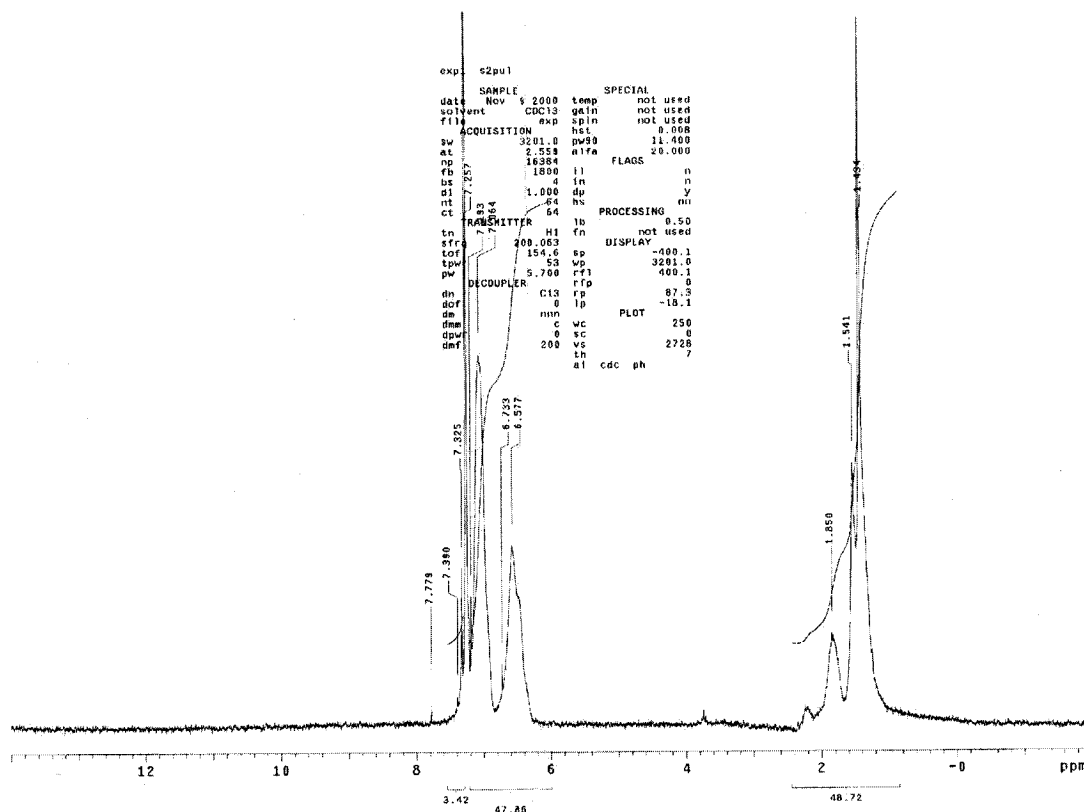


Figure C-3: NMR spectrum of  $\text{PS-}b\text{-Pt-BuA}$  block copolymer.

The strong signal at  $\delta = 7.24$  ppm is due to the solvent chloroform and its integration was not used in any of the calculations. The proton signals present at  $\delta = 6\text{-}7$  ppm represent the phenolic protons of the styrene block. The signals present at  $\delta = 1\text{-}2$  ppm represent all of the *t*-BuA protons and the protons in the backbone of the PS block. The integral of the peak at  $\delta = 6\text{-}7$  ppm was divided by five (since there are 5 protons present on the benzyl ring). The result was called  $\text{PS}_x$ . To calculate  $\text{PAA}_y$ , the integration

of the  $\delta = 1\text{--}2$  ppm was used. First, three times  $\text{PS}_x$  (the protons from the backbone of the PS chain) was subtracted from the measured integration, and then the result was divided by 12 (the number of protons within one repeat unit of the  $\text{Pt-BuA}$ ). The ratio  $\text{PS}_x / \text{PAA}_y$  gave the relative amounts of the two blocks. Since the block length of the PS block was known from SEC, the ratio  $\text{PS}_x / \text{PAA}_y$  could be used to determine the PAA block length.

Once the relative block lengths of PS to  $\text{Pt-BuA}$  were known, the  $\text{Pt-BuA}$  was converted to PAA by elimination of the *t*-butyl group. Fourier transform infrared spectroscopy (FT-IR) of the  $\text{PS-}b\text{-Pt-BuA}$  polymer before and after the elimination reaction was performed. Figure C-4 contains the FT-IR spectrum of the precursor  $\text{PS}_{325}\text{-}b\text{-PtBA}_{48}$  while figure C-5 contains that of the  $\text{PS}_{325}\text{-}b\text{-PAA}_{48}$  copolymer.

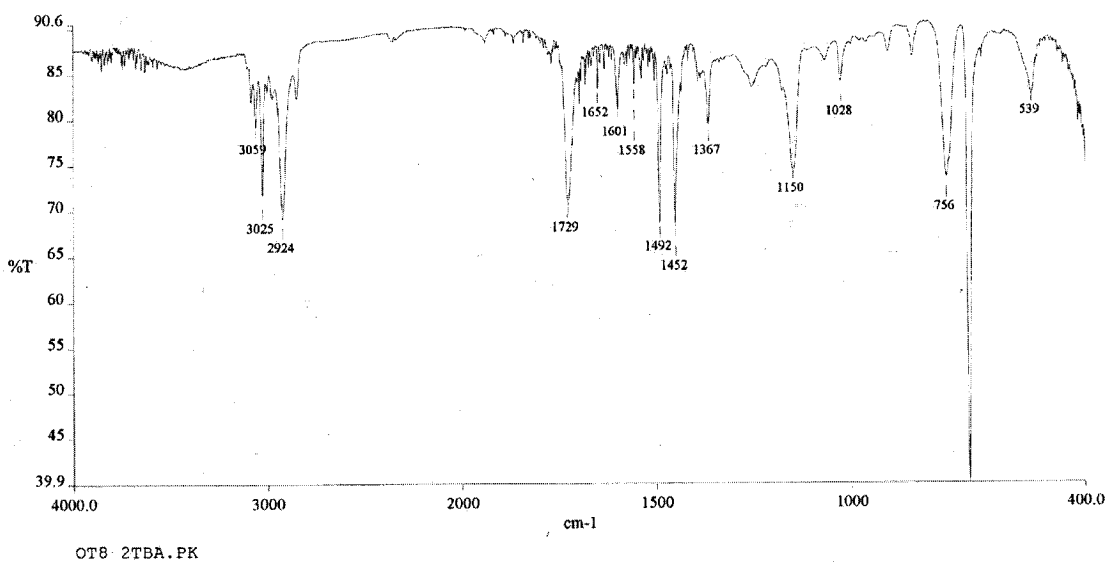


Figure C-4: FTIR spectrum of  $\text{PS-}b\text{-Pt-BuA}$ .

The peaks at different wavelengths, in figure C-4, can be assigned<sup>1,2</sup> as follows. The  $3025\text{ cm}^{-1}$  peak is the  $\text{sp}^2$  C-H stretching, while the  $2924\text{ cm}^{-1}$  peak is the  $\text{sp}^3$  C-H stretching. The  $1729\text{ cm}^{-1}$  peak is due to the ester carbonyl stretch. The *tert*-butyl deformation is represented by the peak at  $1367\text{ cm}^{-1}$ , while the peak at  $1150\text{ cm}^{-1}$

represents the C-O stretch. The large peaks at 756 and 700  $\text{cm}^{-1}$  are due to the presence of monosubstituted phenyl groups.

The removal of the t-butyl group was confirmed by the disappearance of the ester carbonyl bands at 1367  $\text{cm}^{-1}$ , in figure C-4, which means there is no t-butyl deformation. Also the ester carbonyl band originally at 1729  $\text{cm}^{-1}$  has broadened and shifted to 1734  $\text{cm}^{-1}$ , corresponding to the carboxylic acid band in figure C-5.

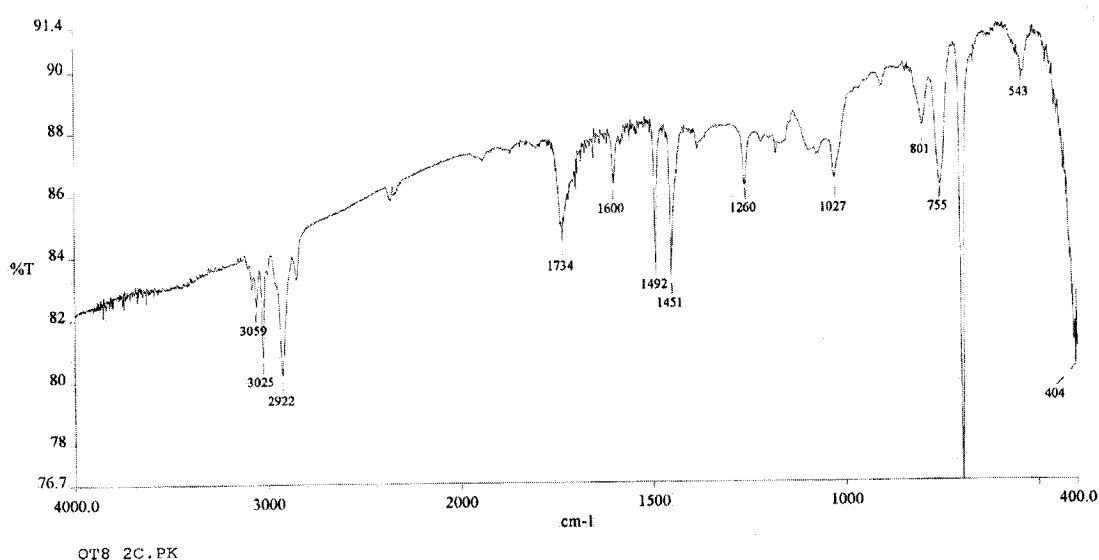
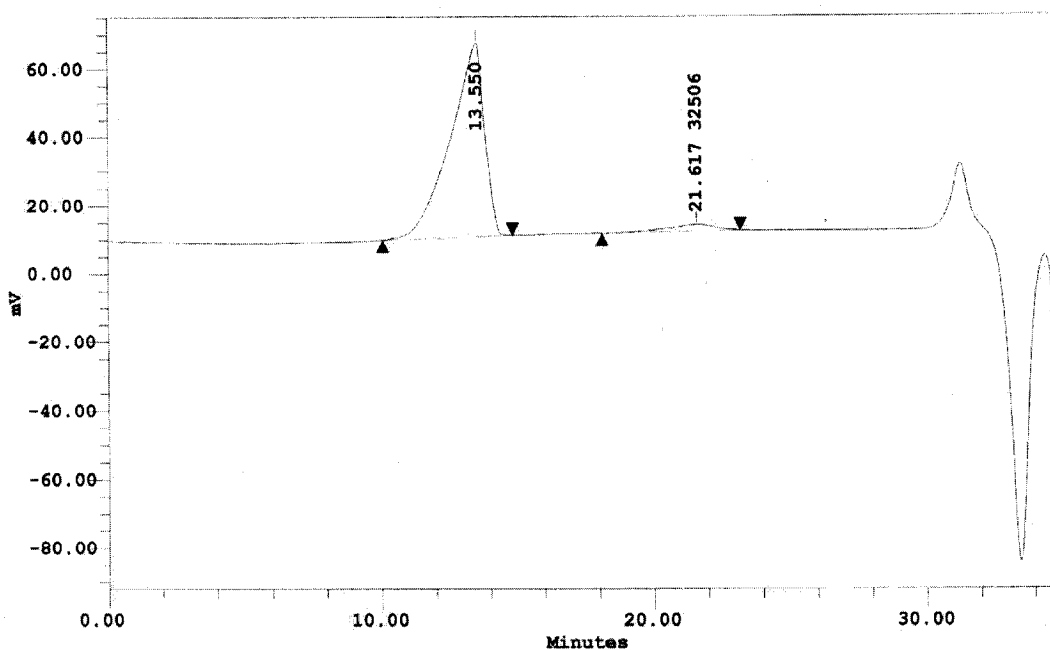


Figure C-5: FTIR spectrum of PS-*b*-PAA.

Once the PS-*b*-PAA copolymers were obtained, the next step was to remove any trace amounts of homopolymer that were not detected earlier by SEC. During the fractionation process, inverse micelles were formed and a sample was taken and analyzed by SEC. Figure C-6 shows the SEC chromatogram of the inverse micelles. A second, very small peak is detected at a higher retention time than the inverse micelles. The retention time of this peak is very similar to that of the PS block (Figure C-1). There is a slight chance that this is single chain diblock that has not aggregated. The relative peak area of the two peaks can give an estimate of the amount of homopolymer in the sample.



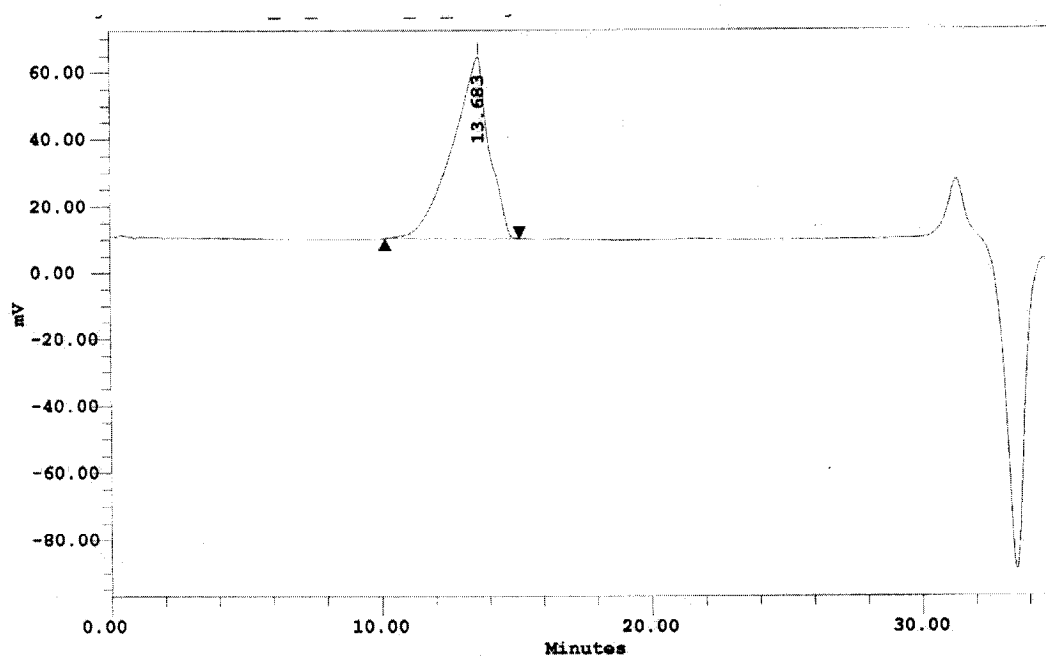
Peak Results

#	Name	Ret Time (min)	% Area	Mn (Daltons)	Mw (Daltons)	Polydispersity
1		13.550	95.72			
2		21.617	4.28	35427	44205	1.247774

Figure C-6: GPC chromatogram of inverse micelles. The extra peak is due to homopolymer.

After the fractionation process, only the peak corresponding to the inverse micelles is present in the SEC chromatogram (figure C-7) suggesting that the extra peak in figure C-6 was due to homopolymer.





Peak Results

#	Name	Ret Time (min)	% Area	Mn (Daltons)	Mw (Daltons)	Polydispersity
1		13.683	100.00			

Figure C-7: GPC chromatogram of inverse micelles after removal of homopolystyrene.

## References

1. Williams, D.; Flemming, I. *Spectroscopic Methods in Organic Chemistry*, 4<sup>th</sup> ed. McGraw-Hill Book Co., Montreal, 1987.
2. Cameron, N. S.; Eisenberg, A.; Brown, G. R.; *Biomacromolecules* **2002**, 3, 116-123.

## APPENDIX D

### MOLECULAR WEIGHT DISTRIBUTIONS

This appendix contains all of the molecular weight distributions that were used for all of the studies in this thesis. The molecular weight distributions of the individual copolymers and the mixtures are presented.

The molecular weight distributions were created using Microsoft Excel. The average molecular weight was determined as in Appendix C. For the PS blocks, the polydispersity was measured by SEC. In the case of the PAA blocks, the polydispersity of the PAA block of the individual copolymer was estimated as described in the experimental section of chapter 2<sup>1,2</sup>. The plot of polydispersity vs. average degree of polymerization that was used to determine the PAA block length polydispersity is included in figure D-1<sup>1</sup>

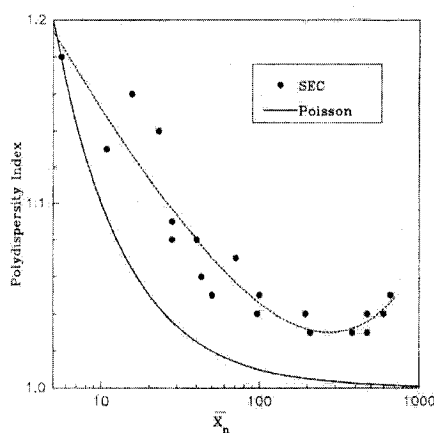
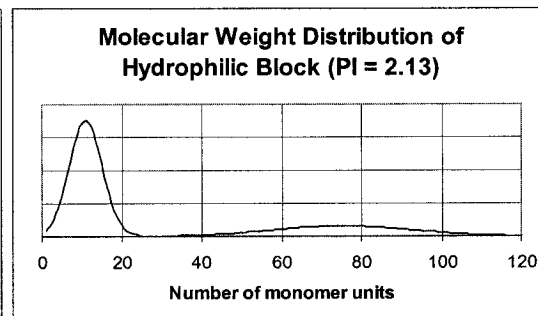
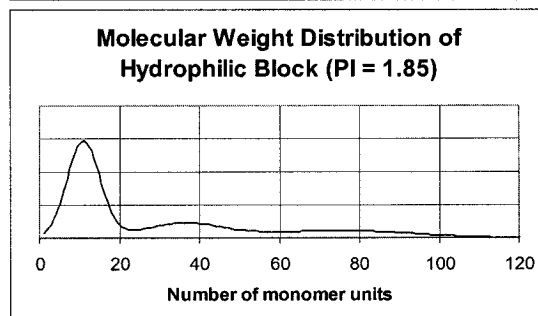
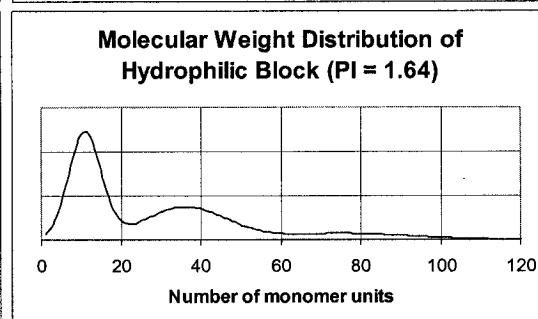
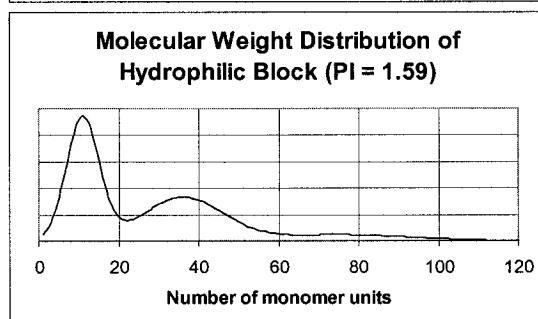
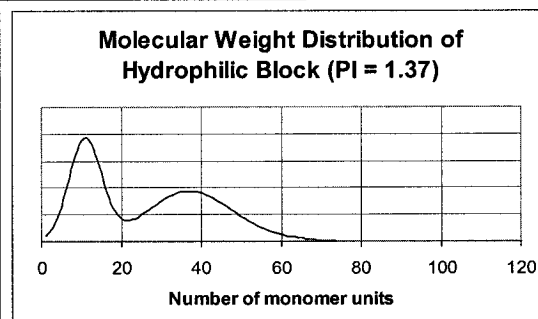
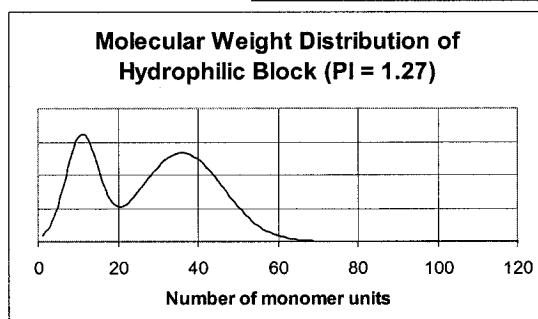
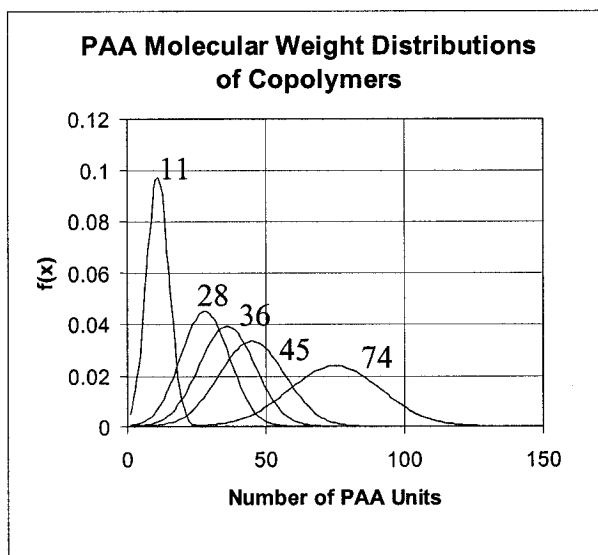
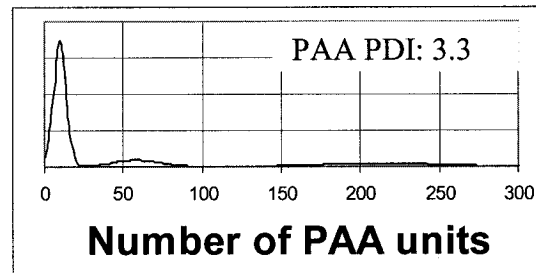
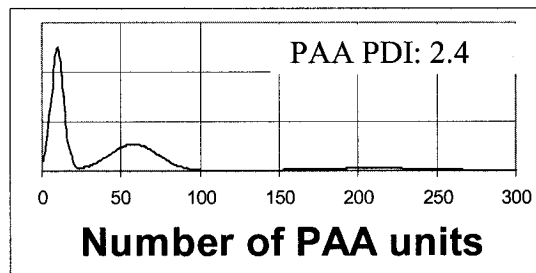
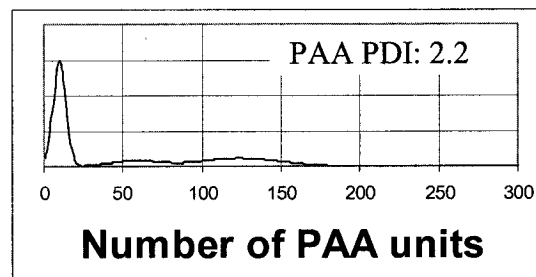
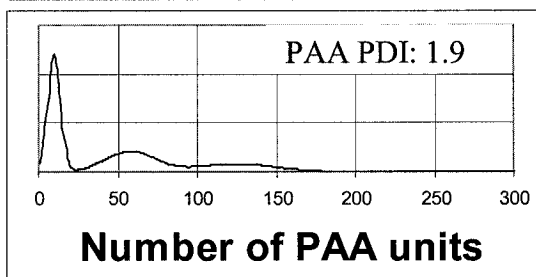
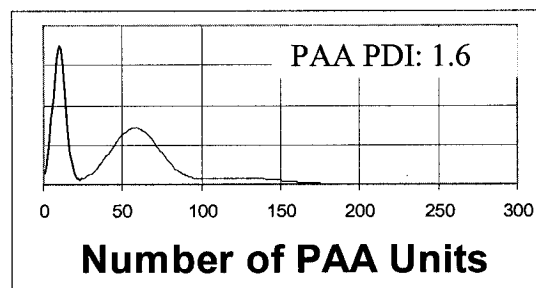
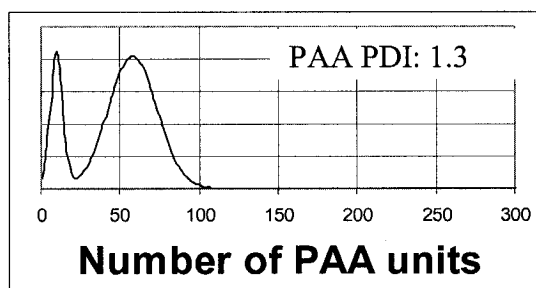
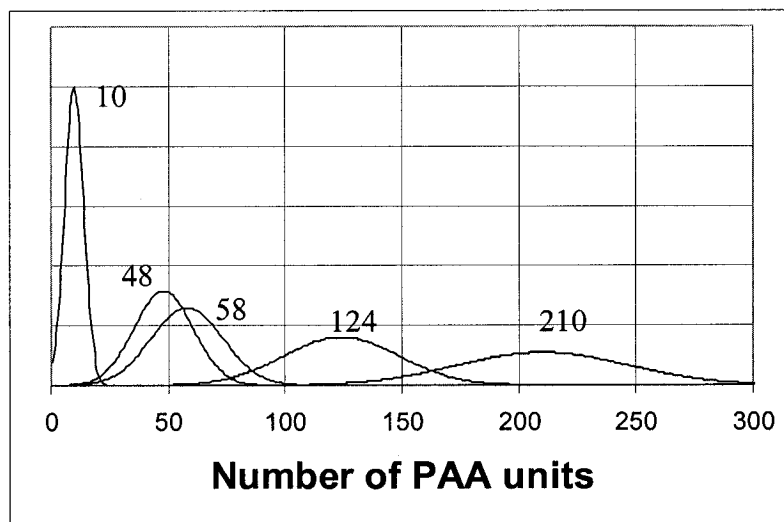


Figure D-1: The measured polydispersity of homopolystyrene of degree of polymerization  $X_n$ . The solid line is the theoretical limit (Poisson distribution). The dotted line is the experimental fit.<sup>1</sup>

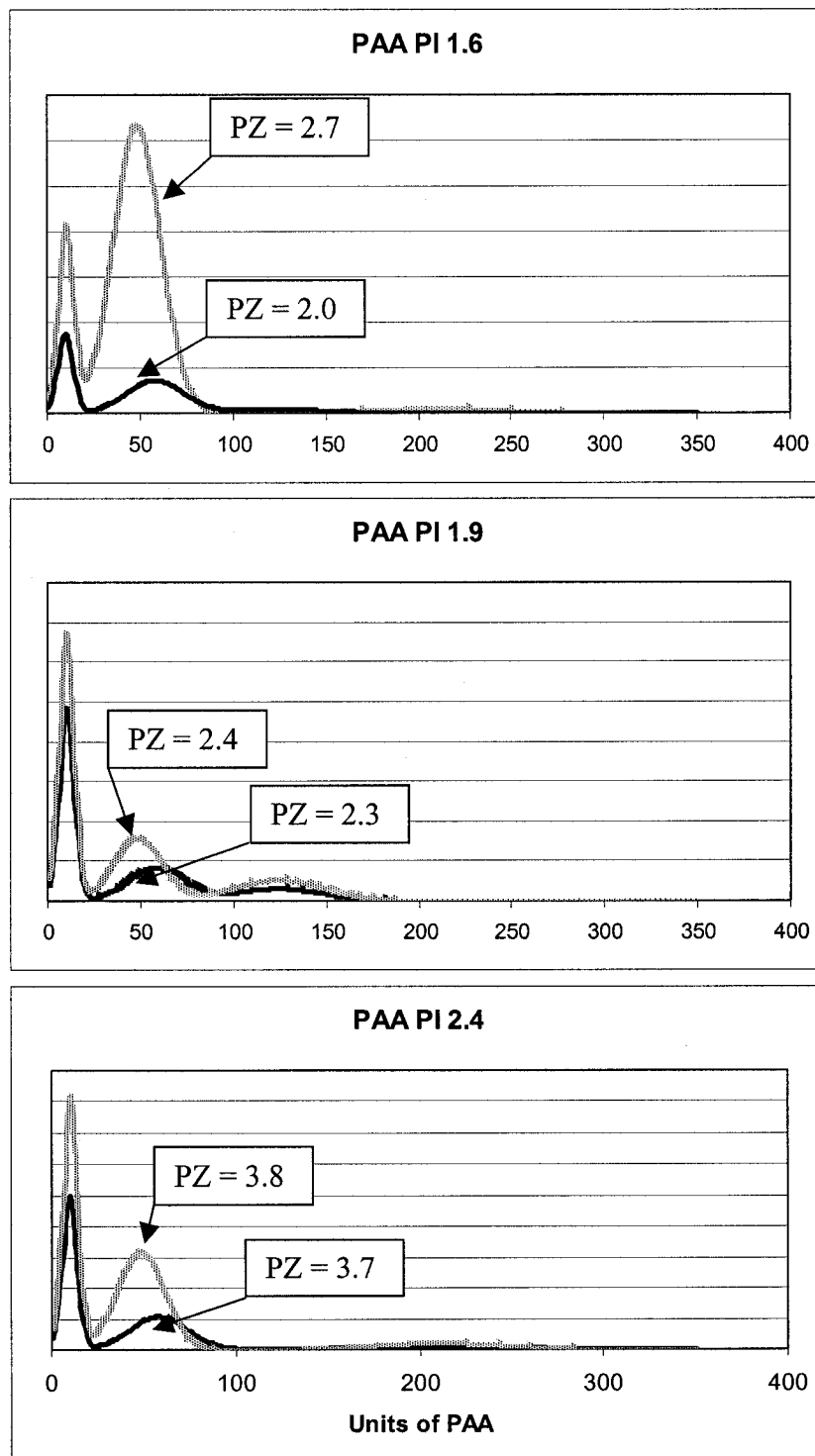
**Molecular Weight Distributions from Chapter 2**

**Molecular Weight Distributions from Chapter 3**

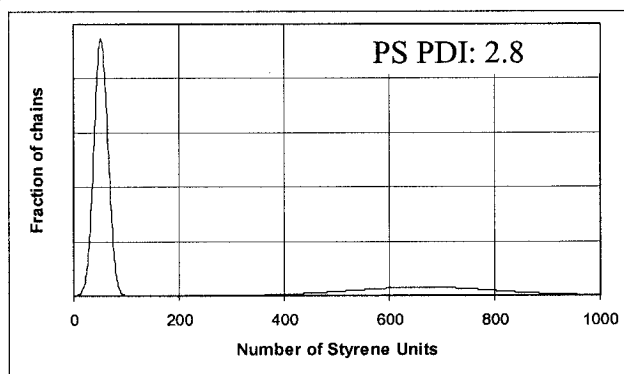
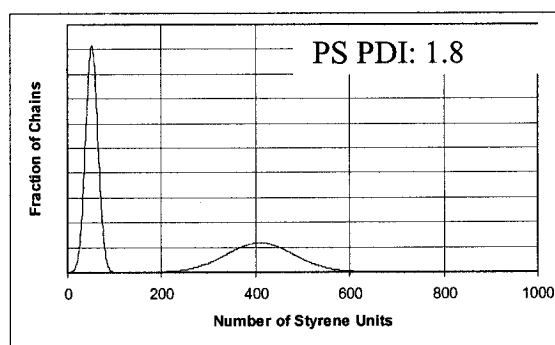
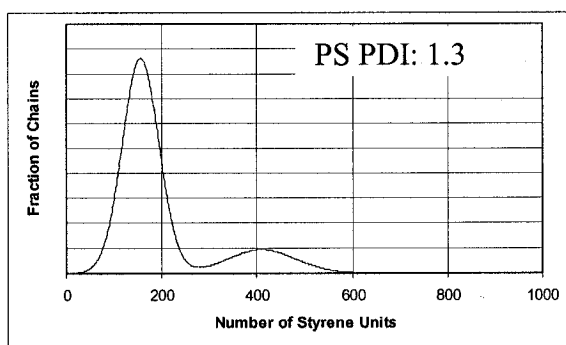
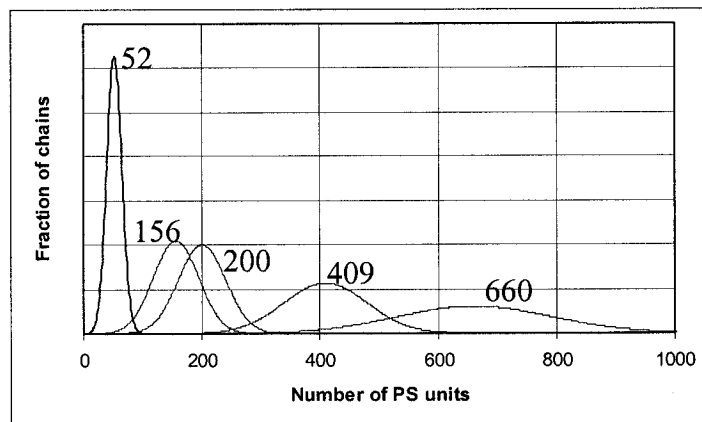


### Molecular Weight Distributions for Chapter 4

The individual molecular weight distributions are the same as those for Chapter 3.



**Molecular weight distributions from chapter 5**



**References**

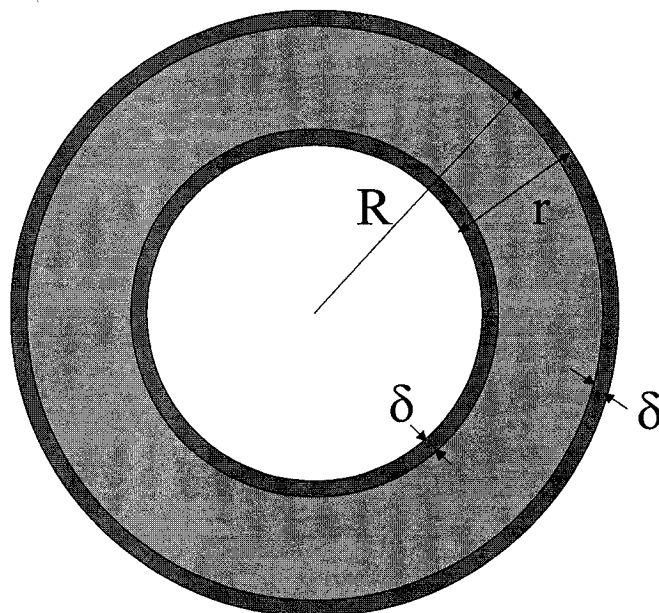
1. Nguyen, D.; Zhong, X.F.; Williams C.E.; Eisenberg, A. *Macromolecules* **1994**, *27*, 5173-5181.
2. Terreau, O.; Luo, L.; Eisenberg, A. *Langmuir* **2003**, *19*, 5601-5607.

## APPENDIX E

---

**CALCULATIONS**


---

**Calculation of Length of Collapsed Corona Chain (Chapter 2)**

From TEM pictures the outer radius,  $R$ , and the wall thickness,  $r$ , of the vesicle can be measured. Because the corona has some electron density it will be seen in the pictures, however it will not be distinguishable from the core. Since the aggregates are solid particles on the TEM grid (the solvent has been evaporated), the corona will be collapsed. To calculate the thickness of the corona,  $\delta$ , the volume fraction of PS to PAA,  $\phi_{PS/PAA}$  can be used.

$$\phi_{PS/PAA} = \frac{V_{PS}}{V_{PAA}} \quad (E-1)$$

where

$$V_{PS} = \frac{N_{PS} \times M_{PS}}{\rho_{PS}} \quad \text{and} \quad V_{PAA} = \frac{N_{PAA} \times M_{PAA}}{\rho_{PAA}} \quad (\text{E-2})$$

where  $V_{PS}$ ,  $N_{PS}$ ,  $M_{PS}$ , and  $\rho_{PS}$  are respectively the volume, number of moles of chains, average molecular weight and density of the polystyrene chains and  $V_{PAA}$ ,  $N_{PAA}$ ,  $M_{PAA}$ , and  $\rho_{PAA}$  are respectively the volume, number of chains, average molecular weight and density of the poly(acrylic acid) chains,

therefore,

$$\varphi_{PS/PAA} = \frac{\frac{N_{PS} \times M_{PS}}{\rho_{PS}}}{\frac{N_{PAA} \times M_{PAA}}{\rho_{PAA}}} = \frac{N_{PS}}{N_{PAA}} \times \frac{M_{PS}}{M_{PAA}} \times \frac{\rho_{PAA}}{\rho_{PS}} \quad (\text{E-3})$$

but, since all of the polymers used are diblock copolymers  $N_{PS} = N_{PAA}$  and assuming a density of 1 g/ml for both polymers;

$$\varphi_{PS/PAA} = \frac{M_{PS}}{M_{PAA}} \quad (\text{E-4})$$

The volume of the PS and the PAA can also be calculated by from the diagram above

$$V_{PS} = \frac{4}{3} \pi \left[ (R - \delta)^3 - (R - r + \delta)^3 \right] \quad (\text{E-5})$$

$$V_{PS} = \frac{4}{3} \pi \left\{ \left[ R^3 - (R - \delta)^3 \right] + \left[ (R - r + \delta)^3 - (R - r)^3 \right] \right\} \quad (\text{E-6})$$

therefore

$$\varphi_{PS} = \frac{\left[ (R - \delta)^3 - (R - r + \delta)^3 \right]}{\left\{ \left[ R^3 - (R - \delta)^3 \right] + \left[ (R - r + \delta)^3 - (R - r)^3 \right] \right\}} \quad (\text{E-7})$$

Let  $P = R - r$



$$\varphi_{PS} = \frac{[(R - \delta)^3 - (P + \delta)^3]}{\{[R^3 - (R - \delta)^3] + [(P + \delta)^3 - P^3]\}} \quad (\text{E-8})$$

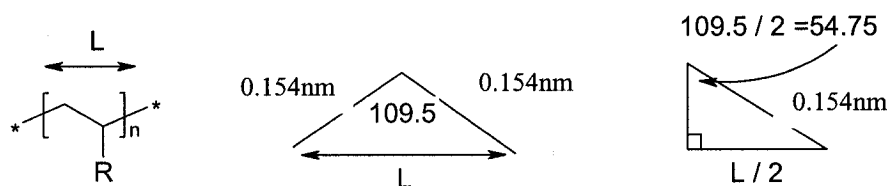
which can be rearranged to give an equation of the form

$$a\delta^3 + b\delta^2 + c\delta + d = 0 \quad (\text{E-9})$$

where  $a = 2(\varphi_{PS/PAA} + 1)$ ,  $b = -3r(\varphi_{PS/PAA} + 1)$ ,  $c = 3(R^2 + (R-r)^2)(\varphi_{PS/PAA} + 1)$ , and  $d = (R-r)^3 - R^3$ . For each sample of vesicles the average outer radius, wall thickness and  $\varphi_{PS/PAA}$  (as determined by Equation E-4) were used in the coefficients of Equation E-8 and a spreadsheet was used to plot the equation. The x intercept gave the value of  $\delta$  and was approximately 1 nm for all of the samples, which is getting close to the limit of detection of the transmission electron microscope.

### **Calculation of Extended vs. Collapsed Corona Chain Lengths**

All of the collapsed corona chain lengths were calculated to be slightly less than 1 nm. The fully extended chain length was calculated by multiplying the average number of monomer units by the average length of one monomer. The difference between the two was then calculated. To calculate the length of one monomer,  $L$ , simple geometry is used.



The length of one monomer unit is equal to the distance between the first and third carbon atoms in the polymer backbone. Since the C-C bond length is known to be  $0.167\text{ nm}$ , a simple isosceles triangle can be constructed with the two equal sides having lengths of  $0.154\text{ nm}$  and the third side has a length of  $L$ . The angle between the two equal sides will be  $109.5^\circ$ , the  $sp^3$  hybridized angle. This triangle can be cut in half to give a right

angled triangle with the hypotenuse equal to the length of the C-C bond and the angle opposite of the  $L/2$  side equal to  $54.75^\circ$ . The sine of the angle is equal to  $L/(2 \times 0.154 \text{ nm})$ .

Therefore

$$L = 2 \times (0.154 \text{ nm}) \times \sin 54.75 = 0.25 \text{ nm} \quad (\text{E-11})$$

### **Calculation of Aggregation Number (Chapter 3)**

The aggregation number was calculated by dividing the volume of the core of the micelle by the volume of a single polymer chain. To simplify the calculation, the dark areas observed in the TEM pictures were treated as being polystyrene only. This is a reasonable assumption as the volume fraction of PS to PAA was very high due to the high asymmetry of the relative lengths of the different blocks. Also, in chapter 2 (the calculation is above in this appendix), the corona was determined to have an average thickness less than 1 nm showing that the corona is negligible in these calculations.

$$N_{agg} = \frac{V_{s,r,v}}{V_{PS}} \quad (\text{E-12})$$

The volume of the core of the micelle or rod was a simply geometry calculation

$$\text{For spheres} \quad V_s = \frac{4}{3} \pi \left( \frac{d_s}{2} \right)^3 \quad (\text{E-13})$$

where  $d_s$  is the measured average diameter of the micelles.

$$\text{For rods} \quad V_r = \pi \left( \frac{d_r}{2} \right)^2 l \quad (\text{E-14})$$

where  $d_r$  is the measured average diameter of the rod and  $l$  is the measured average length of the rod.

For vesicles, the polystyrene volume was calculated by subtracting the volume of the empty sphere in the middle of the vesicle from the volume of the whole aggregate.

$$\text{For vesicles} \quad V_v = \frac{4}{3} \pi (R^3 - (R - r)^3) \quad (\text{E-15})$$

Where  $R$  is equal to the average measured outer diameter of the vesicle and  $r$  is equal to the average measured wall thickness.

The volume of one polystyrene chain was calculated by multiplying the volume of one styrene monomer with the average number of monomer units.

$$V_{PS} = N_s V_{St} \quad (\text{E-16})$$

where

$$V_{st} = \frac{MW_{St}}{\rho_{St}} \quad (\text{E-17})$$

where  $MW_{St}$  is the molecular weight of the styrene monomer and  $\rho_{St}$  is the density of styrene.